

## CHAPTER 1

### INTRODUCTION

#### 1.1 Research motivation

The bubble column reactor is one type of multiphase reactor, which is widely used in chemical, biochemical, petrochemical industries, genetic-engineering reactors, fermentation and waste water treatment etc., to enhance reaction between gas and liquid phase. Gas is dispersed in continuous phase of liquid in the column. Bubble column reactor advantages are easy for construction since no moving parts, require less maintenance and cost, have a large liquid holdup and have a high interfacial area concentration which enhances the mass and heat transfer between gas and liquid phases. Reaction and mixing between gas and liquid phase in bubble column are reported to be caused by the action of vortices via stretching, tearing and folding (A. A. Kulkarni & Joshi, 2005; G. Yang, Du, & Fan, 2007; N. Yang, Wu, Chen, Wang, & Li, 2011). Therefore, the performance of a reactor is dependent on bubble flow characteristics, the motion and the rise of bubbles in bubble column can be very complex depending on various parameters such as the size and shape of the bubble, the density and viscosity ratios between liquid and gas, surface tension force, drag force, etc. Non-dimensional numbers of Reynolds number, Weber number, Morton number, Bond number and Archimedes number are used to categorise the flow in bubble column. Single bubble rise characteristics are experimentally studied in details in bubble column, e.g., see refs (Badam, Buwa, & Durst, 2007; Bari & Robinson, 2013; Davidson & Schüler, 1997; Deckwer & Schumpe, 1993; Jamialahmadi, Zehtaban, Müller-Steinhagen, Sarrafi, & Smith, 2001; R Krishna & Sie, 2000). However, due to some limitations in experimental equipment and measurements, there are still some difficulties to obtain an accurate data on bubble terminal velocity, bubble shape changes, velocity profile, bubble coalescence

dynamics etc, in various physical properties or system parameters (N. Yang et al., 2011). Therefore, numerical investigation provides an alternative means to obtain detailed information on the complex bubble flow characteristics in bubble column. In recent years, numerical algorithms and computing power for computational fluid dynamics analysis advances and this helps for better physical understanding of two-phase flow problem likes single bubble rising behaviour. The focus of the present work is to investigate numerically the formation and raise characteristics of a single bubble in bubble column.

## **1.2 Objectives**

The objectives of this study are:

- To investigate the formation of bubble from orifice for different boundary and operating conditions using CFD.

Specifically, the effect of the size of orifice diameters is tested using a constant inlet gas velocity boundary condition; the effect of the fluid property (Bond and Reynolds numbers) are investigated.

- To investigate the effect of column angles to rise velocity of a single bubble using CFD.

Specifically, the effect of bubble column angle (i.e., trapezoidal column) on free bubble rise characteristics (i.e., instantaneous velocity, bubble shape changes, bubble trajectory etc) is investigated.

- To investigate bubble coalescence process using CFD

Specifically, the bubble coalescence in co-axial and parallel arrangements is investigated; the effects of the fluid property (viscosity and surface tension coefficient) are investigated.

### **1.3 Scope of the thesis**

This study investigated the formation and rise characteristics of a single bubble in bubble column. Air and glycerine solution were used as gas phase and liquid phase respectively for the investigation of formation and coalescence process of bubbles. Water was used for the investigation of column angle on free bubble rise characteristics. For the present study, a single bubble formation characteristics from an orifice was investigated in different conditions of liquid properties such as the effect of Bond number (which indicates the change of surface tension from 0.063 N/m to 0.0063 N/m) when the other properties of liquid kept constant; the effect of Reynolds number (which indicates the change of liquid viscosity from 0.074 Pa.s to 0.001 Pa.s) when the other properties of liquid kept constant. Furthermore, the rise characteristics of free bubble in different column angle ( $0^\circ$  to  $9^\circ$ ), a detailed mechanisms of co-axial and parallel bubble coalescence processes, shape changes phenomena and velocity profile were also investigated, when one property of liquid was changed as well as the other properties kept constant. The aim of the study is to obtain detailed knowledge of a single bubble formation and rise characteristics in bubble column using CFD. Volume of fluid with continuum surface force model was used. The outcomes from this study would be beneficial for the right choice of orifice size of sparger design and fundamental phenomenon of gas-liquid flow characteristics in a bubble column.

There are some limitations of the present studies such as (i) A 2D domain without axi-symmetric was chosen due to capture a asymmetry bubble formation, rise characteristics and shape of bubble from bottom to the top of the column; (ii) the domain has represented 2D cross sectional view of cylindrical bubble column and a careful interpretation is required whenever to use the 2D results to 3D cases; (iii) the bubble formation and rise characteristics in stagnant liquid were considered as laminar;

(iv) the study was also considered without heat and mass transfer between gas and liquid.

#### **1.4 Thesis outline**

The dissertation consists of six chapters which are organized in the following ways: Chapter 1 offers a brief overview of the research topic, objectives and scope of the thesis. In Chapter 2, reviews of existing literature pertaining to previous experimental, theoretical, and numerical research on bubble motion have been given. In Chapter 3, governing equations, boundary conditions, simulation cases and bubble formation characteristics are explained. Chapter 4 deals with the couple level set volume of fluid numerical method and the results of the effect of column angle on single bubble dynamics. In Chapter 5, numerical results of co-axial and parallel bubble coalescence mechanism in rectangular channel filled with stagnant liquid are explained. Finally, Chapter 6 summarizes the important findings and conclusions of the study and it includes some suggestions for further research on bubble motion in bubble column.

## CHAPTER 2

### LITERATURE REVIEW

#### 2.1 General background

Bubble column reactors are widely used to enhance reactions and mixing between the gas and liquid phase in petrochemical processes in chemical industries. The degree of reaction and mixing is found to be strongly dependent on bubble flow characteristics. A number of experimental studies (Badam et al., 2007; Bari & Robinson, 2013; Bolaños-Jiménez, Sevilla, Martínez-Bazán, & Gordillo, 2008; Davidson & Schüler, 1997; Deckwer & Schumpe, 1993; Jamialahmadi et al., 2001; R Krishna & Sie, 2000; L. Zhang & Shoji, 2001) have been done to characterize the bubble flow in bubble columns. Parameters such as rise velocity, bubble volume, the bubble deformation, the size of orifice, the shape of distributor, operating conditions (e.g., the pressure, the temperature, the liquid and gas density, the viscosity etc) were investigated. In addition, a number of numerical studies (Albadawi, Donoghue, Robinson, Murray, & Delauré, 2013; Bari & Robinson, 2013; Buwa & Ranade, 2002; Chakraborty, Biswas, & Ghoshdastidar, 2011; Chakraborty et al., 2009b; Gerlach, Alleborn, Buwa, & Durst, 2007; Ma, Liu, Zu, & Tang, 2012; Ohta, Kikuchi, Yoshida, & Sussman, 2011; Valencia, Cordova, & Ortega, 2002) have been done in recent years to investigate the bubble flow characteristics such as bubble trajectory, bubble formation dynamics, bubble shape, bubble deformation, liquid flow field around the rising bubble etc in the bubble column.

A typical bubble column is shown in Figure 2.1, in which gas fed through a distributor or sparger to generate bubbles in a medium of liquid (Figure 2.1a) or liquid-solid suspensions (Figure 2.1b). Generally, bubble column has a large length to diameter ratio, or aspect ratio. The liquid (slurry) is used either as semi-batch (zero liquid velocity) or as continuous mode (co-current or counter-current with respect to the

gas flow). For the continuous mode, the liquid velocity is lower than the gas velocity. There are many types of sparger used in the bubble column, see Figure 2.1c for examples. Orifice size of sparger varies from 0.7 mm to 2 mm and inlet gas velocity varies from 0.5 to 20 m/s per orifice on average (Buwa & Ranade, 2002; Hua & Lou, 2007; A. A. Kulkarni & Joshi, 2005).

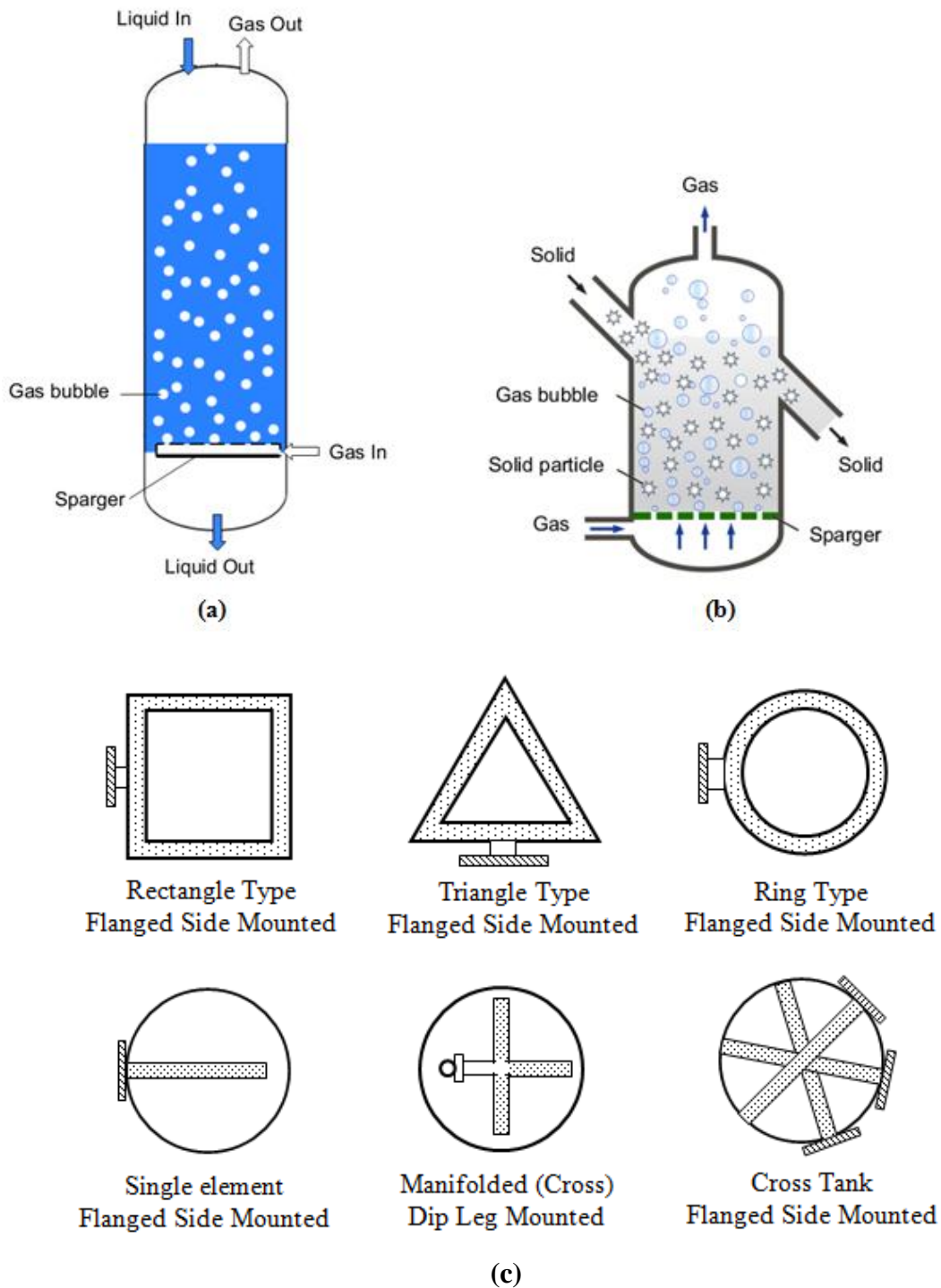


**Figure 2.1:** Schematics of bubble column configuration of liquid-gas (a) and of liquid-solid-gas (b) and (c) different types of spargers (A. A. Kulkarni & Joshi, 2005).

## 2.2 Bubble formation stages

Bubble formation and rise mechanism is a good example of a two-phase problem. Bubble volume increases when air flow through an orifice increases. When the opposing forces, i.e., mass inertia force, drag force surpass the lift force etc., bubble detaches from the orifice and starts to rise due to buoyancy. According to Zhang & Shoji (2001), bubble formation has two stages, i.e., the expansion stage and the elongation stage. Figure 2.2 show the bubble formation mechanism at the elongation stage. At bubble formation stage, there are five types of force mainly act on a bubble; such as the gas momentum flux ( $F_m$ ) and the buoyancy force ( $F_b$ ) acts on the vertical direction, this force are balanced by opposite forces of the mass inertia force ( $F_i$ ), the drag force ( $F_d$ ) and the surface tension force ( $F_\sigma$ ) (L. Zhang & Shoji, 2001).

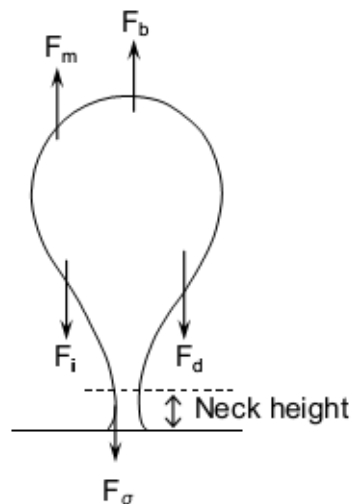


**Figure 2.2:** Schematic diagram of bubble formation mechanism at elongation stage. Note:  $F_m$ : Gas momentum flux;  $F_b$ : Buoyancy force;  $F_i$ : Added mass inertia force;  $F_d$ : Drag force and  $F_\sigma$ : Surface tension force (L. Zhang & Shoji, 2001).

### 2.2.1 Expansion stage

In the expansion stage, bubble grows radially due to incoming gas (or air) flow, but the base of bubble is still attached to an orifice. This process continues as long as the opposing forces (i.e., against bubble release) dominates the lifting forces. The expansion stage will come to the end when the opposing forces become equal to or larger than the lifting forces.

### 2.2.2 Elongation stage

In the elongation stage, a continuous gas (air) flow through an orifice results in a further growth of the bubble size. The bubble starts to lift off from the orifice but is still attached to it; the bubble forms a neck shape near the orifice. The neck also starts to grow with the gas influx. Eventually, the neck becomes very thin and pinches off from the orifice (or bubble detachment). According to Kim, Kamotani, & Ostrach (1994), bubble neck collapses when the neck length becomes larger than or equal to the orifice diameter.

### 2.2.3 Bubble detachment

When a bubble neck pinches off, a new force balance acting on the bubble develops. The upper part of a detached bubble maintains its shape due to inertia, but the lower part shrinks towards the bubble centre. After detachment or pinch off, the buoyancy force, inertia force and drag forces are considered as the main forces in a bubble rise, which is depicted in Figure 2.3. In this case, the buoyancy force is balanced by the opposite forces of inertia and drag.

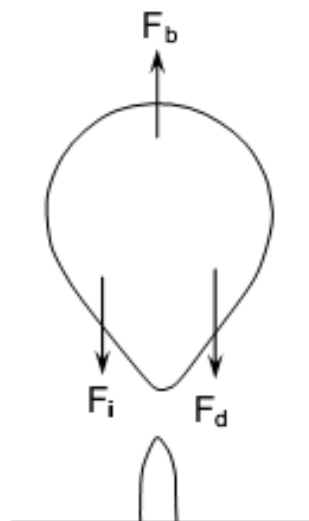


**Figure 2.3:** Bubble detachment or bubble pinch off. Note:  $F_b$ : Buoyancy force;  $F_i$ : Added mass inertia force;  $F_d$ : Drag force (L. Zhang & Shoji, 2001).

### **2.3 Study of single bubble formation**

The study of a single bubble formation through an orifice in the bubble column will help to understand the bubble size, bubble shape and bubble formation characteristics. Therefore, extensive experimental studies have been carried out to investigate a single bubble formation through an orifice under normal pressure condition and constant gas flow condition (Badam et al., 2007; Bari & Robinson, 2013; Jamialahmadi et al., 2001; A. A. Kulkarni & Joshi, 2005; Y. Zhang, Xiao, & Tan, 2005). Studies were also done at elevated pressures (Lin, Tsuchiya, & Fan, 1998; Tse, Martin, Mcfarlane, & Nienow, 1998; G. Yang, Luo, Lau, & Fan, 2000). For example, Davidson & Schüler (1997) experimentally investigated the air bubble formation characteristics through a number of orifice diameters in high viscosity liquids (500-1040 cp) under two types of flow conditions, i.e., under constant gas flow rates (0-50 ml/s) and constant gas pressure conditions. For a constant gas flow rate, the volume of the bubble that detaches is found to be dependent on the gas flow rate and kinematic viscosity of the liquid. The effect of the orifice diameters is found small. However, for the constant gas pressure condition, the bubble volume is found to be dependent on the orifice diameters, the gas density and viscosity; and the surface tension of the liquid. Jamialahmadi et al. (2001) investigated the air bubble formation in different types of liquid solutions under constant flow conditions and developed a nonlinear correlation to predict bubble diameter. The authors suggested that the bubble volume is strongly dependent on the orifice diameter, the surface tension and the liquid viscosity. Badam et al. (2007) investigated the bubble formation characteristics from a submerged orifice under constant gas flow conditions in water and propanol solution. They have found that the volume of bubble and the bubble formation time increases with the increase of the orifice diameter and the surface tension coefficient. Bari & Robinson (2013) investigated air bubble growth in water for different gas flow rates using submerged orifice diameters. The hydrostatic pressure is

found to have a significant effect on the bubble elongation during the bubble mid growth stage.

The formation characteristics of a single bubble under various conditions have also been investigated numerically (Albadawi et al., 2013; Buwa & Ranade, 2002; Chakraborty et al., 2011; Chakraborty et al., 2009b; Di Bari, Lakehal, & Robinson, 2013; Gerlach et al., 2007; Gerlach et al., 2005; Ma et al., 2012; Ohta et al., 2011). For example, Chakraborty et al. (2011) used the combined Level Set and Volume of Fluid (CLSVOF) methods to determine the position of the gas liquid interface for a case where the gas is supplied through an orifice into a moving liquid under microgravity environments. They reported that an increase of the liquid velocity in the column decreases the bubble size and the bubble formation time. Albadawi et al. (2013) used CLSVOF methods to investigate the growth of the bubble formation and the bubble detachment using four different flow rates (i.e., 50, 100, 150, 200 mlph) through an orifice diameter of 1.6 mm; a higher flow rates forms a bigger bubbles. Ma et al. (2012) is used VOF-CSF model to investigate the effect liquids properties on the bubble formation. They found that a bigger size of bubbles is formed by increasing the surface tension coefficient and liquid viscosity. But a small size of bubble is formed by increasing the liquid density.

#### **2.4 Single bubble rise velocity**

Single bubble rising behaviour has been extensively investigated. A rising bubble can be characterized in terms of its rise velocity and its diameter or size. For small bubbles (e.g. less than 1 mm), the viscous and the surface tension force dominates the bubble rise velocity. In this situation, the Hadamard-Rybczynski theory and the Stokes' theory can be applicable (Fan, 1989; A. A. Kulkarni & Joshi, 2005). But when the diameter of the bubble is greater than 1 mm, those liquid properties is not dominating the bubble

rise velocity significantly. In this situation, the Mendelson, (1967) equation is widely applicable (Fan, 1989; R Krishna et al., 1999; A. A. Kulkarni & Joshi, 2005). When the diameter of the bubble is intermediate (i.e., 4 mm to 10 mm), the buoyancy and surface tension force plays an important role for fluctuation of bubble motion (or spiral trajectory path). In this situation, it is difficult to obtain accurate velocity of the bubbles.

Several techniques have proposed (R Krishna, Wilkinson, & Van Dierendonck, 1991) to estimate of the bubble rise velocity based on the bubble size. In fact, the most well known technique is also by Krishna and co-workers (R Krishna et al., 1991; Rajamani Krishna, De Swart, Hennephof, Ellenberger, & Hoefsloot, 1994). They classified the bubble sizes in two groups, which is large bubble and small bubble and developed a simplified equation for the regime of bubbly flow. On contrary, some other researchers reported that the bubbly flow depends not only on the bubble size but also on operating conditions such as the pressure, the temperature, the fluid properties and column diameters (Coutanceau & Thizon, 1981; R Krishna, Urseanu, Van Baten, & Ellenberger, 1999; Schäfer, Merten, & Eigenberger, 2002). Therefore, a number of correlations are established to predict the accurate bubble rise velocity and some of popular correlations are given in Table 2.1.

**Table 2.1:** Established correlations to predict the bubble rise velocity from literature (R Krishna et al., 1999; R Krishna et al., 1991; Rajamani Krishna et al., 1994; H. Li & Prakash, 2000; Moo-Young & Blanch, 1981; Tomiyama, Celata, Hosokawa, & Yoshida, 2002).

Authors	Correlation
Krishna and Rajamani (1994)	$\varepsilon_{g,hom} = \frac{U_g}{U_{b,small}} ; \varepsilon_{b,heter} = \frac{U_{g,trans}}{U_{b,sm}}$

T able 2.1 Continue

---

Stroke's equation	$U_{b,small} = \frac{g\rho}{18\mu} d_b^2 ; Re < 1$
Hadamard–Rybczynski equation	$U_b = \frac{g\rho}{18\mu} d_b^2$
Wilkinson equation	$\frac{U_{b,small} \mu_l}{\sigma} = 2.25 \left( \frac{\sigma^3 \rho_l}{g\mu_l} \right)^{-0.273} \left( \frac{\rho_l}{g\rho_l} \right)^{0.03}$
Mendelson equation	$U_b = \left( \frac{2\sigma}{\rho_l d_b} + \frac{gd_b}{2} \right)^{0.5}$
Developed by Tomyama et al. (2002).	$U_b = \left( \frac{2\sigma}{\rho_l d_b} + \frac{\Delta\rho g d_b}{2} \right)^{0.5}$
Developed by Li and Prakash (2000).	$U_{b,sm} = U_{b,sm 0} \left( 1 + \frac{1.073}{U_{b,sm 0}} \phi_s \right)$
Developed by Krishna et al. (1999) for wall effect.	$U_{b,large} = \begin{cases} 0.62\sqrt{gd_b} ; & d_b/D_t < 0.07 \\ 0.62\sqrt{gd_b} (1.1 \exp(-1.55d_b/D_t)); & 0.07 < d_b/D_t < 0.4 \\ 0.236\sqrt{gD_t}; & d_b/D_t > 0.4 \end{cases}$

---

A single bubble rise velocity was investigated under various conditions of liquid density, viscosity, surface tension and column diameter etc through experimental studies (Coutanceau & Thizon, 1981; R Krishna et al., 1999; R Krishna & Van Baten, 1999; Raymond & Rosant, 2000; Tsuge, Hamamoto, & Hibino, 1984; Uno & Kintner, 1956) and numerical studies (Chakraborty et al., 2009a; Ma et al., 2012; Ohta, Kikuchi, Yoshida, & Sussman, 2007). The conclusions of these studies are the single bubble rise velocity decreases with the increase of the liquid density and viscosity and also with the decrease of the column diameter. For example, Uno & Kintner (1956) experimentally investigated the single bubble rise characteristics in four different quiescent liquids and different sized column diameters. The authors have suggested an empirical correlation for fluids with Morton (Mo) ranges from  $O(10^{-5})$  to  $O(10^{-11})$  and three different bubble

regimes (spherical, ellipsoidal, and spherical cap). The tube diameters and initial bubble radii ranges from 2.09 to 15 cm and from 0.1 to 1.2 cm, respectively and these cases of a high Reynolds (Re) number. Similarly, Tsuge et al. (1984) has proposed empirical and semi empirical correlations for single bubble drops for  $Re = 500$ . Coutanceau & Thizon (1981) had investigated the wall effects on single bubble behaviour in highly viscous liquids using both theoretical and experimental methods in which bubble is set to rise along the axis of a vertical circular tube filled with a highly viscous liquid. The terminal speed of a spherical bubble is found to be affected by the wall effect. Krishna et al. (1999) experimentally investigated the rise velocities of single bubbles in the size range of 3~80 mm in cylindrical columns filled with water of diameters ranging from 10 mm to 630 mm. The authors has shown the significant effect of the wall on single bubbles rising in smaller diameter columns and suggested a modification to Mendelson (1967) equation to describe the bubble rising velocity inclusive of the wall effect.

## 2.5 Bubble shape deformation

The bubble shape is an important aspect for bubble motion. The bubble shape depends on bubble wake effect and physical properties of the surrounding liquid or medium and resultant forces acting on the bubble, namely surface tension, viscous and buoyancy forces (Dahya Bhaga & Weber, 1981). The bubble rise characteristics in the stagnant fluid under the influence of the buoyancy force can be grouped into three main regimes; they are the spherical, oblate ellipsoidal, and spherical or ellipsoidal caps, which are shown in Figure 2.4. The shape of the bubble can be related to three dimensionless parameters, namely, the Eötvös number (Eo) or Bond number (Bo), Morton number (Mo), and Reynolds number (Re). Eötvös number gives the ratio between the body force (gravitational force) and the surface tension force, which is-

$$Eo \text{ or } Bo = \frac{g \Delta\rho d_b^2}{\sigma} \quad (2.1)$$

Morton number mainly describes the properties of the continuous surrounding fluid such as density and viscosity, which is-

$$Mo = \frac{g\mu_l^4}{\rho_l\sigma^3} \quad (2.2)$$

Reynolds number is defined as the ratio between the inertial forces and the viscous forces, which is

$$Re = \frac{\rho_l U_b d_b}{\mu_l} \quad (2.3)$$

where  $d_b$  is the bubble diameter,  $\Delta\rho$  is the density difference between the components,  $\rho_l$  is the liquid density,  $g$  is the gravitational acceleration,  $\sigma$  is the surface tension,  $\mu_l$  is the viscosity of the liquid, and  $U_b$  is the terminal velocity of the bubble.

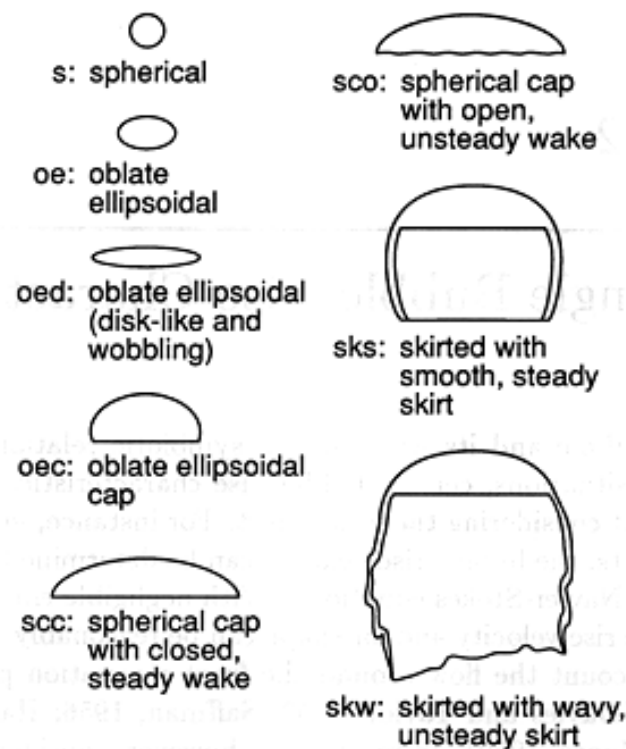


**Figure 2.4:** Various bubble shapes observed in Newtonian fluids (Dahya Bhaga & Weber, 1981).

When the diameter of bubble is small (e.g. less than 1 mm), the viscous force and the surface tension force dominates and this means that bubble surface retains its origin

shape or spherical shape. When the diameter of bubble is greater than 1 mm, the bubble shape can change from spherical to ellipsoidal shape. But when the diameter of bubble is an intermediate (e.g., greater than 1 mm to less than 18 mm), the surface tension and the buoyancy force play an important role for variations in bubble shape and rise dynamics. The intermediate sizes of bubbles have complex shape such as ellipsoidal, ellipsoidal cap shape and these bubbles are likely to rise in a spiral trajectory path due to the effective forces. When the diameter of a bubble is larger (e.g., greater than 18 mm), the buoyancy force dominates over the other forces resulting a development of spherical cap shape bubble (R. Clift, 2005; Fan & Tsuchiya, 1990).

Bubble shape can be described using bubble aspect ratio, which is the ratio of the bubble height (h) to bubble width (w) or vice versa (Dahya Bhaga & Weber, 1981). Researchers developed some correlations through experimental studies to describe the relationship between bubble shapes and motion in various liquids (Dahya Bhaga & Weber, 1981; Bozzano & Dente, 2001; RC Chen & Chou, 1998; R. Clift, 2005; Grace, 1973; Tsuchiya & Fan, 1988; G. Yang et al., 2007). Bubble shapes are found to be dependent on the viscosity ratio, the density ratio and the surface tension force. For example, Clift (1978) reviewed studies carried from years 1930 to 1977 dealing with the fluid dynamics, heat and mass transfer of bubbles and drops. They developed a graphical correlation of bubble shape and terminal velocity for a wide range of Morton numbers ( $1.7 \times 10^{-12} < Mo < 1.2 \times 10^3$ ). A more comprehensive range of experimental data and a study of correlation of bubble rise velocity and bubble shape deformation were presented by Dahya Bhaga & Weber (1981). In addition, the authors had also carried out numerical investigations, in which a bubble is introduced in liquid to visualize the velocity field around the rising bubble based on the Reynolds number. Zudin (1995) proposed an analytical solution for shape evaluation and rise velocity for large bubbles. The rise velocity of a single bubble and shape deformation in a stagnant liquid was

studied by Bozzano & Dente (2001). The authors introduced a friction coefficient to evaluate the bubble velocity and shape for various flow regimes. Davies & Taylor (1950) proposed formulation to calculate the rise velocity of spherical cap bubbles. Some of important correlations for bubble shape evaluation (or bubble aspect ratio) are summarized in Table 2.2.

**Table 2.2:** Correlations for bubble aspect ratio, ( $E=h/w$ ) (R. Clift, 2005; Fan & Tsuchiya, 1990; Okawa, Tanaka, Kataoka, & Mori, 2003; Wellek, Agrawal, & Skelland, 1966).

Authors	Correlation
Fan & Tsuchiya (1990).	$E = \begin{cases} 1 ; & Ta < 1 \\ 0.81 + 0.2 \tanh[1.8(0.4 - \log_{10} Ta)]^3 ; & 1 \leq Ta < 39.8 \\ 0.24 ; & 39.8 \leq Ta \end{cases}$ <p>Ranges: <math>Mo &lt; 10^{-3}</math> (pure liquids)</p>
Clift et al. (2005).	$E = \frac{1}{1 + 0.163 Eo^{0.757}}$ <p>Ranges: <math>Mo &lt; 10^{-3}</math>; <math>Eo &lt; 40</math> (contaminated liquids)</p>
Okawa et al. (2003).	$E = \frac{1}{1 + 1.97 Eo^{1.3}} ; \text{ Ranges: } Eo < 30$
Wellek et al. (1966)	$E = \frac{1}{1 + 0.091 We^{0.95}} ; \text{ Ranges: } We < 10$

Note: Correlations of bubble aspect ratio are presented as a function of bubble Tadaki number ( $Ta = Re Mo^{0.23}$ ) for pure liquids system.

## 2.6 Bubble coalescence

The bubble coalescence dynamics plays an important role on overall performance of a system as well as in heat and mass transfer between gas and liquid. Thus the detailed knowledge of pair bubble coalescence dynamics such as bubbles shape, collision time,

bubble shape after coalescence etc., can lead to gain better insight of bubble coalescence characteristics. The bubble coalescence process is defined as two or more bubbles merge to form a bigger bubble. Small bubbles are formed from bubble breakup. The mechanism of bubble coalescence can be interpreted into three stages, namely (a) bubbles collision (b) formation of thin liquid film and trapping and (c) rupture of the liquid film (Crabtree & Bridgwater, 1971; Oolman & Blanch, 1986). When the bubbles close to contact each other, the collision force of bubbles increases than the surface tension force resulting in a formation of thin liquid film between the contact areas. Typically, this liquid film thickness varies from  $10^{-5}$  to  $10^{-6}$  m. When liquid film is thinner more due to the impact from collision force than the liquid film will be rupture resulting in bubble coalescence. This film rupture mechanism occurs in a millisecond of time.

Bubble coalescence is not only depends on the fluid properties but also depends on the flow structure of fluid between the bubble gap that controls the force of collision, the coalescence time and duration of the collision (Chesters, 1991; Tse et al., 1998). The bubble coalescence has been reported by many researchers (Chi & Leal, 1989; Ma et al., 2012; Pinto, Pinheiro, & Campos, 1998; Ribeiro Jr & Mewes, 2006). But a limited experimental works (D Bhaga & Weber, 1980; Higuera, 2005; Manasseh, Yoshida, & Rudman, 1998; Oolman & Blanch, 1986; Stover, Tobias, & Denn, 1997) have been done on bubble coalescence investigation because of complex nature of a bubble shape changes phenomenon during bubble coalescence and limitation of experimental equipment.

## **2.7 Multiphase flow simulation using CFD**

Computational fluid dynamics (CFD) is a very effective means to investigate gas-liquid flows in bubble column due to significant advancements in numerical techniques and

computational power. In general, there are three types CFD of approaches that are commonly employed for this type of study and they are Eulerian–Eulerian (E–E) method, Eulerian–Lagrangian (E–L) method and the interface tracking method (Ahmadzadeh, Saranjam, Hoseini Fard, & Binesh, 2013; Tryggvason et al., 2001). The E–E two fluid model treats the gas bubble or particles as a pseudo-continuum phase (Salomons, Blumrich, & Heimann, 2002) and therefore does not provide flow details of individual bubbles. In the E–L model, gas is treated as a continuum phase and particles are considered as a discrete phase and motion of particles are tracked individually. This model can predict deformation of a gas bubble in a solid phase. The interface tracking method has two types of methods, namely front-tracking method and volume tracking method. The first is based on Lagrangian grid system and the latter is based on Eulerian framework. A high degree of accuracy is achieved using front-tracking but this method requires huge computational power and time. Instead, the volume-tracking method is often preferred for its efficiency and less intensive in computational power. The interface is constructed using some special functions like fractional volume-of-fluid (VOF) (Hirt & Nichols, 1981).

The VOF method is designed for two or more immiscible fluids where the position of the interface between the fluids is of interest (Rabha & Buwa, 2010). The level-set (LS) method can be used with VOF to improve the interface tracking and shapes of bubble (Osher & Fedkiw, 2001). In this method, the surface tension force at the interface can be incorporated into the flow momentum equation as a source term using the continuum surface force (CSF) method (Brackbill, Kothe, & Zemach, 1992). The significant advantage of this method is the much lower computational cost in comparison to that required for E-E and E-L approaches. However, VOF method can be less accurate for interface calculations on its own but this can be improved using the combination of the LS and VOF methods, namely CLSVOF which combine the

advantages of both the LS and the VOF methods (Q. Li, Ouyang, Yang, & Li, 2012) and can handle a flow problems involving large topological changes and interface deformations such as bubble shape, bubble formation and bubble coalescence process with easy.

## **2.8 Summary**

In summary, various studies have been carried out experimentally to investigate a single bubble formation mechanism from an orifice, wall effect on free bubble rising characteristics and bubble coalescence process. For example, the study of the changes in the bubble contact angle as well as its formation at orifice and the rising characteristics of a single bubble in non-uniform columns is limited, e.g., see refs (Bari & Robinson, 2013; Krishna et al., 1999; Manasseh, Yoshida, & Rudman, 1998). The present work provides much detailed information on the formation of bubble from orifice (e.g., expansion, elongation and pinch off, bubble equivalent diameter, and bubble detachment time), the effect of Bond number, the effect of Reynolds number on bubble formation, the rising characteristics of a single bubble in non-uniform columns (e.g., bubble rising behaviour, the spatial distribution, the shape deformation and characteristics of the bubble with wall effects due to the different types of trapezoidal cavity) and bubble coalescence process, which is very difficult to be obtained from experimental studies. Therefore, the purpose of the present work is to fulfil above the gap with detailed explanation using CFD method.

## CHAPTER 3

### STUDY OF A SINGLE BUBBLE FORMATION CHARACTERISTICS USING CFD

This chapter describes the study of bubble formation from an orifice in stagnant fluids. The work carried out in this chapter provides detailed information on the formation of a bubble from orifice under various operating conditions.

#### 3.1 Introduction

The study of a single bubble formation through an orifice in the bubble column is important to understand the bubble size, bubble shape and bubble formation characteristics. Experimental studies have been carried out to investigate a single bubble formation through an orifice under normal pressure conditions and constant gas flow condition (Badam et al., 2007; Bari & Robinson, 2013; Jamialahmadi et al., 2001; A. A. Kulkarni & Joshi, 2005; Y. Zhang, Xiao, & Tan, 2005). For example, Jamialahmadi et al., (2001) investigated the air bubble formation in different types of liquid solutions under constant flow conditions and developed a nonlinear correlation to predict bubble diameter. The authors suggested that the bubble volume is strongly dependent on the orifice diameter, the surface tension and the liquid viscosity. Bari & Robinson, (2013) investigated the quasi-static bubble growth in water for different gas injection rates (i.e., 10 mlph and 100 mlph) using orifices of 0.58, 1.05 and 1.6 mm. In this study, the orifice size was found to have a great effect on the bubble shape, contact pressure force and departure characteristics of the bubble. The formation characteristics of a single bubble under various conditions have also been investigated numerically (Albadawi et al., 2013; Buwa & Ranade, 2002; Chakraborty et al., 2011; Chakraborty et al., 2009b; Di Bari, Lakehal, & Robinson, 2013; Gerlach et al., 2007; Gerlach et al., 2005; Ma et al.,

2012; Ohta et al., 2011). For example, Gerlach et al. (2007) investigated the bubble formation dynamics from submerged orifice diameters (i.e., 2 mm and 3 mm) under constant inflow conditions (i.e., 1 ml/min to 250 ml/min) using combined level set and volume of fluid (CLSVOF) methods. The bubble volume was found to be dependent on the gas flow rate, density, viscosity and surface tension coefficient. Ma et al., (2012) used VOF-CSF model to investigate the effect liquids properties on the bubble formation. They found that a bigger size of bubble was formed by increasing the surface tension coefficient and liquid viscosity. Albadawi et al., (2013) used CLSVOF methods to investigate the growth of the bubble formation and the bubble detachment using four different flow rates (i.e., 50, 100, 150, 200 mlph) through an orifice diameter of 1.6 mm; a higher flow rate forms a bigger bubble due to faster development of air pressure inside the bubble.

In summary, a detailed study of the changes in the bubble contact angle and its formation details at orifice in a glycerine solution is not available. There are some works in which water are tested, which has a different physical property from the glycerine solution, e.g., see refs (Di Bari, Lakehal, & Robinson, 2013; Gerlach et al., 2007; Gerlach et al., 2005). The present study provides much detailed information on the formation of a bubble from orifice (e.g., expansion, elongation and pinch off, bubble equivalent diameter, and bubble detachment time), which is very difficult to be obtained from experimental studies. For example, the initial formation of a bubble from an orifice is dependent on the size of the orifice (i.e., orifice diameters ranging from 0.5 mm to 1.5 mm) for an inlet gas velocity boundary conditions. The effect of the Bond numbers (which represent the variation of surface tension) and the effect of Reynolds numbers (which represent the variation of liquid viscosity) on the bubble formation will be investigated using the VOF model.

## 3.2 Methods

### 3.2.1 Governing equations

#### 3.2.1.1 Equations of mass and momentum

For an incompressible Newtonian fluid, the continuity and the momentum equations are as follows:

$$\nabla \cdot \vec{V} = 0 \quad (3.1)$$

$$\frac{\partial}{\partial t}(\rho \vec{V}) + \nabla \cdot (\rho \vec{V} \vec{V}) = -\nabla P + \nabla \cdot [\mu \{\nabla \cdot \vec{V} + (\nabla \cdot \vec{V})^T\}] + \rho \vec{g} + \vec{F} \quad (3.2)$$

Where  $\vec{V}$ ,  $\rho$ ,  $\mu$ ,  $P$ ,  $t$ ,  $\vec{g} = (0, -g)$  and  $\vec{F}$  is the velocity vector, the density of the fluid, the viscosity of the fluid, the pressure, the time, the gravitational acceleration and the volume force, respectively.

#### 3.2.1.2 Volume fraction equation

In the volume of fluid (VOF) model, the gas-liquid interface boundary is tracked by solving the volume fraction continuity equation, which is as follows:

$$\frac{\partial}{\partial t}(\alpha_z) + \vec{V} \cdot \nabla \alpha_z = 0 \quad (3.3)$$

To solve the above equation in each control volume, the volume fraction of all phases is unity. The volume of each phase is calculated by volume-average values. For example, the  $Z^{\text{th}}$  fluid's volume fraction  $\alpha_z$  is given as:

$$\alpha_z = \frac{\text{Volume of the } Z^{\text{th}} \text{ fluid in unit}}{\text{Volume of the unit}} \quad (3.4)$$

And the conditions of each cell are shown below:

- $\alpha_z = 0$  ; the cell is in gaseous phase (of the  $Z^{\text{th}}$  fluid)
- $\alpha_z = 1$  ; the cell is in liquid phase (of the  $Z^{\text{th}}$  fluid)
- $0 < \alpha_z < 1$ ; the cell is at the interface between the gaseous and liquid phases

The volume fraction equation solves the secondary phase (i.e., gaseous phase) and the calculation is based on the following constraints:

$$\sum_{z=0}^n \alpha_z = 0 \quad \text{and} \quad \sum_{z=0}^n \alpha_z = 1 \quad (3.5)$$

In-general, for  $n$ -phase system, the volume-fraction-averaged density ( $\rho$ ) and viscosity ( $\mu$ ) are calculated using the following equation:

$$\rho = \sum \alpha_z \rho_z \quad \text{and} \quad \mu = \sum \alpha_z \mu_z \quad (3.6)$$

### 3.2.1.3 Continuum surface force (CSF) equation

The dynamic stress balance at the interface of the phases is realized through the CSF model, which is incorporated into the momentum equation by introducing a volume force  $\vec{F}$  as described by Brackbill et al., (1992). This volume force is calculated from the volume fraction data using-

$$\vec{F} = \frac{2\sigma k \nabla \cdot \alpha_l}{(\rho_g + \rho_l)} \quad (3.7)$$

Where  $k$  is the surface curvature of the interface which is defined in terms of the divergence of the unit vector,  $\hat{n}$  and it is calculated by using the following equations:

$$k = (\nabla \cdot \hat{n}) = \frac{1}{|\vec{n}|} \left[ \left( \frac{\vec{n}}{|\vec{n}|} \cdot \nabla \right) |\vec{n}| - (\nabla \cdot \vec{n}) \right]; \text{ Where } \hat{n} = \frac{\vec{n}}{|\vec{n}|} \quad (3.8)$$

In this study, geometric reconstruction scheme that is based on the piece linear interface calculation (PLIC) (Youngs, 1982) is used to trace the gas-liquid interface. For PLIC, it assumes that the interface between two fluids has a linear slop within each cell, and uses this linear shape for calculation of the advection of fluid through the cell faces. The first step in this reconstruction scheme is calculating the position of the linear interface relative to the centre of each partially filled cell, based on information about the volume fraction. The second step is calculating the adverting amount of fluid through each face

using computed linear interface representation and information about normal and tangential velocity distribution on the face. The third step is to calculate the volume fraction in each cell using the balance of fluxes calculated during the previous step (Rider et al. 1998).

### **3.2.2 Boundary conditions**

A two dimensional (2D) domain is used to represent the formation of bubble from an orifice in a bubble column. A full 2D domain has been used in refs (Ma et al., 2012; Liu et al., 2013; Gupta and Kumar, 2008) and such domain is used to investigate asymmetry in bubble shape and formation characteristics in a domain. Equations for a full 2D domain are solved, with  $0 < X < D$  and  $0 < Y < H$ , in which  $D$  &  $H$  is the diameter & height, respectively of the domain. This domain represents 2D cross sectional view of a cylindrical bubble column. An orifice of different diameters is used as a gas inlet and is located at the bottom wall of the column. This inlet is assigned as ‘velocity inlet’ boundary condition (BC). The top wall is assigned as pressure outlet BC. The side walls are assigned as no slip BC. The operating pressure is set to be equal to the ambient pressure, i.e., 101325 Pa and the gravitational force ( $g$ ) of  $9.81 \text{ m/s}^2$  is assigned along the (–ve)  $Y$  direction.

### **3.2.3 Numerical methods**

Ansys-Fluent CFD commercial package (Fluent, 2006), which is based on the finite volume method, is used to solve the governing equations. To minimize the numerical diffusion, the QUICK scheme was applied to solve the momentum equation. The pressure implicit with splitting operators (PISO) algorithm was used for the pressure-velocity coupling, which allows for a rapid convergence rate without a significant loss of the solution stability and accuracy (Akhtar, Pareek, & Tade, 2007). The pressure was

solved using the PRESTO! scheme. The transient model is based on an explicit scheme and a time step of 0.0001 s was used which gives a Courant number of 0.25. Under relaxation factors of 0.3 and 0.7 were set for the pressure and momentum, respectively to assist the convergence. Scaled residual of  $1 \times 10^{-6}$  was set as the convergence criteria for all the governing equations.

### 3.2.4 Simulation cases

A total of 19 simulation cases were carried out for the purpose of bubble formation process from an orifice. A summary of all the simulation cases is given Table 3.1.

#### (i) (Cases 1-3)

First three cases (Cases 1-3) were used to investigate the effect of orifice diameters,  $d_o$  (i.e., 0.5 mm, 1 mm, 1.5 mm) on the bubble formation at a constant gas inlet velocity,  $U_g$  of 0.2 m/s. A 2D rectangular domain with  $H = 100$  mm height and  $D = 50$  mm width as shown in Figure 3.1 is used to study the bubble formation from an orifice.

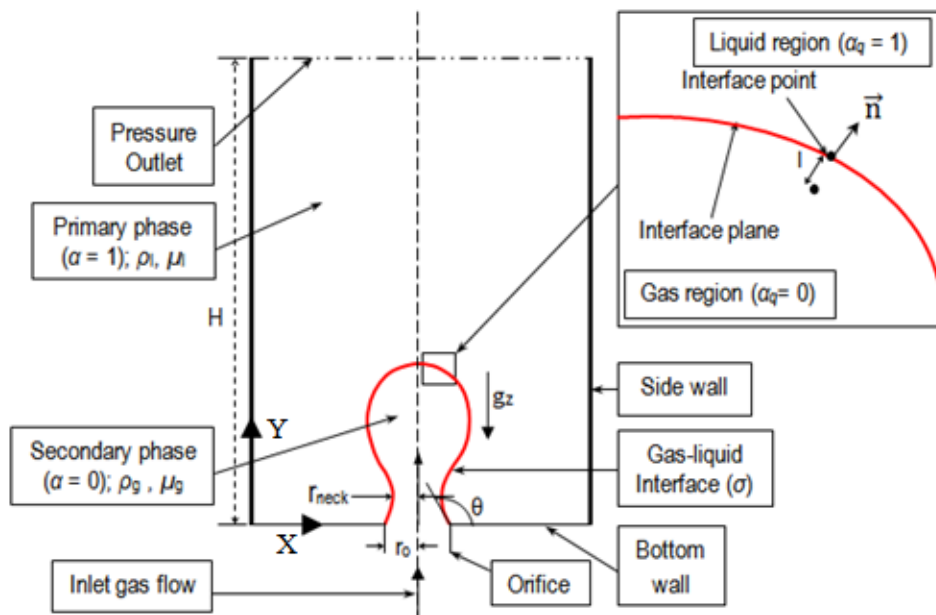


**Figure 3.1:** Computational domain of the simulation.

A constant gas velocity of 0.2 m/s is supplied through orifice diameters of 0.5 mm, 1 mm and 1.5 mm. The varying sizes of orifices are selected based on that which issued in

industrial bubble columns, see refs. (Buwa & Ranade, 2002; Gupta & Roy, 2013; A. Kulkarni, Ekambara, & Joshi, 2007). Air is fed into the glycerine solution through the orifices and the bubble formation process and the bubble shape are investigated numerically. The effect of column wall to the bubble is negligible since the bubble size is very small in comparison to the column diameter.

(ii) (Cases 4-11)

Four cases (Cases 4-7) were used to investigate the effect of Bond number in range of 0.04-0.47, which is varied using the surface tension coefficient and density values, using  $U_g = 0.2$  m/s and  $d_o = 1$  mm. The next four cases (Cases 8-11) is similar to Cases 4-7, but the density of the liquid is reduced to be the same as that of water.

(iii) (Cases 12-19)

Cases 12-15 were used to investigate the effect of Reynolds number in range of 1.35 - 120, which is varied using the liquid viscosity and density values, using  $U_g = 0.2$  m/s and  $d_o = 1$  mm. The last four cases (Cases 16-19) is similar to Cases 12-15, but the density of the liquid is reduced to be the same as that of water. Glycerine solution (82% glycerine and 18% water) is used as the liquid phase and air is used as the gaseous phase. The material property of the liquid density,  $\rho_1 = 1205$  kg/m<sup>3</sup>, viscosity,  $\mu_1 = 0.076$  Pa.s and surface tension,  $\sigma = 0.063$  N/m are taken from Raymond & Rosant, (2000).

**Table 3.1** Simulation cases.

<i>Case</i>	$\rho_1$ (kg/m <sup>3</sup> )	$\mu_1$ (Pa.s)	$\sigma$ (N/m)	$d_o$ (mm)	$Bo_\sigma$	$Re_\mu$	<i>Inlet BC,</i> $U_g$ (m/s)	<i>Purpose</i>
1-3	1205	0.076	0.063	0.5, 1, 1.5.	0.012, 0.047, 0.11.	0.2 - 2.45	0.2	To investigate the effect of orifice diameters on the bubble formation mechanism.
4 - 7	1205	0.076	0.063; 0.019; 0.011; 0.0063	1	0.047, 0.15, 0.26, 0.47	1.6	0.2	To investigate the effect of Bond number on the bubble formation mechanism.

**Table 3.1** continue

8 - 11	1000	0.076	0.063; 0.019; 0.011; 0.0063	1	0.04, 0.128, 0.221, 0.4	1.35	0.2	To reduce the density to be the same as that of water.
12-15	1205	0.076; 0.050; 0.025; 0.001	0.063	1	0.047	1.60; 2.41; 4.82; 120	0.2	To investigate the effect of Reynolds number on the bubble formation mechanism.
16-19	1000	0.076; 0.050; 0.025; 0.001	0.063	1	0.047	1.35; 2.00; 4.00; 100	0.2	To reduce the density to be the same as that of water.

*Noted:*  $U_g$  represented the inlet gas velocity.

### 3.2.5 Limitations

There are some limitations of the present studies such as:

- (i) A 2D domain without axi-symmetric was chosen due to capture a asymmetry bubble formation, rise characteristics and shape of bubble from bottom to the top of the column.
- (ii) The domain has represented 2D cross sectional view of cylindrical bubble column and a careful interpretation is required whenever to use the 2D results to 3D cases.
- (iii) The bubble formation and rise characteristics in stagnant liquid were considered as laminar.
- (iv) The study was also considered without heat and mass transfer between gas and liquid.

### 3.2.6 Mesh dependency study

A uniformed structured grid with cell dimensions of  $0.25 \text{ mm} \times 0.25 \text{ mm}$  is used everywhere in the domain as shown in Figure 3.2a. The effect of mesh sizes on results was investigated using three types of meshes, i.e.,  $0.20 \text{ mm} \times 0.20 \text{ mm}$ ,  $0.25 \text{ mm} \times 0.25 \text{ mm}$  and  $0.30 \text{ mm} \times 0.30 \text{ mm}$ , resulting in a total number of elements of 126252, 80000 and 56112, respectively.

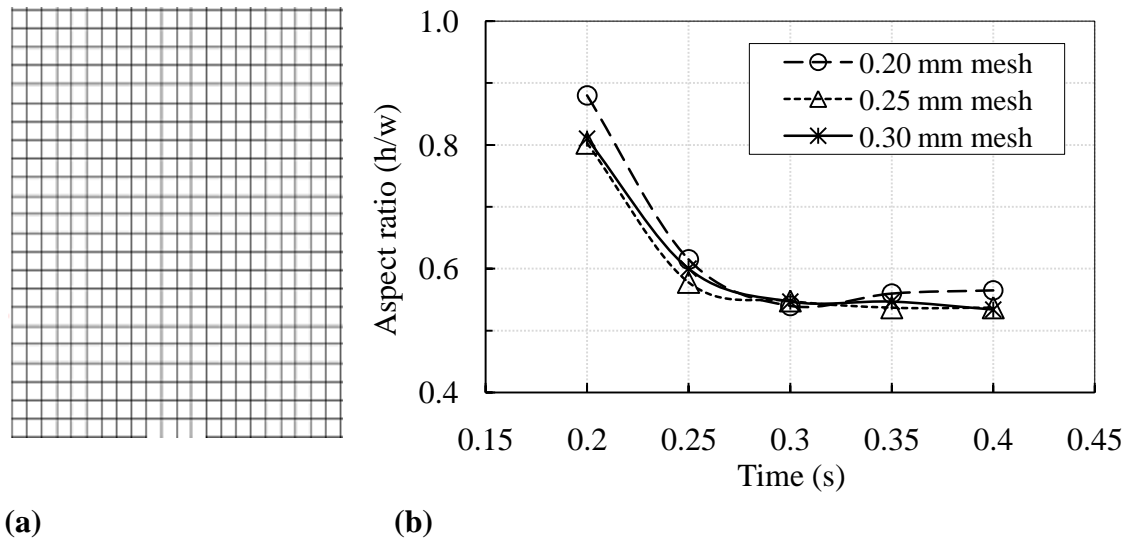


**Figure 3.2:** (a) A uniform structured grid or mesh near the orifice and (b) bubble aspect ratio versus time using different size of meshes.

For this mesh dependency study, the bubble aspect ratio is investigated using 0.2 m/s inlet gas velocity through a 1 mm orifice diameter. The aspect ratio is given as the ratio of the bubble height to width. Figure 3.2b shows the aspect ratio with the increase in the simulation time for the three types of meshes. Note that the results of aspect ratio were taken, when the bubble had detached itself from the orifice. The results obtained using the three types of meshes show a slight difference in that for the 0.25 mm × 0.25 mm mesh, the difference was even smaller. For this reason, the mesh with 0.25 mm × 0.25 mm dimensions was selected for the current study to comprise accuracy and the computation cost. The validation of the present works as follows.

### 3.3 Results and discussion

#### 3.3.1 Validation of CFD model for bubble formation mechanism

The present CFD results have been compared with experimental results of other studies from literature. The bubble formation mechanism is investigated for validation purposes in the liquid medium of the glycerine solution in the column. An orifice diameter of 1 mm and an inlet gas velocity of 0.2 m/s at the orifice are used. The numerically

computed bubble and its shapes near the orifice in the glycerine solution are compared with that from experiments investigations of Davidson & Schüler, (1997). Figures 3.3a and 3.3b show bubble's expansions, elongations and detachment stages at the orifice of our CFD model and the experimental investigation. Note that, the blue colour represents the liquid phase, which is the glycerine solution, and the red colour represents the gas phase, respectively. These comparisons show a good agreement and indicate that the present CFD model is capable in predicting accurate results for the investigation of single bubble formation mechanism, bubble shape and dynamics in a bubble column. In the bubble expansion stage in Figure 3.3a, the bubble expands and grows vertically longer due to the constant incoming gas flow. The bubble is attached to the mouth of the orifice but the bubble shape changes from a circular shape (early stage of expansion) to a slender neck shape (later stage of expansion). In the elongation stage, the neck of the bubble near the orifice grows longer and slender due to the constant inlet gas flow but the neck is still connected to the orifice. In detachment stage, the slender neck pinches off and the bubble detaches from the orifice mouth. It is clear that the CFD model is able to show the mechanism of bubble generation from orifice.

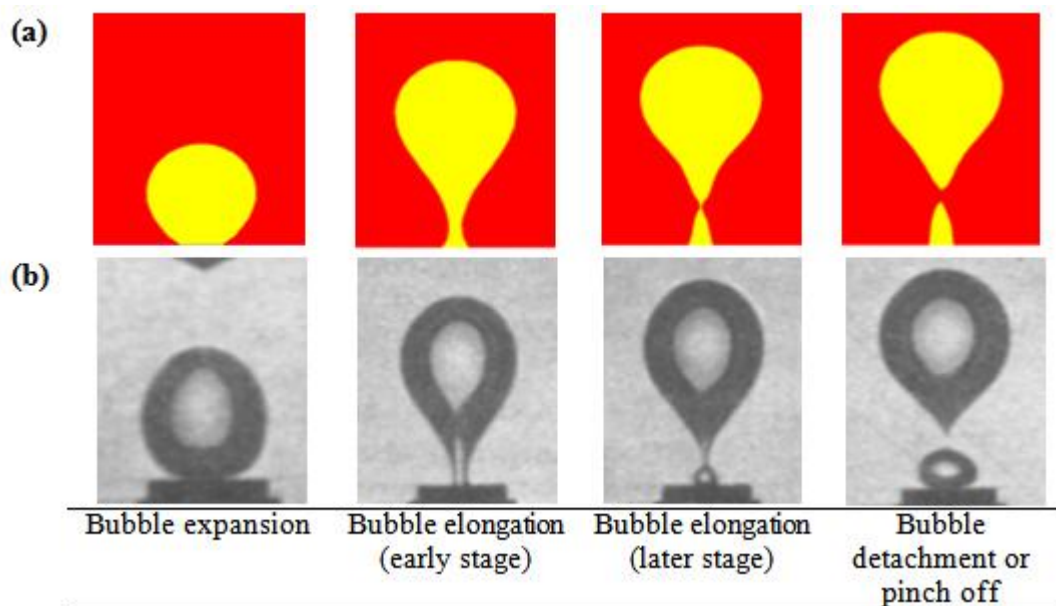


**Figure 3.3:** (a) Numerically computed bubble shapes and (b) experiments bubble shape from Davidson & Schüler (1997) at orifice diameter of 1 mm orifice diameter and  $U_g = 0.2$  m/s.

### 3.3.2 Effect of orifice diameter (Cases 1-3)

#### 3.3.2.1 Development of instantaneous contact angle and pressure

A constant inlet gas velocity of 0.2 m/s is supplied through the orifice diameters of 0.5 mm, 1 mm and 1.5 mm. This was to investigate the effect of the orifice diameter on the bubble formation. The contact angle ( $\theta$ ) is measured between the base of the orifice and the bubble and the history of this value for the three orifice diameters is presented in Figures 3.4 under the constant inlet velocity. Generally,  $\theta$  of the three orifices, at first, decreases rapidly and then increase largely before the bubble pinch-off happens. The decrease is due to the bubble growth where  $\theta$  changes from an obtuse angle to an acute angle due to its contact pressure. During the bubble growing stage, the buoyancy force plays a role in stretching the bubble upward and consequently,  $\theta$  reaches a minimum value of around  $43^\circ$ .  $\theta$  remains unchanged or only undergoes minor changes at this minimum for some period of time until the end of the bubble expansion stage (or when the bubble grows to its largest volume). This is very obvious for the case of the 0.5 mm orifice diameter while it is less significant for the 1.5 mm orifice diameter under the constant velocity boundary conditions. The change of  $\theta$  is quicker for the 1.5 mm orifice diameter than that for the other two orifice diameters.

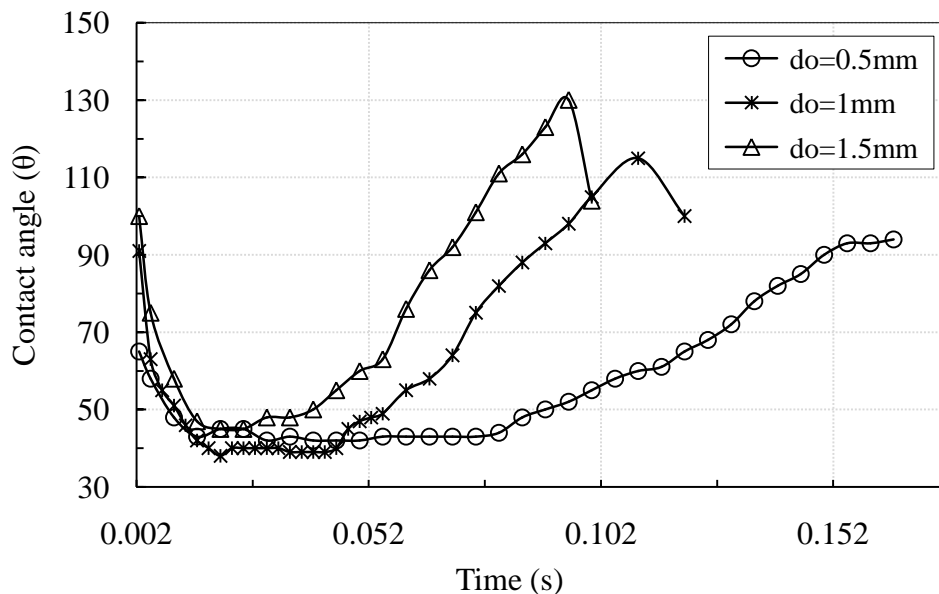


**Figure 3.4:** History of contact angle for different orifice diameters.

The bubble volume as a function of the instantaneous contact angle ( $\theta$ ) for different orifice diameters at the constant inlet gas velocity (or in term of different flow rate conditions) is given in Figure 3.5. The results calculated using empirical correlation of Fritz (1963), which is independent orifice size, for both air-water and air-glycerin are included in the figure for comparison. In addition, experimental data of Gerlach et al. (2005) for orifice flow rates of  $1.67e-7 \text{ m}^3/\text{s}$  and  $1.67e-8 \text{ m}^3/\text{s}$ , which are close to that in our study, for air-water is also included. First compare Fritz (1963) and Gerlach et al. (2005); Gerlach et al. (2005) have shown significant variations in result compared with that of Fritz (1963); The consistent results are limited only for the contact angle above  $90^\circ$  and for the lowest flow rate studied; the difference significantly increases with the increase of flow rates (more results based on different flow rates are given in Gerlach et al. (2007) and are not present herein).

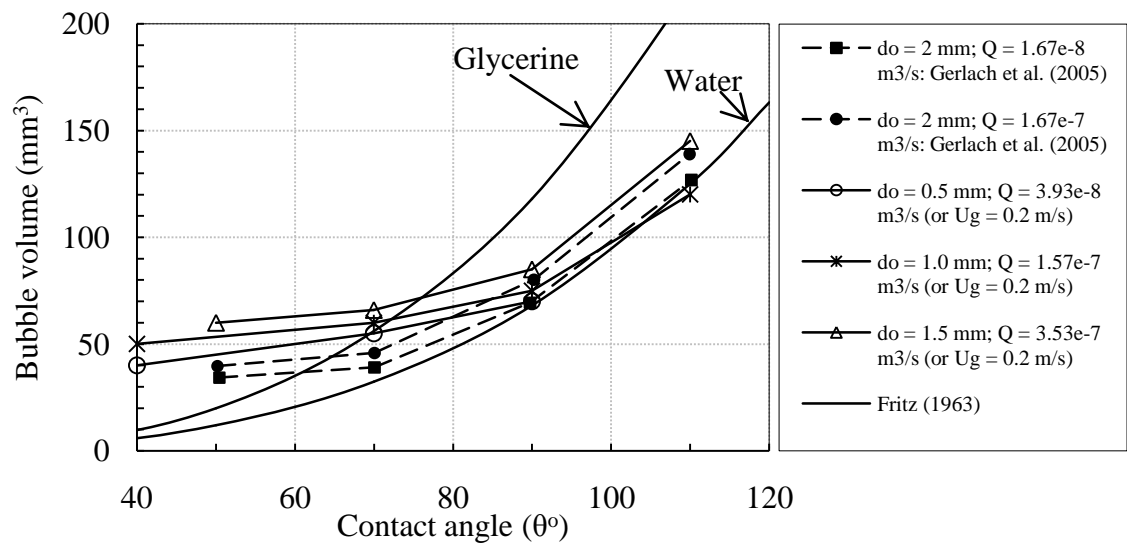


**Figure 3.5:** Bubble volume as a function of instantaneous contact angle.

Comparing Gerlach et al. (2005) and the present study, on average, the results are quite close to each other; some differences are observed and this may have resulted due to the difference fluid property used where Gerlach et al. (2005) is based on air-water and the present study is based on air-glycerin. For example, comparing  $Q = 1.67e-7 \text{ m}^3/\text{s}$  of

Gerlach et al. (2005) and  $1.57 \times 10^{-7} \text{ m}^3/\text{s}$  from our study, the maximum difference is about 32% and 10% for contact angle less and more than  $80^\circ$ , respectively. Lastly, compare Fritz and the present study for air-glycerin; significant difference is seen and this may have resulted from not considering the effect of orifice in Fritz (1963) correlation.

In general, the pressure inside the bubble and the dynamic pressure, which mainly act on the bubble dome surface, are dependent on the bubble volume. The magnitude of the difference in pressure across the curved gaseous–liquid interface is characterized by the Young–Laplace equation, which is given as  $\Delta P = \sigma (1/r_o + 1/r_c)$ ; where  $\Delta P$ ,  $r_o$  and  $r_c$  is the pressure difference around the bubble, the orifice radius and the bubble curvature radius respectively. When the radius bubble curvature is equal to the radius of the orifice, the bubble attains a perfect hemispherical shape (hs) and has the largest dynamics pressure. Figure 3.6 shows the history of the ratio of the dynamic pressure over the maximum dynamic pressure, on the bubble dome surface at the constant inlet gas velocity of 0.2 m/s.

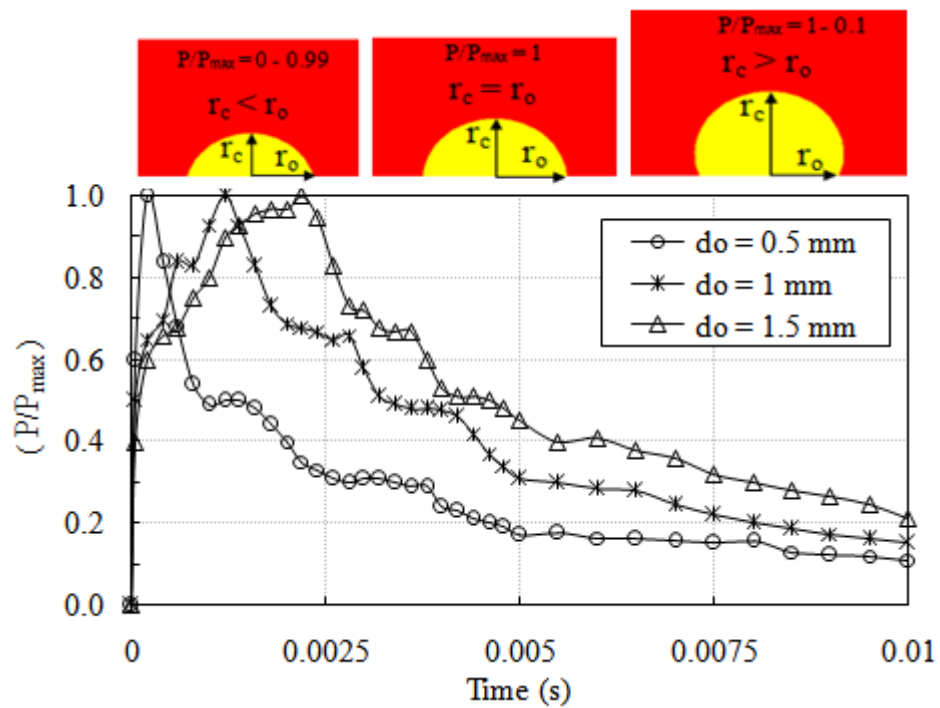


**Figure 3.6:** Differential pressure ( $P/P_{max}$ ) of the bubble before reaching the hemispherical shape

Generally, the value rapidly increases before reducing and the fastest increase is seen for the smallest orifice (i.e., 0.5 mm) and a relatively slower increase is seen for the largest orifice (1.5 mm). After the peak, the value of 1.5 mm orifice remains the highest among the cases despite a sharp reduction. This ratio value can also be used to describe the development of bubble shape and the peak value indicates that a perfect hemispherical shape has been attained. This result shows that, under the same inlet velocity conditions, the bubble develops quicker in a smaller orifice. The history of the pressure inside the bubble, referred to as the static pressure for the three cases of different orifice diameters at the constant inlet gas velocity of 0.2 m/s is shown in Figure 3.7. It can be seen that the pressure drops exponentially for all cases with an asymptotic value of 40Pa for all the cases under the constant inlet velocity; the 1.5 mm orifice is the first case followed by the 1 mm and 0.5 mm orifice diameters.

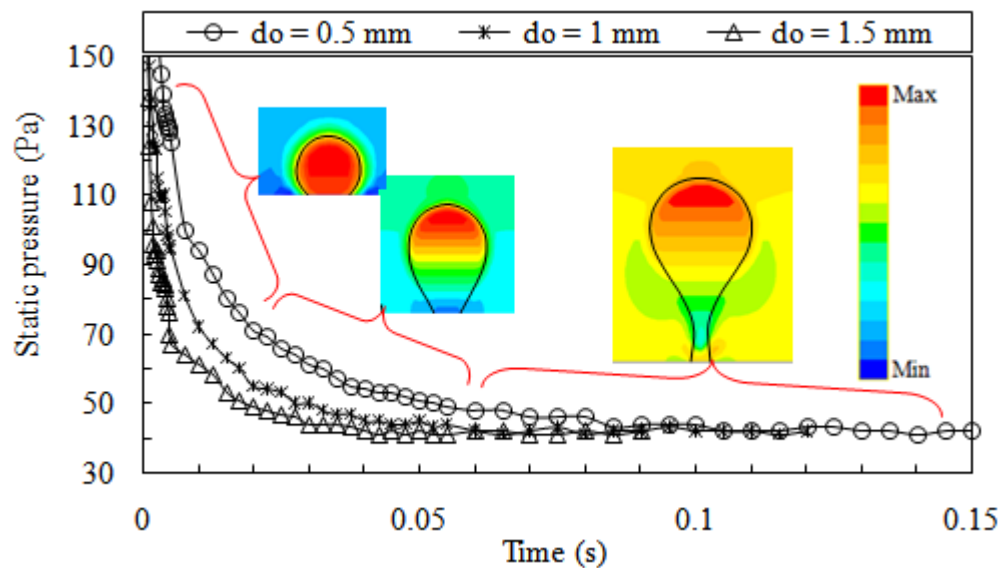


**Figure 3.7:** Static gas pressure of the bubble versus time.

Figure 3.8 shows the relationship between the orifice diameter and the duration needed for the bubble to depart from the orifice for the first bubble (or leading bubble), the second bubble and the third bubble, under the constant inlet gas velocity of 0.2 m/s. Generally, the bubble detachment time decreases under the constant inlet gas velocity

with the increase in the orifice diameter for all the bubbles. The first bubble has the longest detachment time. While the third bubble has a longer detachment time than the second bubble, the formation of the third bubble is affected by the dynamics of the first and second bubbles which changes the pressure and turbulence near the orifice.

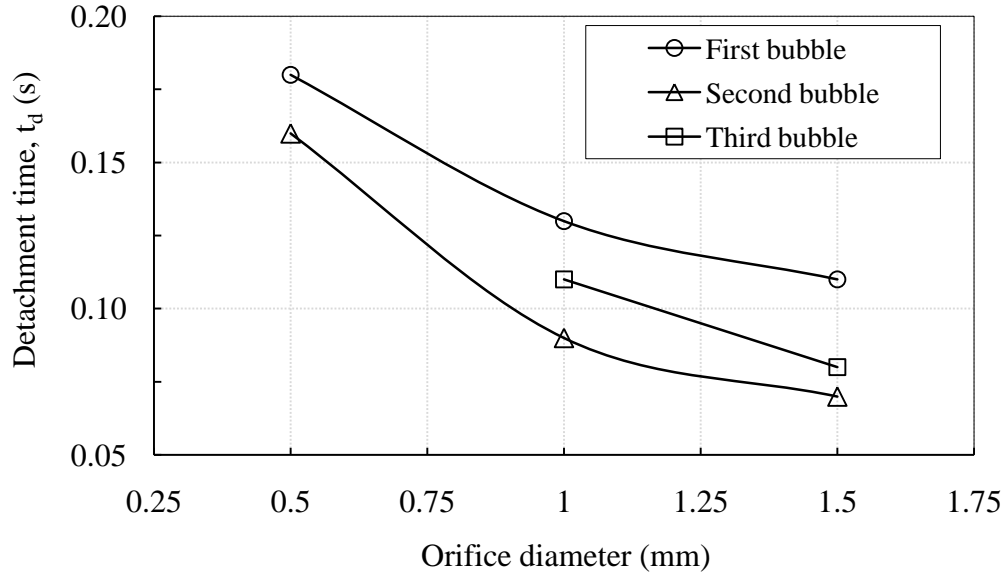


**Figure 3.8:** Effect of orifice diameters on the bubble detachment time.

### 3.3.2.2 Predicted bubble diameter and shape of bubble

An appropriate bubble diameter and bubble volume is important for efficient heat and mass transfers. In this study, bubble departure diameter is calculated via the multiplication of the volume flow rate and the bubble departure time (Badam et al., 2007) which is defined as,  $d_p = (1.5d_o^2 U_g t_d)^{1/3}$ . The calculated result is also compared with the studies by Jamialahmadi et al., (2001), Bhavaraju, Mashelkar, & Blanch, (1978) and Gaddis & Vogelpohl, (1986) correlations that were based on experimental work. For example, Jamialahmadi et al., (2001) developed a correlation of the range in liquid properties;  $\rho_l = (1000 - 1300) \text{ kg/m}^3$ ;  $\mu_l = (0.001 - 0.09) \text{ Pa}\cdot\text{s}$ ;  $\sigma = (0.02 - 0.08) \text{ N/m}$  and  $d_o = (0.5 - 4) \text{ mm}$ . This equation has been derived based on the orifice Bond number (Bo), Froude number (Fr) and Grashof number (Gr) for predicting the bubble departure diameter. The correlation equation is as follows,  $d_p = d_o (5/\text{Bo}^{1.08} + 9.261\text{Fr}^{0.36}/\text{Ga}^{0.39} +$

$2.147Fr^{0.51})^{1/3}$ . Bhavaraju et al., (1978) have also developed the correlation of  $d_p = 3.23 d_o (\rho_l U_g d_o / \mu_l)^{-0.1} \times (U_g^2 \pi^2 / 16 g d_o)^{0.21}$  to locate bubble departure diameters. In a similar vein, Gaddis & Vogelpohl, (1986) investigated the range of liquid properties;  $\rho_l = (1000 - 1320) \text{ kg/m}^3$ ;  $\sigma = (0.06 - 0.08) \text{ N/m}$ ;  $\mu_l = (0.001 - 1) \text{ Pa}\cdot\text{s}$ ;  $d_o = (0.2 - 6) \text{ mm}$  to develop the correlation of  $d_p = [(6d_o\sigma/g\rho_l)^{(4/3)} + (81\mu_l U_g d_o^2/4g\rho_l) + (135U_g^2 d_o^4/64g)^{(4/5)}]^{(1/4)}$  to predict the bubble departure diameter. Figure 3.9 illustrates the bubble departure diameter in relation to the function of orifice diameter. It is found that the bubble departure diameter progressively increases with increasing orifice diameter due to the influence of the contact pressure. The numerical results (circle point) evince a similar trend with the three correlations and relative error as less than 4% under the constant inlet gas velocity of 0.2 m/s. These results again indicate that the present model is capable to predict accurate results.

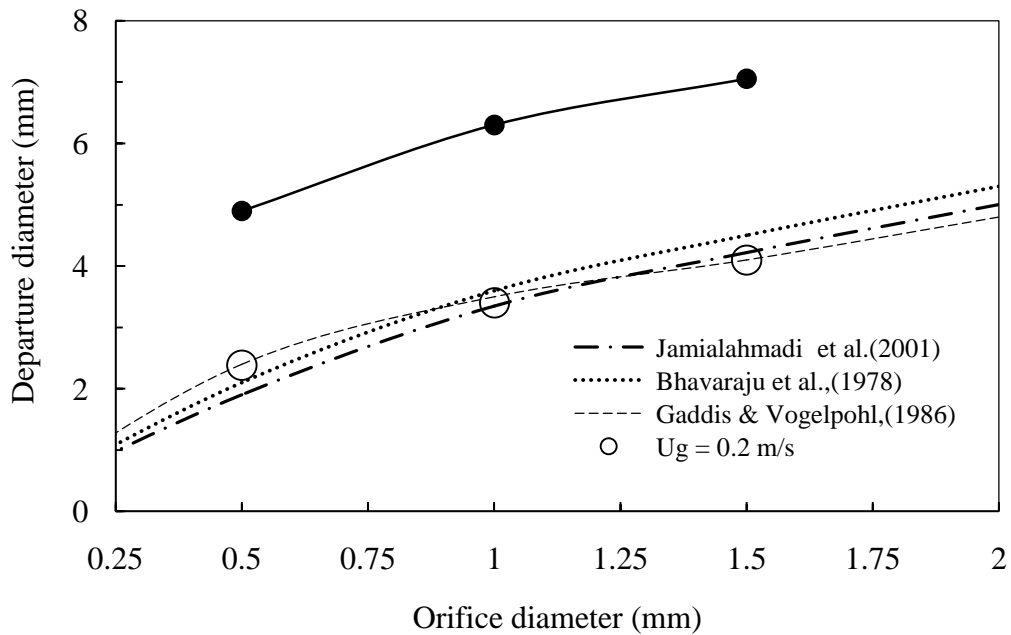


**Figure 3.9:** Bubble departure diameter versus orifice diameter. The results calculated from correlations of Jamialahmadi et al. (2001), Bhavaraju et al. (1978), Gaddis & Vogelpohl (1986) are also included.

In addition, the solid line (see in Figure 3.9) corresponds with the calculation results by the following equation, (Raymond & Rosant, 2000)  $d_e = (d_h/d_w^2)^{1/3}$ , where  $d_h$  and  $d_w$  is the bubble height to the bubble width. The bubble equivalent diameter ( $d_e$ ) is measured

after the bubble pinch off and when close to a spherical shape. It is found that the bubble equivalent diameter values are estimated at 52% higher on average than the bubble departure diameter for both conditions of gas flow. Or, the bubble equivalent diameter (solid line in Figure 3.9) almost parallel to the bubble departure diameter (circle point) and maintained around 2.78 mm additional value with the bubble departure diameter values.

The effect of the orifice diameters in the range of 0.5 mm to 1.5 mm on the bubble formation and flow using a constant inlet gas velocity of 0.2 m/s is investigated after detachment when the bubble freely moved up. Figures 3.10a, 3.10b and 3.10c show the contour images of the air volume fraction using 0.5, 1 and 1.5 mm orifice diameters, referred to as Case-1, Case-2 and Case-3, respectively, from 0.1 s to 0.4 s numerical time. At  $t = 0.1$  s, the leading bubble of these three cases is still connected to the orifice but is in different bubble formation stages. The bubbles of Case-1, Case-2 and Case-3 are at the expansion stage, at elongation stage and the detachment stage, respectively. At  $t = 0.2$  s, the leading bubble for Case-1 has detached itself from the orifice and is rising up with the help of the buoyancy force. The bubble has an imperfect spherical (s) shape (or is in the process of changing into an oblate ellipsoidal (oe) shape) and the second bubble is at the formation stage. At the same time, the leading bubble of Cases-2 and 3 have formed into the oblate ellipsoidal (oe). The second bubble is at the elongation stage for Case-2 but has detached itself from the orifice for Case-3. At  $t = 0.3$  s, the leading bubbles for Cases-1 and 2 retain their oblate ellipsoidal (oe) shapes while rising. The second bubble of Case-B tails the leading bubble. However, the second bubble of Case-3 undergoes a coalescence process with the leading bubble, see  $t = 0.3$ s (Figure 3.10c). It is observed that in Figure 3.10c, a small amount of the liquid is trapped inside the bubble immediately after the bubble's coalescence. The same observation has been reported in the experimental investigation of Takada, Misawa,

Tomiya, & Hosokawa, (2001). The cause is reported as the high inertia of the liquid. Therefore, the liquid is not able to come out completely from the coalesced bubble within a short time (Takada et al., 2001).

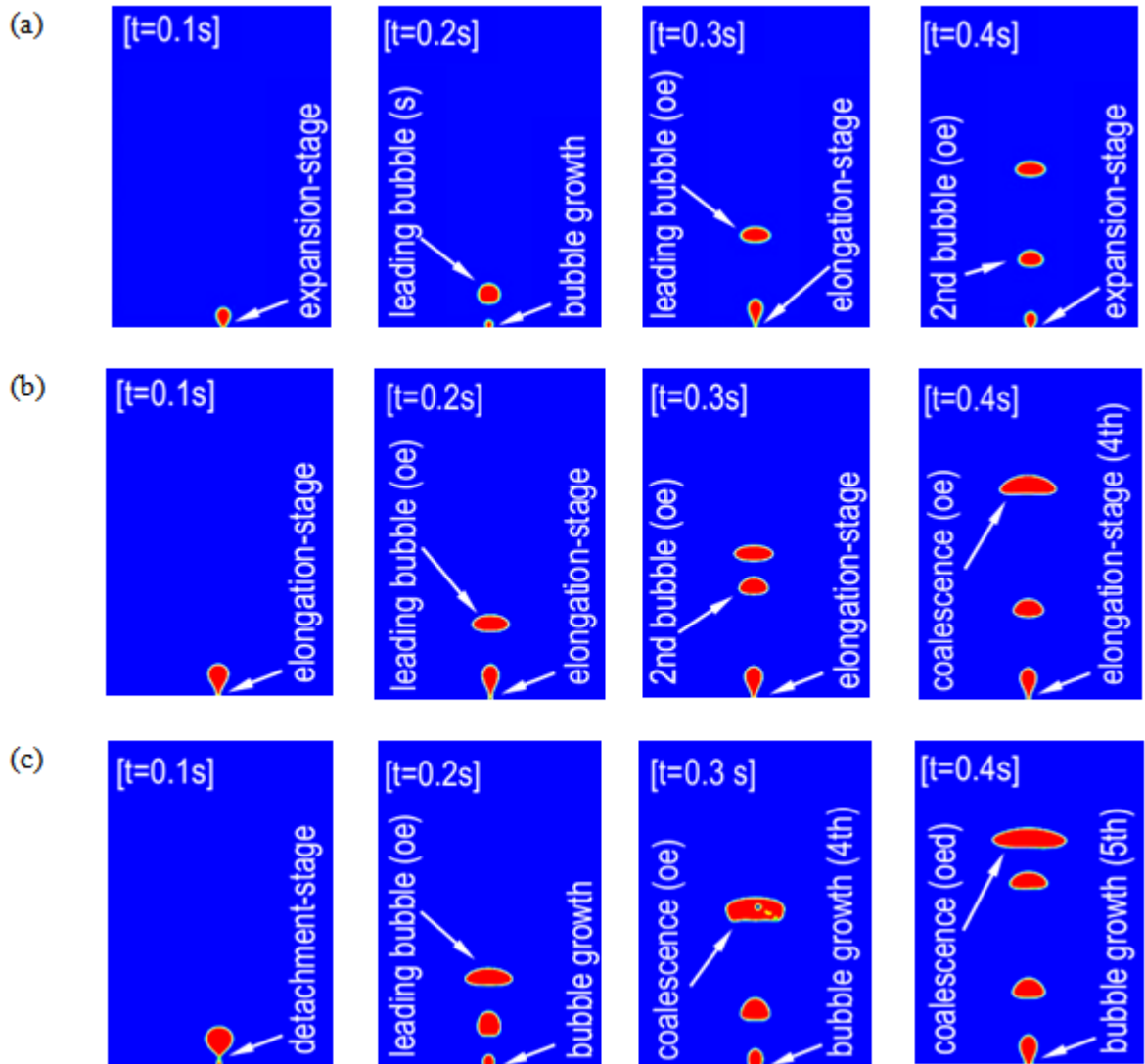


**Figure 3.10:** Effect of orifice size on bubble formation and shape at inlet gas velocity of 0.2 m/s (a)  $d_o = 0.5$  mm (b)  $d_o = 1$  mm (c)  $d_o = 1.5$  mm; (oe, oblate ellipsoidal; oec, oblate ellipsoidal cap; oed, oblate ellipsoidal disk; s, spherical). Note that the shape definition is taken from Grace (1973).

At  $t = 0.4$  s, the shapes of the leading bubble are not the same for the three cases. It is in a symmetrical oblate ellipsoidal (oe) shape at a horizontal plane (Figure 3.10a) for Case-1; an asymmetrical oblate ellipsoidal (oe) shape at the horizontal plane (Figure 3.10b) for Case-2; and an oblate ellipsoidal disk (oed) shape (Figure 3.10c) for Case-3, respectively. These ‘oe’ for Case-2 and ‘oed’ for Case-3 are formed due to the rest of

wake after the bubble coalescences. At same time, the third bubble for Case-1 is at expansion stage; while the fourth and fifth bubbles are at elongation stage for Cases-2 and 3 respectively, as observed. Note that the definition for the bubble shapes is based on the shape regime map for isolated bubbles in liquids, taken from Grace, (1973).

Figure 3.11 shows the bubble rising distance of the leading bubble and the second bubble based on time for Case-1 to Case-3. A big orifice diameter causes a higher instantaneous bubble rise velocity which can be observed from the rise distance of the bubble. This also means that the bubble rise distance at a particular time is different whereby it is the highest for the 1.5 mm orifice (Case-3) and the lowest for the 0.5 mm orifice (Case-1). In addition, the difference in the leading bubble rise distance varies around 0 to 13% between Case-3 (do = 1.5 mm) and Case-2 (do = 1 mm) and around 0 to 32% between Case-2 (do = 1 mm) and Case-1 (do = 0.5 mm). These variations can occur due to the significant changes of buoyancy from the effect of the orifice diameters.

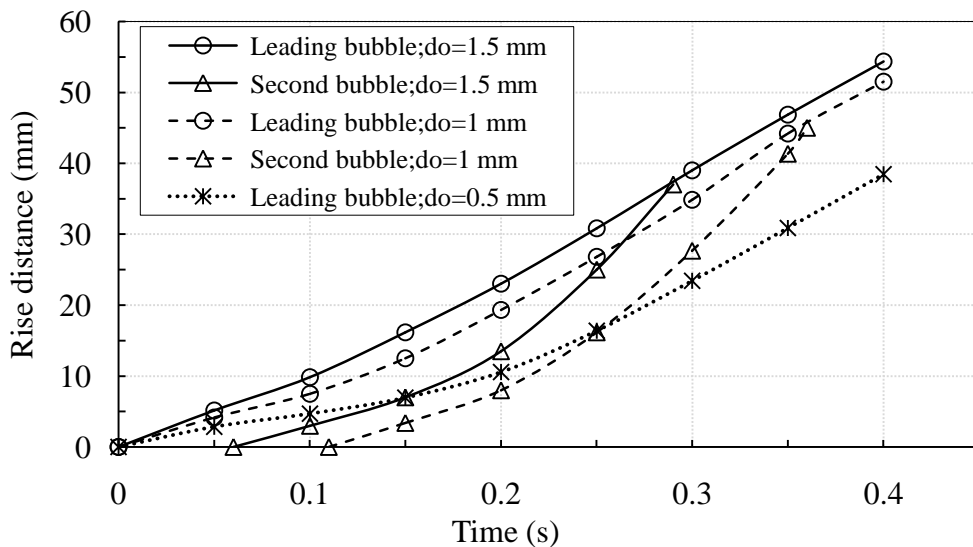


**Figure 3.11:** Bubbles rise distance at a constant inlet gas velocity of 0.2 m/s for different orifices. Note that the arrow indicates the bubble coalescence positions.

On the other side, the effect of the orifice diameters on the bubble coalescences is also represented by Figure 3.11. Note that, the arrow sign indicates the bubble coalescence at time that corresponds to the bubble position. It can be observed that the second bubble

for Case-3 ( $d_o = 1.5$  mm) and Case-2 ( $d_o = 1$  mm) are kept at around 52% and 58% relative distance with the leading bubble from the initial time (0 s) of 0.20 s respectively. Subsequently, these relative distances are decreased or the second bubbles rise fast because of the wake effect of the leading bubble and collide with the leading bubble at the time of 0.28 s and 0.36 s for Case-3 ( $d_o = 1.5$  mm) and Case-2 ( $d_o = 1$  mm), while the corresponding rise distance value is 38 mm and 45 mm, respectively. Case-1 ( $d_o = 0.5$  mm) does not evince bubble coalescences. Therefore, the big orifice diameter accelerates the faster bubble coalescence and can be used to manipulate bubble coalescences.

### 3.3.2.3 Effect of Bond number (Cases 4 - 11)

The bubble volume (i.e., calculated based on bubble equivalent diameter) and the orifice Bond number from our simulation is compared with that calculated using correlations from literature (Bari & Robinson, 2013; Jamialahmadi et al., 2001). Bari & Robinson (2013) modified Di Marco, Forgione, & Grassi, (2005) power law equation of  $V_{pr} = [0.6963 V_T (d_o/L_c)^{-0.116}]$  and proposed a new dimensionless equation in terms of the orifice Bond number to predict the dimensionless bubble volume. The dimensionless equation can be written as,  $V^* = [3.78/Bo_o (r')^{0.116}]$ , where the dimensionless radius ( $r'$ ) and orifice Bond number ( $Bo_o$ ) is calculated from the equation of  $r' = [g r_o (\rho_l - \rho_g)^{0.5}] / \sigma^{0.5}$  and  $Bo_o = g (\rho_l - \rho_g) r_o^2 / \sigma$  respectively. Likewise, the correlation of Jamialahmadi et al. (2001) can be written in a dimensionless form based on the orifice Bond number ( $Bo$ ), Froude number ( $Fr$ ) and Grashof number ( $Gr$ ) are assumed as negligible for a quasi-static bubble formation. Thus, the dimensionless bubble volume can be rewritten as,  $V^* = 4.69 Bo_o^{-1.08}$ . The authors reported that the correlation developed has a mean average error of 3.2%. The calculated values from these correlations ( $V^*$ ) and our simulation results ( $V^* = V_{dep}/r_o^3$ ) as a function of orifice Bond number are shown in

Figure 3.12. In general, our data, which is based on air-glycerine system, is closely predicted with the corrections results and the maximum difference is less than 20% for under the constant inlet gas velocity (0.2 m/s) BC. In addition, data on the bubble volume versus  $Bo_o$  from experimental studies of Bari & Robinson (2013), Lesage & Marois (2013) for an air-water system is also included in Figure 3.12 for the orifice Bond ( $Bo_o$ ) number ranging from 0.005 - 0.086. The bubble volume from orifices is about the same under the constant inlet air flow rate BC. However, it is not the case for the constant inlet gas velocity (0.2 m/s) BC and the maximum difference of less than 17% on average is obtained. The differences are occurred due to two different liquids in column (one is glycerin solution and the other is pure water).

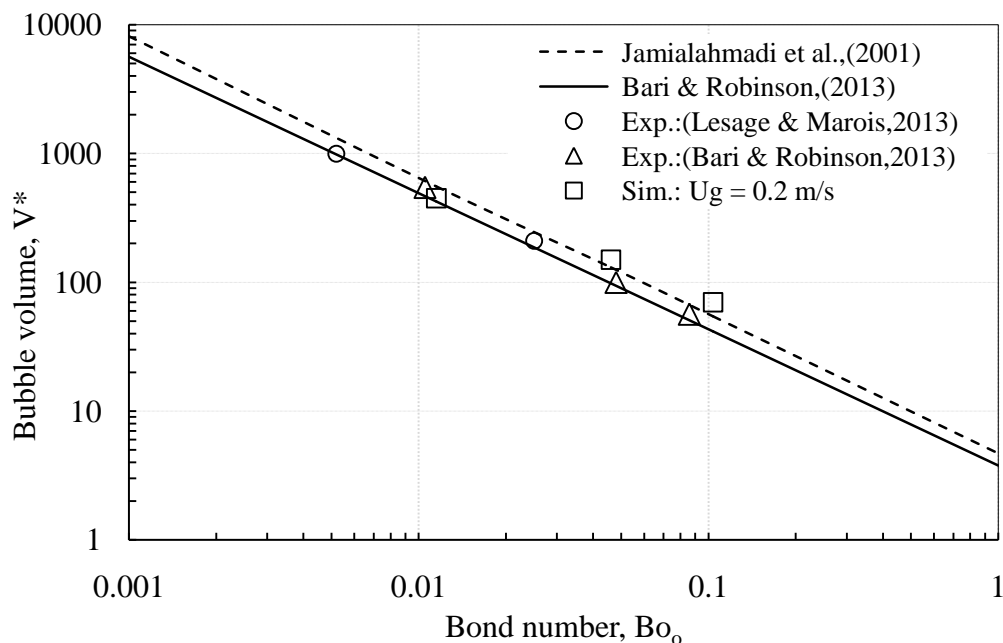


**Figure 3.12:** Dimensionless bubble volume versus the orifice Bond number. Available data for air-water are also included from Bari & Robinson (2013) and Lesage & Marois (2013).

The effect of Bond number,  $Bo_o$ , on the bubble formation dynamics and the bubble shape through an orifice is investigated using Cases 4 to 7.  $Bo_o$  in the range of 0.047 to 0.47 is tested, which is varied using the surface tension coefficient value, see Table 3.1. Orifice diameter,  $d_o = 1$  mm and the constant inlet velocity,  $U_g = 0.2$  m/s is used. Figure

3.13 shows the history of the bubble formation dynamics for Cases 4-7. Note that the period of the bubble formation of these cases are not the same to each other; Case 4 is plotted from  $t = 0.06\text{s} - 0.125\text{s}$ , Case 5 from  $t = 0.045\text{s} - 0.09\text{s}$ , Case 6 from  $t = 0.045\text{s} - 0.085\text{s}$  and Case 7 from  $t = 0.055\text{s} - 0.095\text{s}$ .

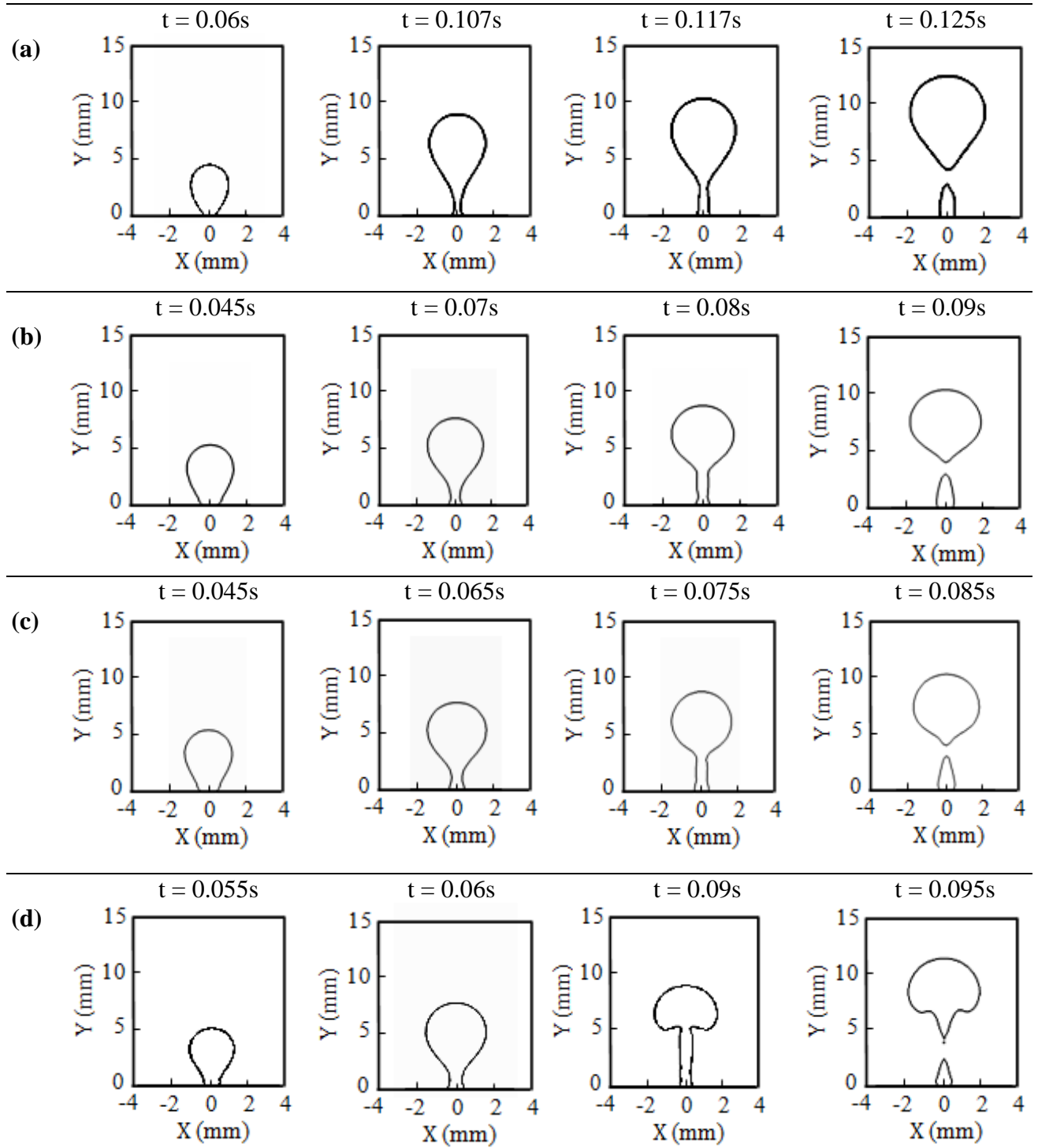


**Figure 3.13:** Bubble shape with dimensionless time for constant  $\rho_r$  and  $\mu_r$  of 1000 and  $\text{Re}_\mu = 1.6$ ; (a)  $\text{Bo}_\sigma = 0.047$  (Case-4); (b)  $\text{Bo}_\sigma = 0.15$  (Case-5); (c)  $\text{Bo}_\sigma = 0.26$  (Case-6) and (d)  $\text{Bo}_\sigma = 0.47$  (Case-7).

The first column in Figure 3.13 shows the growth of the bubble due to the buoyancy force. When the upper portion of the bubble becomes large enough, the bubble gradually becomes more elongated. The buoyancy force tends to lift the upper portion of the bubble whilst the bubble foot remains fixed to the orifice, and as result forming a neck near the bubble base, which is observed in the second column in Figure 3.13 (from left). Further on, when the bubble grows due to the inlet gas velocity, a liquid circulation or vortex (i.e., clock wise form right side and anti-clock wise from left side) around the bubble neck pushes continuously. As a result, the bubble neck is elongated and becomes a slender shape, observed in the third column from left in Figure 3.13. The velocity field around the bubble neck is shown in Figure 3.14. For low  $Bo_\sigma$  number (see in Figure 3.14a), less elongation of bubble neck is observed due to a stronger push of liquid jet near the bubble pinch-off region; Bubble neck tends to increase progressively for a higher  $Bo_\sigma$  number due to a weaker push of liquid jet near the bubble pinch-off region (see in Figure 3.14b-d). For low  $Bo_\sigma$  number, less elongation of bubble neck is observed, which tend increases progressively for high  $Bo_\sigma$  number. For example, the slender bubble neck readings in height for Cases-4 to 7 are 2.5 mm, 2.65 mm, 2.85 mm and 4.8 mm, respectively. In addition, there are distinct differences in changes in the shapes between the results obtained in Figures 3.13a to 3.13d (Case-4 to 7). A high  $Bo_\sigma$  number (low surface tension value), resulting in a significant change in shape is observed from Cases-4 to 7 in Figure 3.13 (third and forth column from left). For example, a mushroom like shape is observed for the high  $Bo_\sigma$  number (Case-7); a closely spherical like shape and a balloon like shape are seen for reduced  $Bo_\sigma$  number of Cases-7 to 4 (increased surface tension value). The mushroom like shape has developed due to a significantly increased liquid drag on the bubble dome.

Consequently, a high  $Bo_\sigma$  numbers (which indicate lower surface tensions), the bubble pinch off time is earlier than the bubbles with the low  $Bo_\sigma$  number (which

indicates higher surface tensions) due to the development of stronger liquid vortex around the bubble's slender neck. But the  $Bo_\sigma$  of 0.47 (or Case-7) takes more time for bubble pinch off due to a very low resistance to stop the bubble slender neck rupture near the orifice, resulting in further elongation of the bubble neck with progressed in time (see Figure 3.13d at  $t = 0.09s$ ).

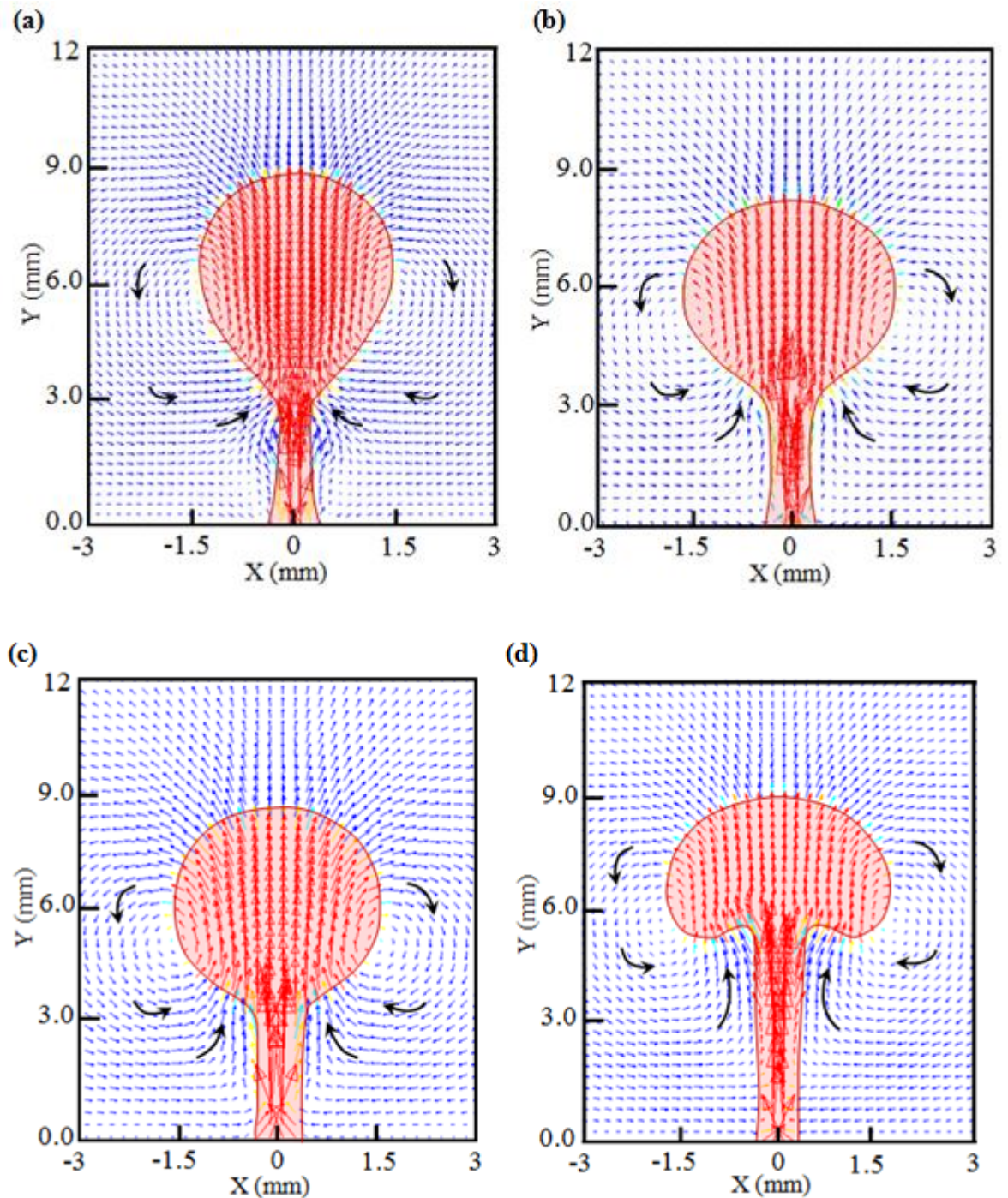


**Figure 3.14:** Velocity field around the bubble neck for constant  $\rho_r$  and  $\mu_r$  of 1000 and  $Re_b = 1.60$ ; (a)  $Bo_\sigma = 0.047$ ;  $t = 0.117s$  (Case-4); (b)  $Bo_\sigma = 0.15$ ;  $t = 0.08s$  (Case-5); (c)  $Bo_\sigma = 0.26$ ;  $t = 0.075s$  (Case-6) and (d)  $Bo_\sigma = 0.47$ ;  $t = 0.09s$  (Case-7).

On the other hand, the surface tension force is always trying to maintain a shape with a minimum surface energy; as a result harder stretching has developed over the bubble surface for the  $Bo_\sigma$  of 0.47 (or Case-7). These effects cause a late pinch off for lower  $Bo_\sigma$  number of the bubble.

Figure 3.15 compares the pinch-off time versus  $Bo_\sigma$  number for Cases 4-7 and Cases 8-11. Note that, the density of the liquid in Cases 8-11 is reduced to be the same as that of water. This results in a reduction of the bubble Bond number ( $Bo_\sigma$ ) and Reynolds number ( $Re_\mu$ ) about 16% of that of Cases 4-7. The bubble pinch off for Cases 4-7 are delayed (by 9%) when compared to that of Cases 8-11 suggesting water assist the bubble formation from an orifice.

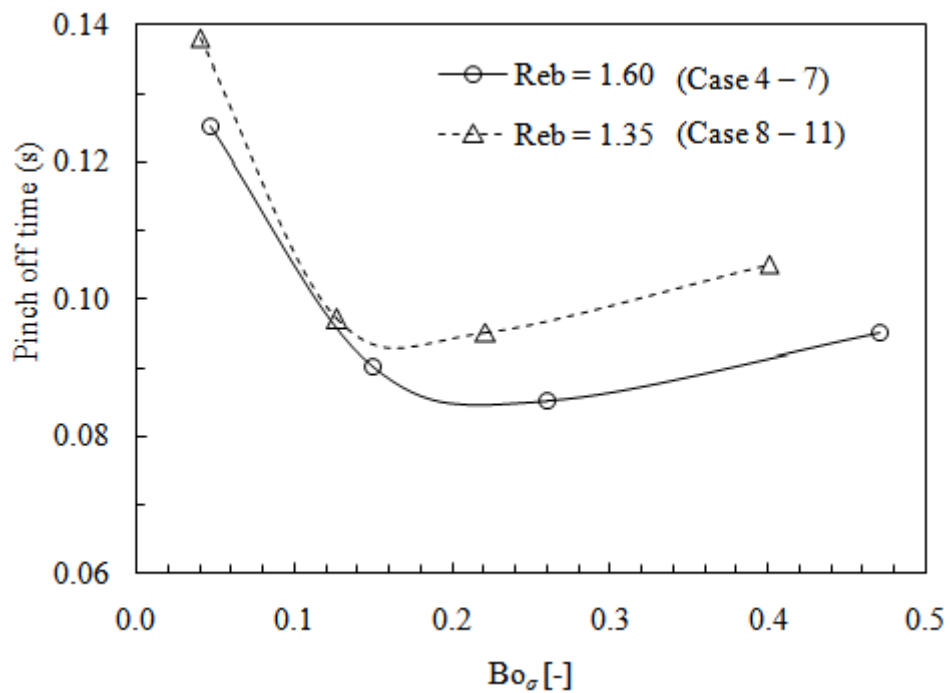


**Figure 3.15:** Bubble pinch-off time as a function of Bond number.

### 3.3.2.4 Effect of Reynolds number (Case 12-19)

The effect of Reynolds number,  $Re_\mu$  on the bubble formation dynamics through an orifice was investigated using Cases 12 to 15.  $Re_\mu$  in the range of 1.60 to 120 was tested, which was varied using the liquid viscosity, see Table 3.1. Orifice diameter,  $d_o =$

1 mm and the inlet gas velocity,  $U_g = 0.2$  m/s was used. Figure 3.16a-d shows that the velocity field near the bubble neck before pinch off for Cases 12-15, respectively.

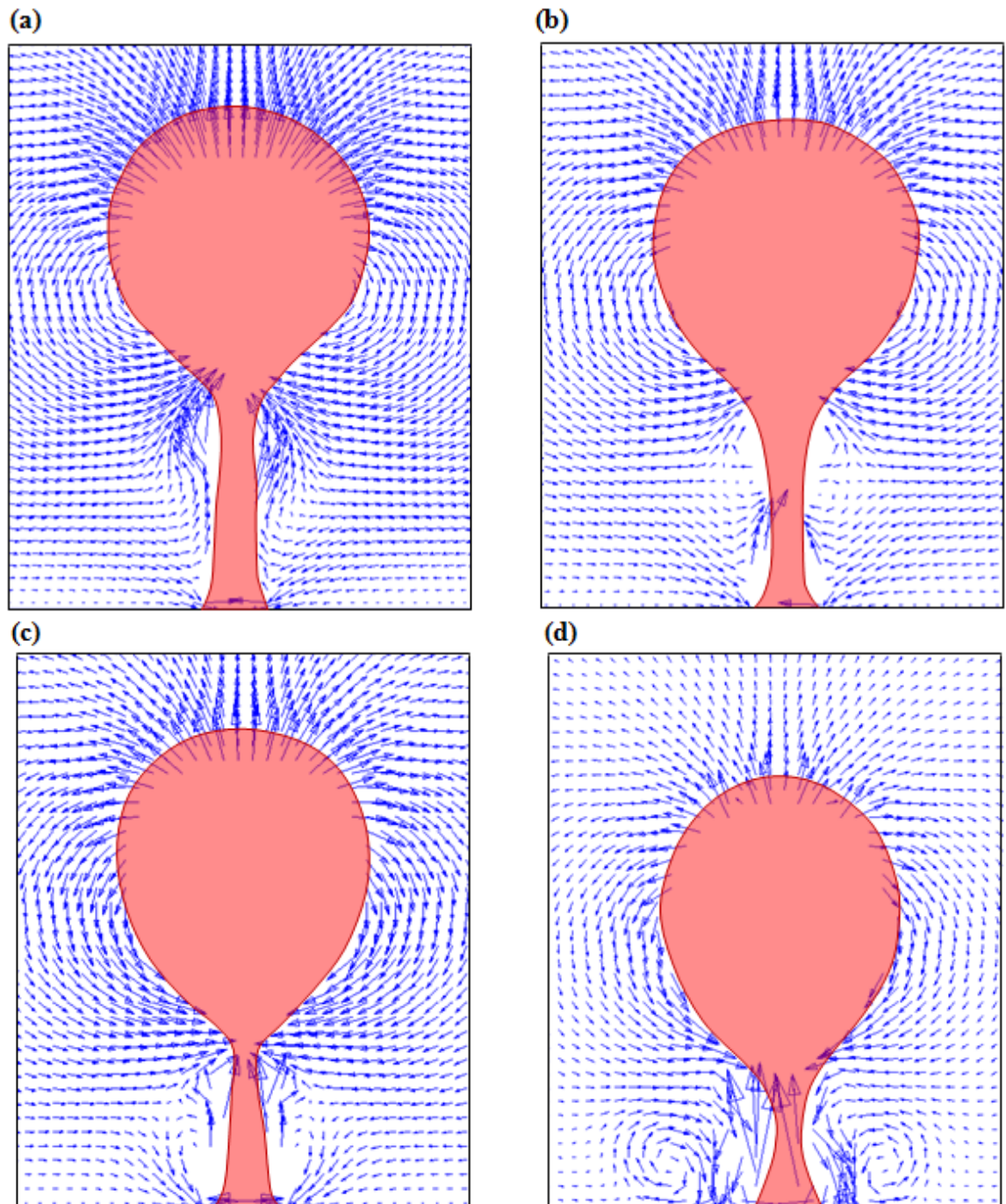


**Figure 3.16:** Velocity field around the bubble neck at  $Bo_\sigma = 0.187$ ; (a)  $Re_\mu = 1.60$ ,  $t = 0.19$ s (Case-12); (b)  $Re_\mu = 2.41$ ,  $t = 0.175$ s (Case-13); (c)  $Re_\mu = 4.82$ ,  $t = 0.162$ s (Case-14); (d)  $Re_\mu = 120$ ,  $t = 0.14$ s (Case-15).

Generally, the buoyancy is one key force for growth of bubble. When the upper portion of the bubble becomes large enough; the bubble gradually turns into more elongated.

The buoyancy force tends to lift the upper portion of the bubble while the bubble foot remains fixed to the orifice, as result forming a neck near the bubble base. Further on, when the bubble grows due to the inlet gas velocity, a liquid circulation around the bubble neck pushes continuously. As a result, the bubble neck is elongated and becomes a slender shape, which is observed in the Cases 12-15 (see in Figure 3.16a-d, respectively). For low  $Re_\mu$  number (see in Figure 3.16a), larger elongation of bubble neck is observed due to stronger push of liquid jet. The push of liquid jet acts on neck region with a longer period, as resulting it develops a low pressure region. This tends to decrease progressively for higher  $Re_\mu$  number due to weak push of liquid jet that allows forming a strong liquid vortex ring near the neck region (see in Figure 3.16b-d). Additionally, in a low  $Re_\mu$  numbers (which indicates high liquid viscosity); the bubble pinch off time is lately than the bubbles with the high  $Re_\mu$  number (which indicates low liquid viscosity) due to the development of weak liquid vortex around the bubble's slender neck. But the high  $Re_\mu$  of 120 (or Case-15) takes less time for bubble pinch off due to stronger vortex ring, which developed near the orifice, resulting in earlier bubble pinch off with less neck elongation of the bubble neck (see Figure 3.16d at  $t = 0.14s$ ). Figure 3.17 compares the pinch-off time versus  $Re_\mu$  number for Cases 12-15 and Cases 16-19.

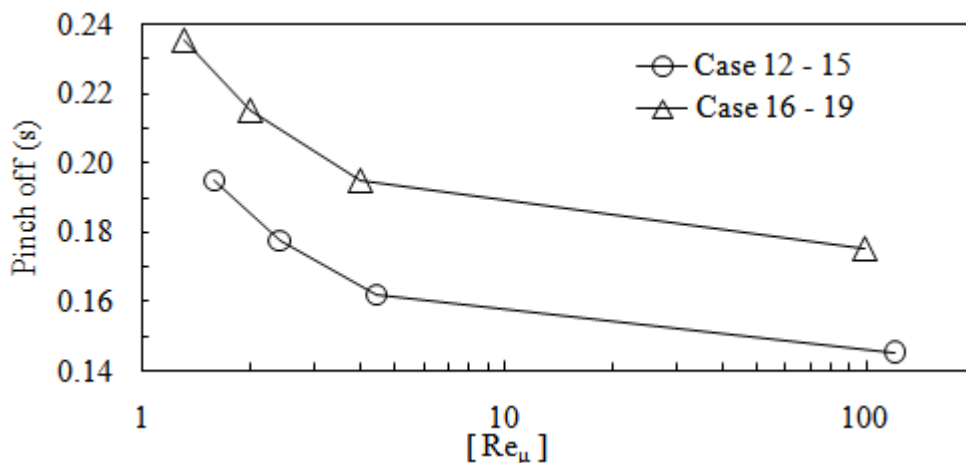


**Figure 3.17:** Bubble pinch-off time as a function of Reynolds number.

Note that, the density of the liquid in Cases 16-19 was reduced as the same as that of water. This results represent the reduction of the bubble Reynolds number ( $Re_\mu$ ) and Bond number ( $Bo_\sigma$ ) about 17% of that of Cases 12-15. The bubble pinch off for Cases 12-15 are delayed (by 20%) when compared to that of Cases 16-19. Figure 3.18a-b shows the bubble neck elongation as a function of Reynolds number and bubble width, respectively.

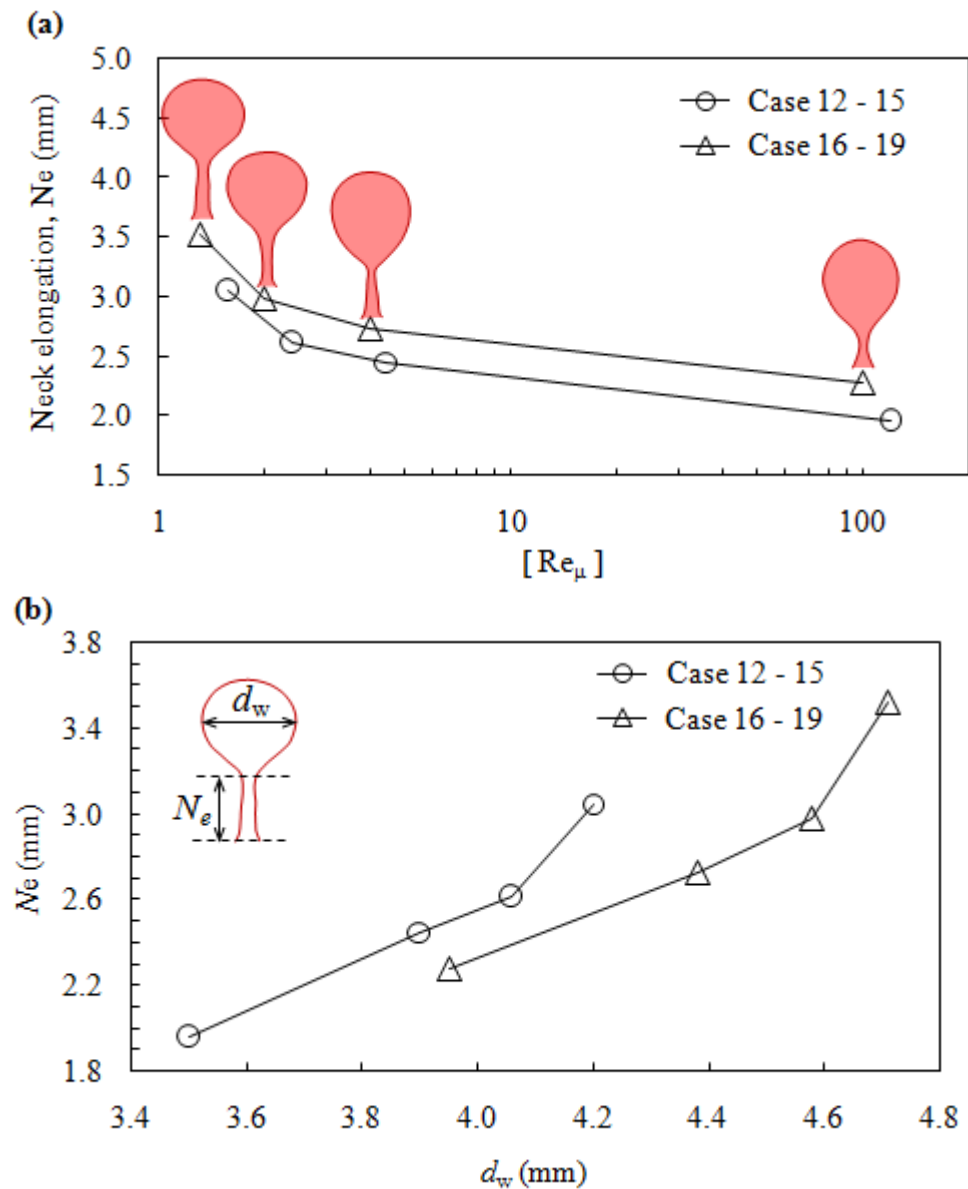


**Figure 3.18:** Bubble neck elongation,  $N_e$  as a function of Reynolds number (a); bubble width,  $d_w$  (b).

It is observed that the bubble neck elongation decreases with the increase of Reynolds number; as well as increases the bubble width for increased Reynolds number of Cases

12-15 and Case 16-19. As compares between the Cases 12-15 and Cases 16-19 in Figure 3.18a, it is found that the bubble elongation height decreases by roughly 15% but the bubble width increases around 13%, when compared to that of Cases 16-19 as can be seen in Figure 3.18b. Thus, the reduction of the bubble Reynolds number ( $Re_\mu$ ) and Bond number ( $Bo_\sigma$ ) about 17% suggest that water assist the bubble formation from an orifice.

### 3.4 Conclusion

In this study, the VOF-CSF method has been used to investigate the effects of orifice sizes ranging from 0.5 mm to 1.5 mm, the effects of Bond numbers ranging from 0.04 to 0.47 and the effects of Reynolds numbers ranging from 1.60 to 120 on bubble formation. The conclusions of this study are-

- The current study has demonstrated the capacity and accuracy of the CFD method to predict bubble velocity, bubble shape and bubble departure diameter for all the cases simulated. This study provides much detailed information on the formation of the bubble from the orifice which is difficult to be obtained from experimental studies.
- The use of a larger orifice diameter (1.5 mm) accelerates the decreasing of the bubble contact angle from an obtuse angle ( $100^\circ$  to  $42^\circ$ ) to an acute angle ( $45^\circ$  to  $130^\circ$ ).
- A larger orifice diameter (1.5 mm) forms a bigger bubble and the bubble requires a shorter time (0.11 s) to detach from the orifice.
- A leading bubble requires a longer time to detach itself from an orifice in comparison to the following bubble (second), and interestingly the third bubble detaches itself much faster than the second bubble.

- An increase in Bond numbers ( $Bo_\sigma$ ) from 0.047 to 0.16 speeds up the bubble pinch-off. However, a further increase in  $Bo_\sigma$  (e.g., 0.17~ 0.47) slows down the bubble pinch-off.
- An increase in Reynolds number ( $Re_\mu$ ) from 1.60 to 120 speeds up the bubble pinch-off.

## **CHAPTER 4**

### **STUDY OF FREE BUBBLE RISE CHARACTERISTICS IN DIFFERENT COLUMN ANGLES USING CFD**

This chapter describes the study of free bubble rise characteristics in stagnant fluids. The work carried out in this chapter provides detailed information of a single bubble rising characteristics (i.e., instantaneous velocity, bubble shape changes, bubble trajectory etc) in different column angle (i.e., trapezoidal column).

#### **4.1 Introduction**

Gas–liquid bubble column reactors are commonly used in chemical and petrochemical processes of many areas of engineering and technologies (Yang et al., 2011; Yang et al., 2007). The generation and rise of the gas bubbles in the reactor stirs up the liquid and intensifies the inter-phase disturbance and the inter-phase contact enhancing the mass and heat transfer. Therefore, various studies have been carried out over a number of years to enhance the further understanding on the characteristics of a free bubble rising in a quiescent liquid through many experimental and numerical investigations e.g., the bubble rise velocities, the bubble shape variation and operating conditions etc., (Coutanceau and Thizon, 1981; Rabha and Buwa, 2010a; Ma et al., 2012; Ajaev and Homsy, 2006; Smolianski et al., 2008; Nilmani et al., 1981; Tomiyama et al., 2002; Gupta and Kumar, 2008). In line with that, the current work investigates the rising characteristics of a free bubble in non-uniform columns. For example, Coutanceau and Thizon, (1981) have investigated the wall effects on single bubble behaviour in highly viscous liquids using both theoretical and experimental methods in which bubble is set to rise along the axis of a vertical circular tube filled with a highly viscous liquid. The terminal speed of a spherical bubble is found to be affected by the wall effect. Krishna

et al., (1999) have experimentally investigated the rise velocities of single bubbles in the size range of 3~80 mm in cylindrical columns filled with water of diameters ranging from 10 mm to 630 mm. The authors has shown the significant effect of the wall on single bubbles rising in smaller diameter columns and suggested a modification to Mendelson (1967) equation to describe the bubble rising velocity inclusive of the wall effect. Mukundakrishnan et al. (2007) have carried out numerical investigation of the axi-symmetric rise and deformation of an initially spherical gas bubble released from rest in a liquid-filled, finite circular cylinder and have shown the significant effect of column wall to the bubble rise velocities and shapes.

Notwithstanding of various experimental and numerical investigations of the rising bubble dynamics in bubble columns at stated above, but there are still many fundamental aspects that requires further investigation. Therefore, the purpose of the present work is to investigate the effect of trapezoidal column to the rise velocity of a single bubble in a quiescent liquid using the CLSVOF numerical methods. The bubble rising behaviour, the spatial distribution, the shape deformation, characteristics of the bubble with wall effects due to the different types of trapezoidal cavity with inclination angles will be investigated.

## 4.2 Methods

### 4.2.1 Governing equations

#### 4.2.1.1 Equations of mass and momentum

For an incompressible Newtonian fluid, the continuity and the momentum equations are as follows:

$$\nabla \cdot \vec{V} = 0 \quad (4.1)$$

$$\frac{\partial}{\partial t} (\rho \vec{V}) + \nabla \cdot (\rho \vec{V} \vec{V}) = -\nabla P + \nabla \cdot [\mu \{ \nabla \cdot \vec{V} + (\nabla \cdot \vec{V})^T \}] + \rho \vec{g} + \vec{F} \quad (4.2)$$

Where  $\vec{V}$ ,  $\rho$ ,  $\mu$ ,  $P$ ,  $t$  and  $g = (0, -g)$  is the velocity vector, the density of the fluid, the viscosity of the fluid, the pressure, the time and the gravitational acceleration, respectively.

#### 4.2.1.2 Level-set function for calculating of gas-liquid interface

In level set (LS) method, a smooth function  $\varphi$  is used to define as the gas-liquid interface position. The function  $\varphi = (\vec{r}, t)$  at a point with position vector,  $\vec{r}$  and time,  $t$  assumes as the following:

$$\varphi(\vec{r}, t) = \begin{cases} +d & \text{in liquid region} \\ 0 & \text{at interface} \\ -d & \text{in gas region} \end{cases} \quad (4.3)$$

Where  $d = d(\vec{r})$  is the shortest distance of the interface from point  $\vec{r}$ . From such a representation of the interface, the unit normal vector  $\vec{n}$  and the mean curvature  $k$  are simply calculated as:

$$\vec{n} = \frac{\nabla\varphi}{|\nabla\varphi|} \Big|_{\varphi=0} \quad \text{and} \quad k = -\nabla \cdot \frac{\nabla\varphi}{|\nabla\varphi|} \quad (4.4)$$

#### 4.2.1.3 Modified momentum equation

The LS function is incorporated in the momentum equation (Eq. 4.2). Therefore the modified momentum equation can be written as:

$$\rho(\varphi) \left( \frac{\partial \vec{V}}{\partial t} + \nabla \cdot (\vec{V}\vec{V}) \right) = -\nabla P + \nabla \cdot \left[ \mu(\varphi) \left\{ \nabla \vec{V} + (\nabla \vec{V})^T \right\} \right] + \rho(\varphi) \vec{g} + \sigma k(\varphi) \nabla H(\varphi) \quad (4.5)$$

To capture the gas-liquid interface motion, the standard advection for the LS function and the volume fraction  $F$  is solved by following equations:

$$\frac{\partial \varphi}{\partial t} + \nabla \cdot (\vec{V}\varphi) = 0 \quad (4.6)$$

$$\frac{\partial F}{\partial t} + \nabla \cdot (\vec{V}F) = 0 \quad (4.7)$$

Volume fraction ( $F$ ) defines as the fraction of the liquid inside a control volume or cell, in which  $F$  takes a value of 0 for pure gas cell; 1 for pure liquid cell and between 0 and 1 for an interface of gas and liquid in the cell. The density and viscosity are calculated from the LS function using:

$$\rho(\varphi) = \rho_l H(\varphi) + \rho_g [1 - H(\varphi)] \quad (4.8)$$

$$\mu(\varphi) = \mu_l H(\varphi) + \mu_g [1 - H(\varphi)] \quad (4.9)$$

Where  $\rho_l$ , and  $\rho_g$ , are the density of liquid and gas;  $\mu_l$  and  $\mu_g$  are the viscosity of liquid and gas respectively.

$$H(\varphi) = \begin{cases} 1 & ; \quad \text{if } \varphi > \varepsilon \\ 0.5[1 + \frac{\varphi}{\varepsilon} - \frac{\sin(\frac{\pi\varphi}{\varepsilon})}{\pi}] & ; \quad \text{if } |\varphi| \leq 0 \\ 0 & ; \quad \text{if } \varphi < -\varepsilon \end{cases} \quad (4.10)$$

Where,  $H(\varphi)$  and  $\varepsilon$  define as the function of Heaviside and numerical thickness of the interface, respectively.

#### 4.2.2 Boundary conditions

A two dimensional (2D) domain is used to represent the flow of a single air bubble in a quiescent water column. A full 2D domain have been used in refs (Ma et al., 2012; Liu et al., 2013; Gupta and Kumar, 2008) and such domain is used to investigate asymmetry in bubble shape and rise characteristics from bottom to the top of the domain. Equations for a full 2D domain are solved, with  $0 < x < D$  and  $0 < z < H$ , in which  $D$  &  $H$  is the diameter & height, respectively of the domain. This domain represents 2D cross sectional view of a cylindrical bubble column. The side and bottom walls of the domain are assigned as ‘no slip’ boundary condition and the top wall as ‘pressure outlet’

boundary condition. The operating pressure is set to be equal to the ambient pressure, i.e., 101325 Pa and the gravitational force ( $g$ ) of  $9.81 \text{ m/s}^2$  are assigned along negative (-ve) Y direction. The numerical methods are similar as discussed in earlier in section 3.4.

#### 4.2.3 Simulation cases

Two dimensional (2D) domain is used to represent the flow of a single air bubble in a quiescent water column. There are four types of cases that were studied. A rectangular domain with the above dimensions is referred to as Case 1 (vertical angle of  $0^\circ$ ) as shown in Figure 4.1a. For Cases 2, 3 and 4, the width of the top wall is reduced to form a trapezoid domain and the side wall has an inclination angle of  $3^\circ$ ,  $6^\circ$  and  $9^\circ$ , respectively (Figure 4.1a). Furthermore, the simulation results of  $1^\circ$  to  $3^\circ$ ;  $4^\circ$  to  $6^\circ$  and  $7^\circ$  to  $9^\circ$  are negligible difference. Therefore, an inclination angle of  $3^\circ$ ,  $6^\circ$  and  $9^\circ$  are selected for the present study to minimize the computation time.

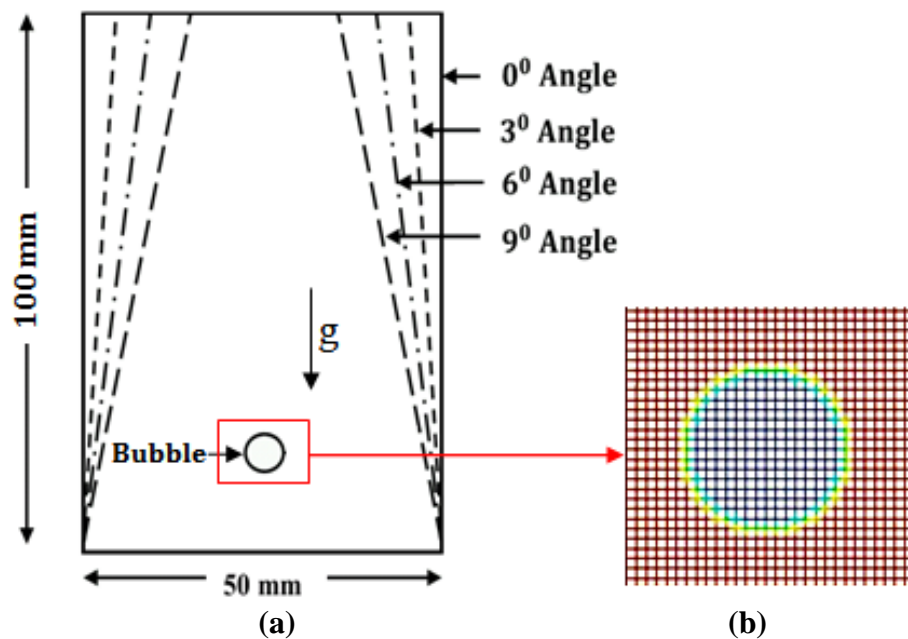


**Figure 4.1:** (a) Computational domain of Column angle  $0^\circ$ ,  $3^\circ$ ,  $6^\circ$  and  $9^\circ$ ; (b) Zoom view on mesh around the bubble.

At the initial stage of a simulation, an air bubble with a diameter of 4 mm is imposed at the centre and 10 mm height from the bottom of the domain. The bubble in a quiescent

liquid will rise under the action of the buoyancy force and the bubble rising velocity and characteristics will be numerically investigated. Based on the initial condition, the Morton number (Mo), the Eötvös number (Eo) and Reynolds number (Re) of the cases in the present study is  $2.5 \times 10^{-11}$ , 2.15, 876, respectively.

#### **4.2.4 Limitations**

The limitations of the present work are similar as that described in section 3.2.5 (Chapter 3).

#### **4.2.5 Mesh dependency study**

Structured mesh has used in this study in which the number and size of cell division of domain walls remain unchanged for all the cases. This also means that the total mesh element is the same for all the cases. This will result in a slightly denser mesh at the top for  $9^\circ$  inclination domain. Each cell has a trapezoidal shape for inclination domains. The effect of the mesh size on results was investigated for Case 1 ( $0^\circ$  channel angle) using three types of meshes. A structured mesh around the bubble as shown in Figure 4.1b is used. The dimensions of each cell in these meshes are 0.25 mm, namely Mesh-1, 0.30 mm (Mesh-2), 0.35 mm (Mesh-3), giving a total element number of 80000, 55778 and 40898, respectively. Relatively, Mesh-1 is a most dense mesh and Mesh-3 is a coarser mesh. For mesh dependency analysis, the bubble rising distance with the increase of time in second is plotted in Figure 4.2 for the different meshes. The results predicted from Mesh-1 and Mesh-2 is almost the same to each other. However, the results predicted from Mesh-3 are slightly different from that of other meshes especially beyond 0.2s. Therefore, Mesh-2, which is less dense than Mesh-3, has been selected to be used for the present study since it provides an accurate result and requires lower computational power.

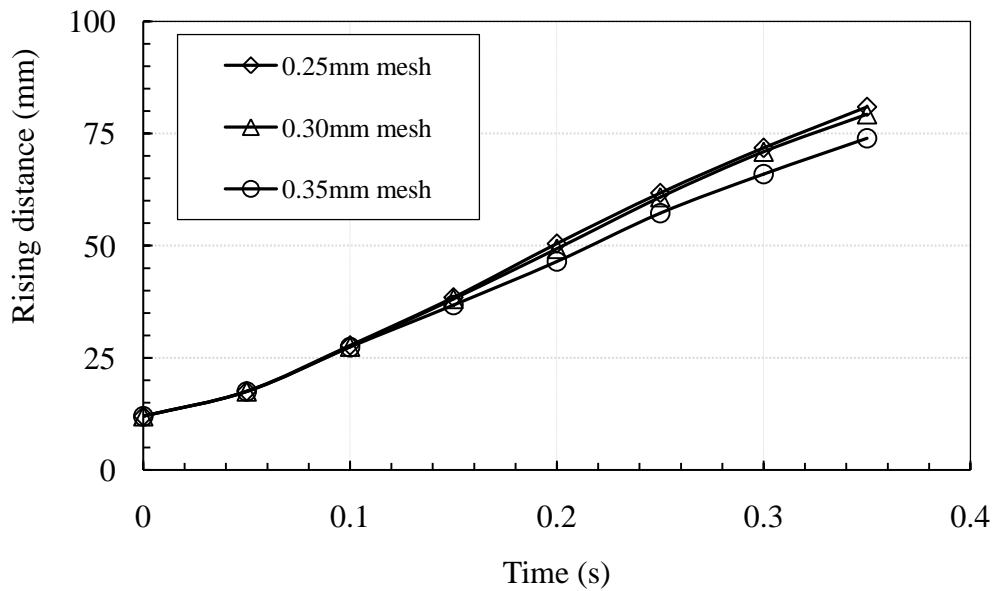


**Figure 4.2:** Mesh dependency test for different types of mesh based on Case 1 ( $0^\circ$  column angle) for the bubble rising distance versus time.

### 4.3 Results and Discussion

#### 4.3.1 Validation of CFD model for single bubble

Results from our CFD models are compared against that from numerical investigations of Ma et al. (2012) and that calculated using Fan-Tsuchiya (Y. Li, Zhang, & Fan, 2000) empirical correlations. In addition, the calculated bubble rise velocity using the empirical correlation by Krishna et al. (1999) which is a modified version of Mendelson, (1967) formulation to include column wall effect is also used for comparison. Figure 4.3a shows the instantaneous rising velocity of a bubble as a function of time in second for Cases 1 to 4 and such results from Ma et al. (2012) are also included. The results of Case 1 ( $0^\circ$  angle) and Ma et al. (2012) are quite consistent to each other with small differences of less than 6%. In general, the velocity of Case 1 at the beginning up to 0.1s increases steeply from 0 to 0.2 m/s. Following that, it becomes relatively uniform with an average value near 0.22 m/s. However, beyond 0.25s, the velocity slightly reduces to 0.18 m/s at 0.35s, which is near the top of the rectangular cavity. The bubble rise velocity calculated using Fan-Tsuchiya et al. (2000) and Krishna et al. (1999) correlations at 0.1MPa for a bubble diameter of 4 mm is 0.197 m/s and

0.2345 m/s and this result is quite close with that of Case 1, which is about 0.21 m/s on average. Therefore, these comparisons provide a good benchmark for the CFD models in the current study.

#### **4.3.2 Effect of channel angles**

Referring to Figure 4.3a, let us first compare Case 1 with Cases 2, 3 and 4 until 0.35s. Figure 4.3b shows the velocity difference in percentage between Case 1 and Cases 2-4, respectively. Up to 0.12s, the velocity distribution of Case 1 is very similar to that of other cases with a difference less than 6%, see Figure 4.3b. Referring from 0.12s until 0.35s, the velocity of Cases 2-4 reduces with the increase of time and this trend is quite different from that of Case 1. From Figure 4.3b, the reduction increases in the order of Case 2, Case 3 and Case 4 or in the order of 3°, 6°, 9° channel angles, where the velocity difference between Case 1 and Case 2 increases consistently until 38%. The velocity and the reduction trend for Cases 3(6°) and 4 (9°) beyond 0.12 is quite similar. From 0.3s to 0.35s, the velocity slightly increases. The velocity difference between Case1 and Case3 (or Case4) increases up to 70 % and then decreases to 40% (or 56% for Case 4) (Figure 4.3b). Now compare Cases 2, 3 and 4 beyond 0.35s. The velocity of the cases starts to fluctuate with an average velocity of 0.1m/s. Figure 4.3c shows the bubble rising velocity profile versus  $d_b/D_t$ , which is the ratio of the initial bubble diameter ( $d_b$ ) to the column diameter ( $D_t$ ) at various vertical heights for Cases 1 to 4. For Case 1, the ratio of  $d_b/D_t$  is constant and this is obvious because it is a rectangular domain whereas  $d_b/D_t$  for other cases increases with the increase vertical height since it is trapezoidal domain. In general, for Cases 2 to 4, the velocity profile is the same as that seen in Figure 4.3a where the velocity increase steeply before decreases and fluctuates with the increase of  $d_b/D_t$ . However, the same peak velocity occurs at the different value of  $d_b/D_t$  for different cases being a lower value for Case 2 and a higher

value for Case 4. Crudely, the velocity profile of Case 4 appears to be a stretch version of that of Case 3 and the same can be said between Case 3 and Case 2.

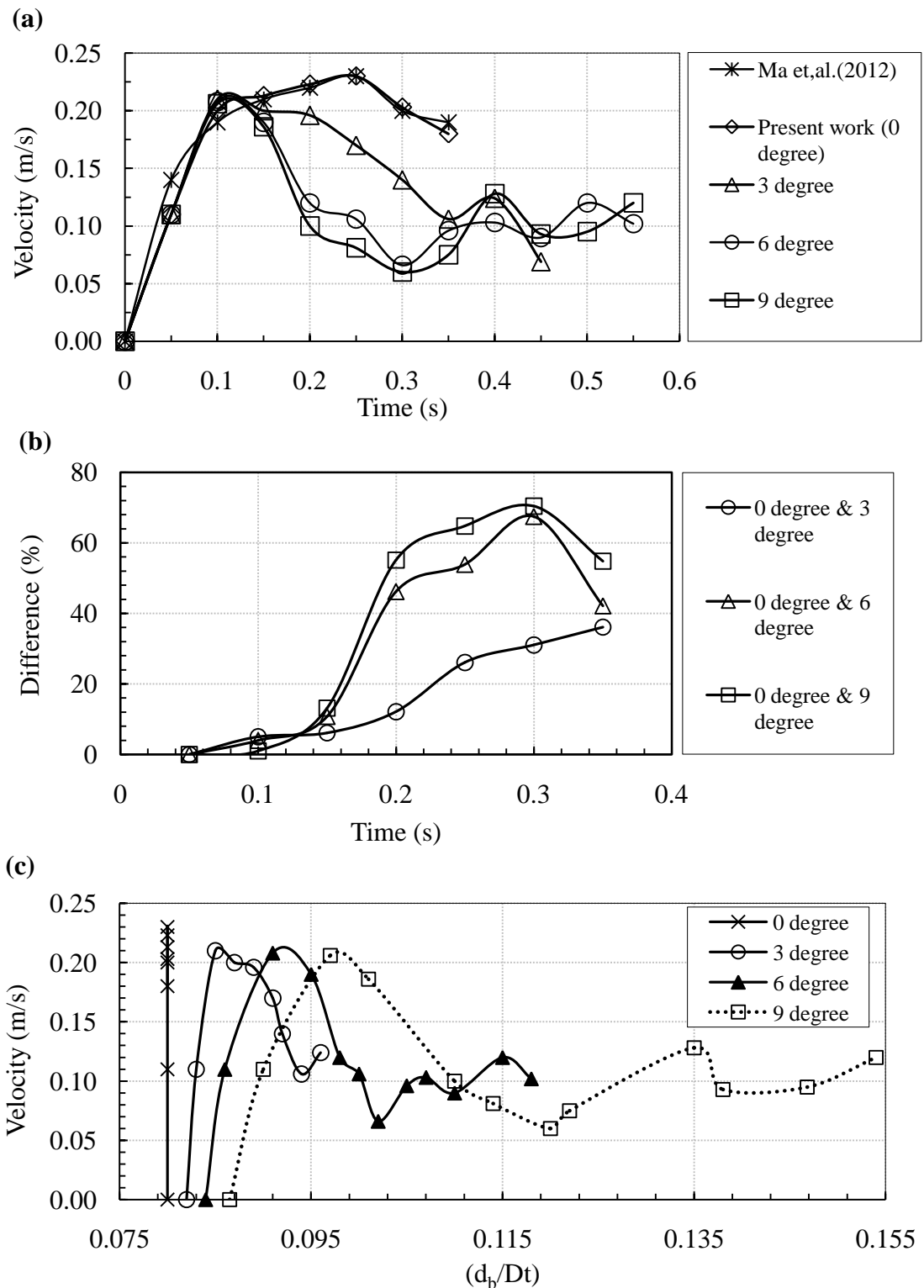
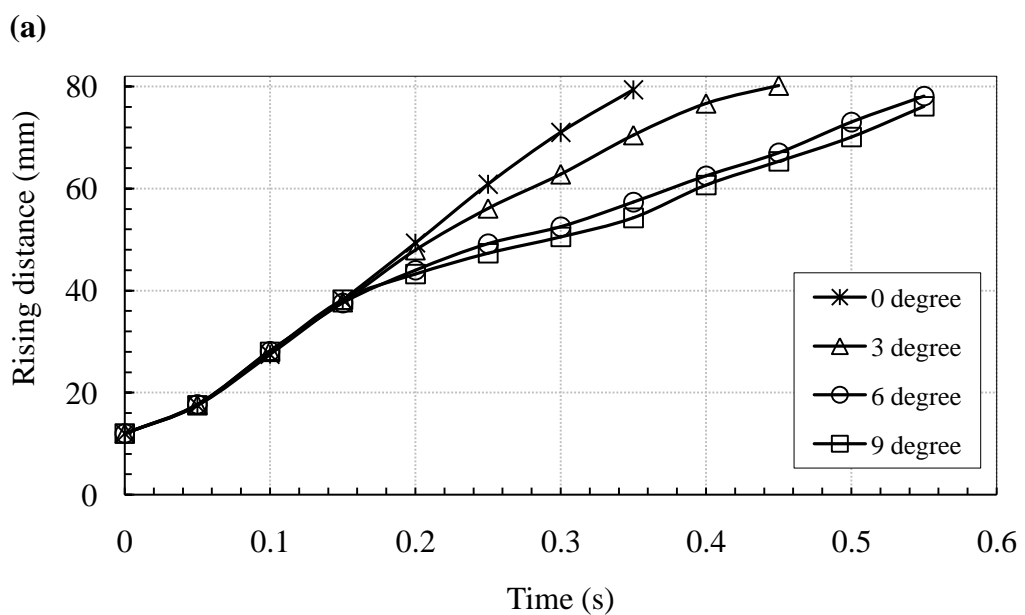


**Figure 4.3:** Bubble rising velocities versus (a) times for Cases 1 ( $0^\circ$  angle), 2 ( $3^\circ$  angle), 3 ( $6^\circ$  angle) and 4 ( $9^\circ$  angle). Such data from Ma et al. (2012) are also included; (b) the difference of the bubble velocity between Case 1 and Cases 2-4; (c) the bubble rising velocity profile versus  $d_b/D_t$ , for different Cases 1-4 respectively.

The above results suggest that the bubble rising velocity reduces with the increase of the inclination angles due to resist of buoyancy or the decrease of the top column width. Secondly, a small velocity fluctuation can be seen near the top of the channel especially for Cases 2, 3 and 4 presumably due to the effect of the trapezoidal cavity. Consequently, this will increase the residing time of bubble in trapezoidal column (or the gas hold up) which has potential enhancement of heat and mass transfer.

Figure 4.4 shows the history of the bubble rising distance with increasing time at different column angles. Figure 4.4a shows the bubble rising distance with the increase of time in second until 80 mm vertical height for Cases1 to 4. Figure 4.4b shows the percentage difference in distance between Case1 and Cases2-4, respectively up to 0.35s. Figure 4.4c shows the vertical height of the bubble versus  $d_b/D_t$  for Cases 1 to 4. First, let us compare Case 1 with other cases which is until 0.35s. Up to 0.16 s, referring to Figure 4.4a, there is no significant difference between cases where the bubble moves up from the initial position of 10mm to 40 mm. After that, the difference is obvious. For example, at 0.35s, the vertical height is about 80, 70, 58 and 55 mm for Cases1, 2, 3 and 4, respectively.



Continue Fig. 4.4

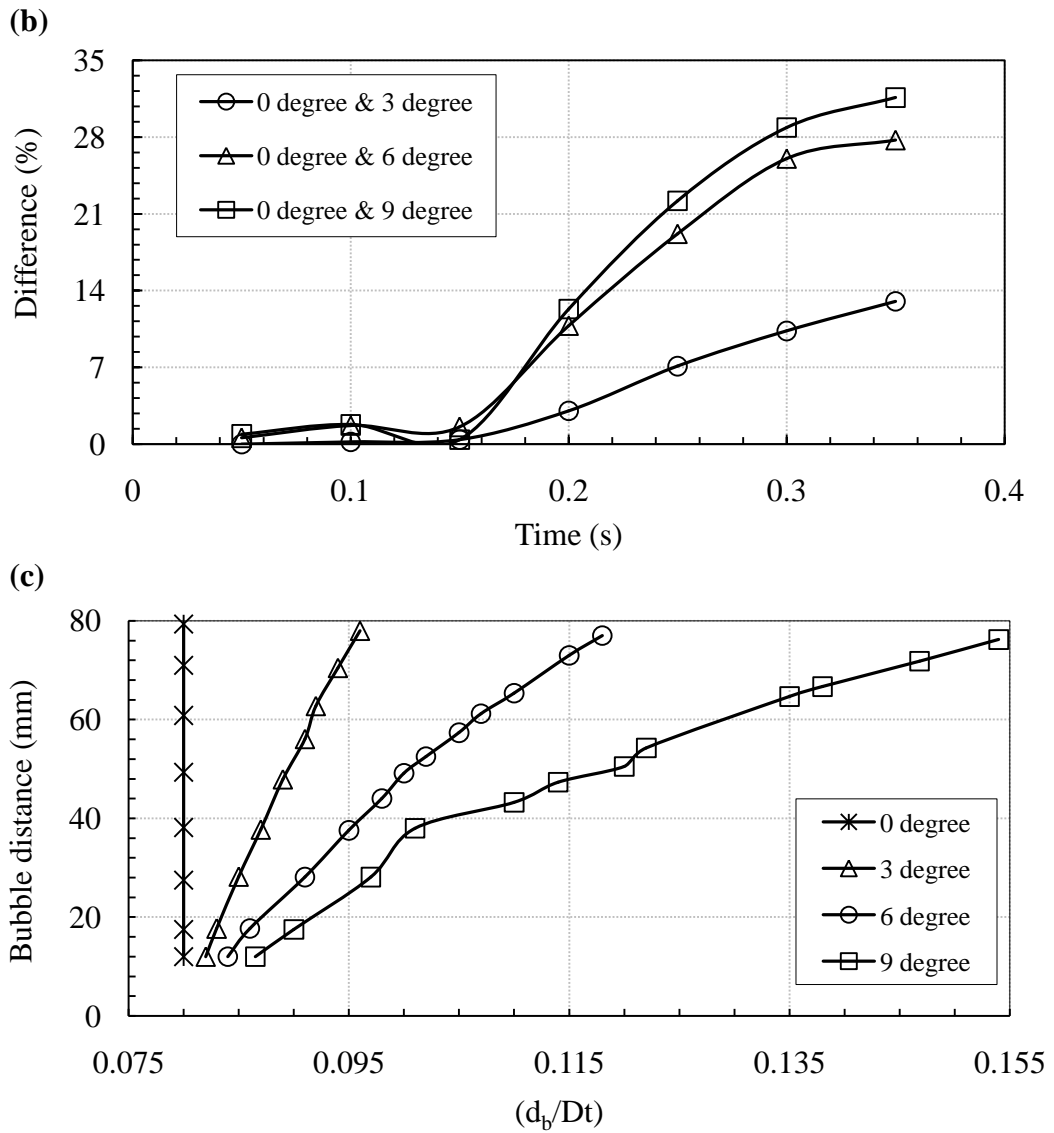
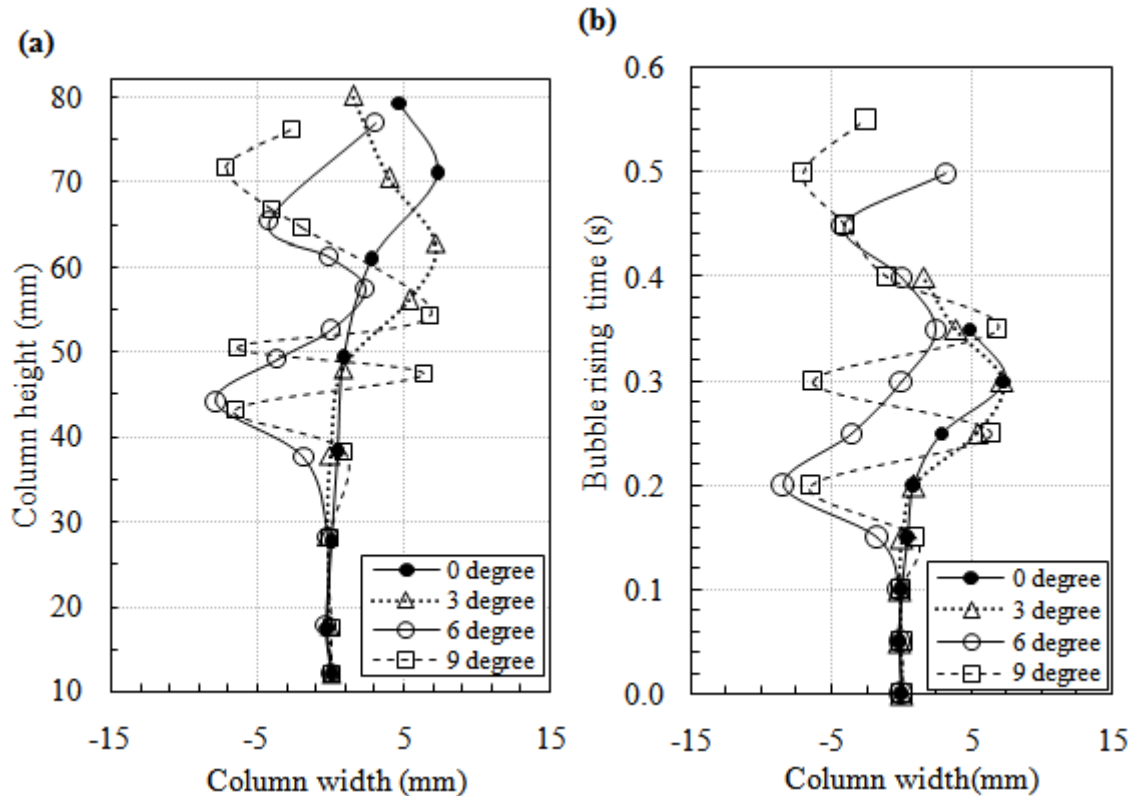


**Figure 4.4:** Bubble rising distance versus (a) times for Cases 1 ( $0^\circ$  angle), 2 ( $3^\circ$  angle), 3 ( $6^\circ$  angle) and 4 ( $9^\circ$  angle); (b) the difference of the bubble rising distance between Case 1 and Cases 2-4; (c) vertical height of the bubble versus  $d_b/D_t$  for different Cases 1-4 respectively.

At this particular time, clearly, Case 1 ( $0^\circ$ ) has the highest vertical distance whereas Case 4 ( $9^\circ$ ) has the shortest vertical distance (Figure 4.4a). The vertical distance of the bubble increases monotonically for all cases. The difference between Case 1 and other cases, referring to Figure 4.4b, show that Case 4 has the highest difference of about 32% followed by Case 3 (28%) and Case 2 (13%). The difference of the vertical height versus time between Case 3 ( $6^\circ$ ) and Case 4 ( $9^\circ$ ) is small in Figure 4.4a despite that the difference in  $d_b/D_t$  value between these two cases in Figure 4.4c is significant.

### 4.3.3 Spatial distribution of a bubble

Figures 4.5a and 4.5b show the trajectory path of the bubble with respect of the column height and time respectively, for Cases 1 to 4. The bubble trajectory path is the same for all cases from the initial position up to 28 mm column height (Figure 4.5a) and 0.1s (Figure 4.5b). After that, the bubble takes different trajectories for difference cases. For Case 1, the bubble remains near the centre for most of the column heights and times. Only at the top of the column or beyond 0.25s, the bubble fluctuates from the centre to the right with the maximum width of 7 mm. The bubble trajectory of Case 2 is similar to that of Case 1 except that the bubble of Case 2 moves to the right hand side at a lower vertical height than that of Case 1 (Figure 4.5a). The bubble trajectory of Case 3 appears to be periodic. The amplitude of the first, second and third half cycle is about 8 mm width to the left, 2.5 mm width to the right and 4 mm width to the left again. The bubble remains largely at the left hand side of the column.



Continue Fig. 4.5

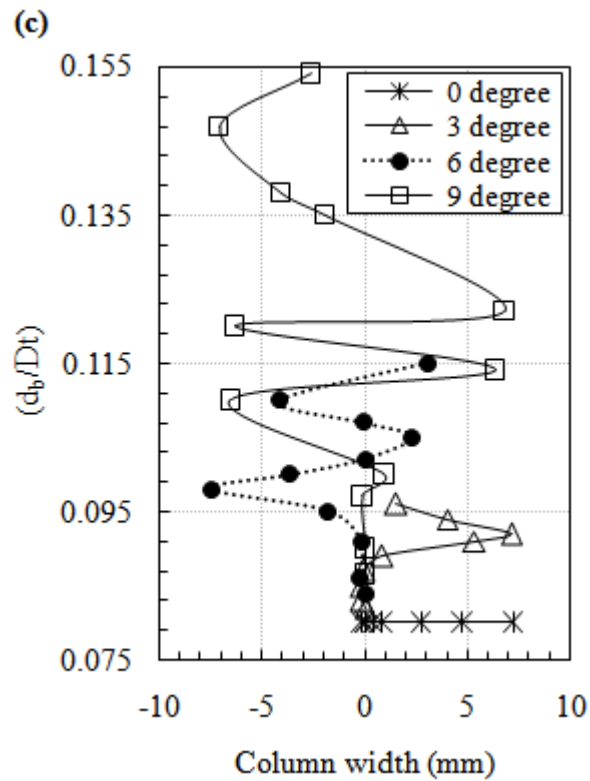


**Figure 4.5:** The trajectory path of the bubble with respect of (a) the column height; (b) rising time; (c) the trajectory of bubble as a function of  $d_b/D_t$  for different Cases 1-4 respectively.

In Case 4 ( $9^\circ$ ), the bubble moves in zigzag motion from the centre to the left and right and this trend continue until near the top of the channel. The frequency of the periodic motion increases with an amplitude of about 7 mm at the left and right of the column. Let us see Figure 4.5c for the trajectory of bubble as a function of  $d_b/D_t$ . The start of the spatial oscillation of the bubble is at a different value of  $d_b/D_t$  for different cases where Case 2 has a lower value and Case 4 has a higher value. The above findings suggest that the trapezoidal column enhances the spatial distribution of a bubble to left and right of the column and may be able to enhance mixing in the liquid.

#### 4.4.4 Bubble morphology

The morphology of the bubble in Case 1 of rectangular cavity and in Cases 2 to 4 of trapezoidal cavity is shown in Figure 4.6a-d, respectively. For quantitative presentation,

the morphology of the bubbles is also presented using an aspect ratio parameter, which is defined as the ratio of major axis to minor axis of an elliptical shape.

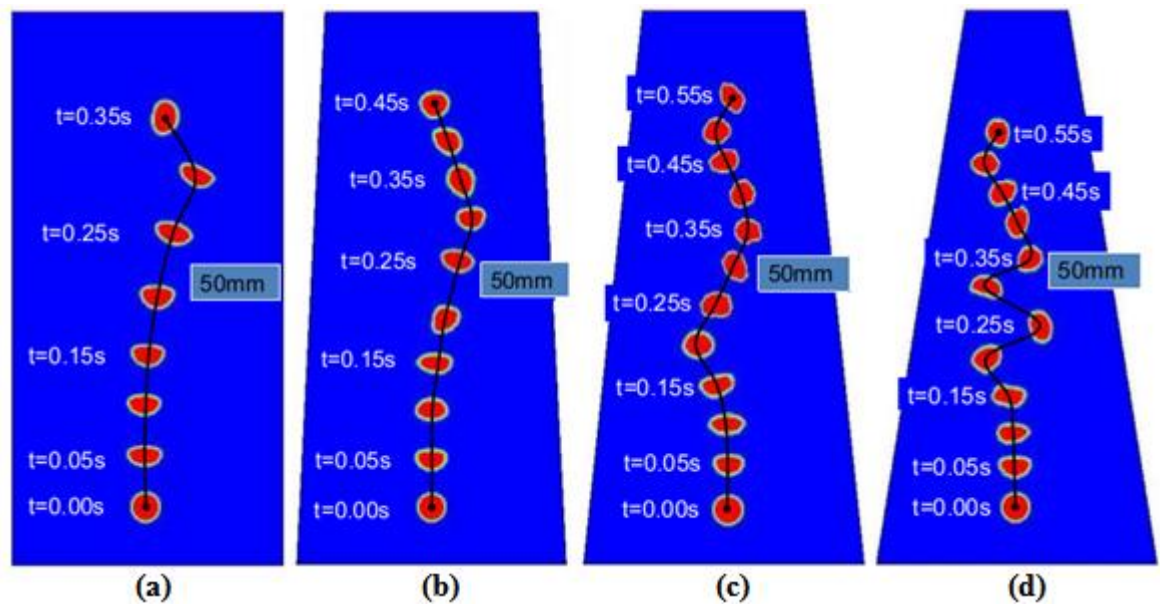


**Figure 4.6:** The morphology of the bubble in Case 1 of (a) rectangular cavity and in Cases 2 to 4 of (b to d) trapezoidal cavity respectively.

Figure 4.7a and 4.7b shows the aspect ratio of the bubble as a function of time and column height for Cases 1 to 4. Starting from the imposed circular shape at the initial condition which has an aspect ratio of unity, the bubble quickly deformed into an elliptical shape in all cases. For example, the bubble in Case 1 has deformed to an elliptical shape with an aspect ratio about 0.5 within 0.06 second (or 20 mm height), and at this particular time, the bubble has the largest deformation in comparison to that of the other cases. After this time or height, the aspect ratio of Case 1 bubble slightly increases remains on average of 0.6 until to the top of the column, indicating that the changes in the bubble shape are no significant beyond 0.1 s. The bubbles in Cases 2-4 also deform to the minimum aspect ratio of 0.5 but it is achieved at a slightly longer time, i.e., 0.1- 0.15s or vertical height of 28-40 mm, in comparison to that of Case 1. After that, the aspect ratio of these cases increases to a highest value before fluctuate with the increase of the time or the vertical height representing a change the bubbles

shape from an elliptic shape to more likely toward a circle and vice versa. In other words, the elliptical bubble tends to regain a circular-like shape and then go back to an elliptical shape and this can be seen in Figure 4.6. In this regard, the increase of the aspect ratio is the highest for Case 2, which occurs at 0.25s or 55 mm vertical height. The highest increase for Case 3 is at 0.22s or about 47 mm vertical height and for Case 4 is at 0.2 s or about 42 mm vertical height. Let us see Figure 4.7c to investigate the effect of the ratio of  $d_b/D_t$  to the shape of bubble for Cases 1 to 4. The fluctuations in bubble shape start at different values of  $d_b/D_t$  for different cases, being the lowest for Case 2 and the highest for Case 4. Figure 4.7d shows the velocity versus the aspect ratio for a 4 mm size of bubble for all our cases. Tomiyama et al. (2002) developed a correlation based on bubble terminal velocity, aspect ratio ( $E = h/w$ ) and fluid properties for a rectangular column. The correlation can be written for ( $E < 1$ ):  $V_T = \left[ \left\{ \sin^{-1} (1 - E^2)^{1/2} - E (1 - E^2)^{1/2} \right\} / (1 - E^2) \right] \times \left[ 8\sigma E^{4/3} / d_b \rho_l + (\Delta\rho g d_b E^{2/3} / 2\rho_l (1 - E^2)) \right]^{1/2}$ . Experimental data on velocity and aspect ratio for a 4 mm bubble from Tomiyama et al. (2002) and that calculated using his correlation for a rectangular column is also included in the figure. Our simulation result for a  $0^\circ$  angle (Case 1) agrees well with Tomiyama et al. (2002) correlation and experimental data with less than 6% error. When the column angle is increased from  $3^\circ$  to  $9^\circ$ , the values of the velocity vs. aspect ratio are distributed non-uniformly below the correlation line. When the column angle is increased from  $3^\circ$  to  $9^\circ$ , the data of the velocity vs. the aspect ratio are distributed under Tomiyama et al. (2002) correlation. A lower value is found for a  $9^\circ$  inclination angle (Case 4) in comparison to  $3^\circ$  (Case 2) and  $6^\circ$  (Case 3). Thus, the column angle has an effect not only on bubble velocity, but also on the bubble aspect ratio or shape deformation.

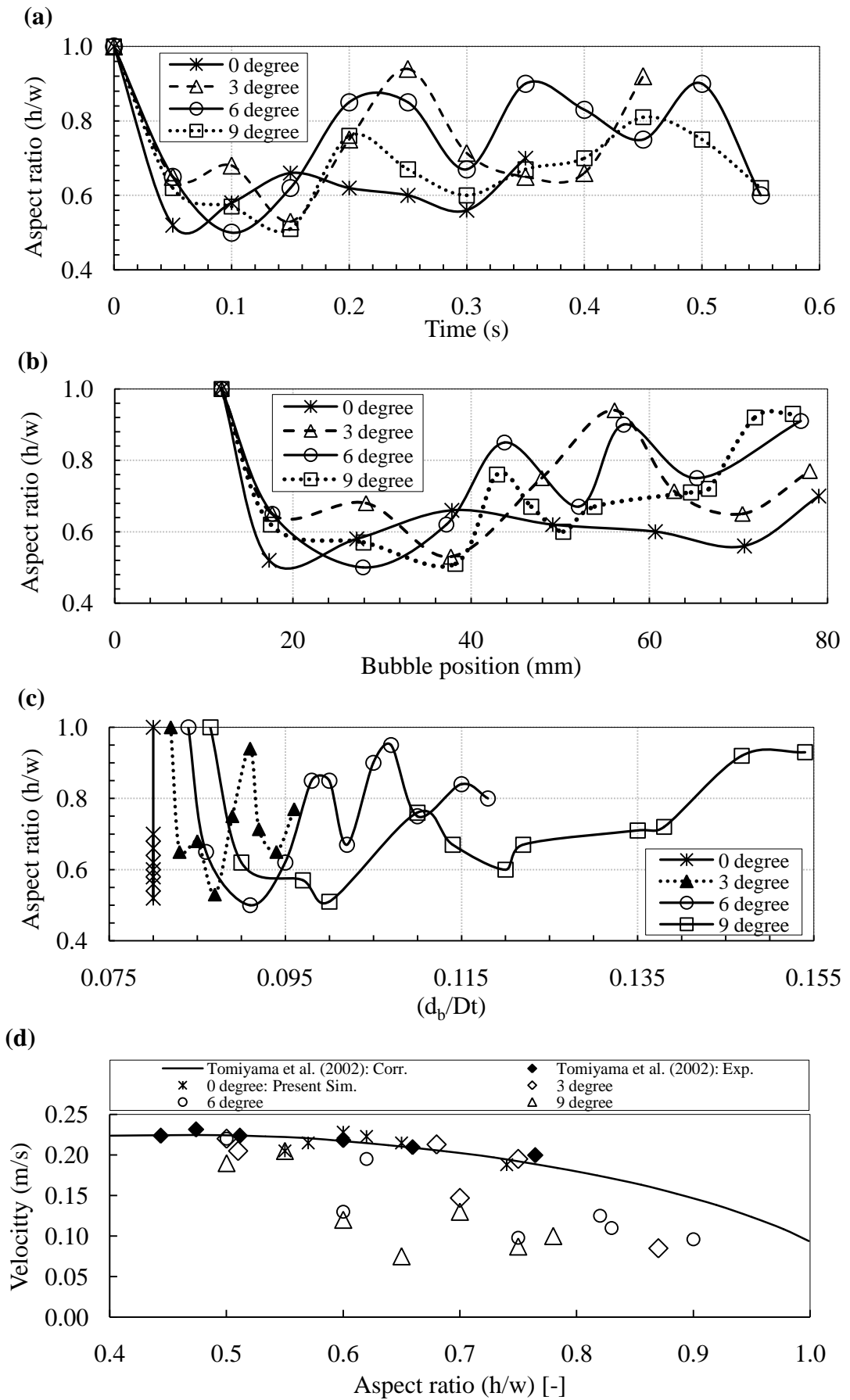


**Figure 4.7:** The aspect ratio of the bubble as a function of (a) time; (b) column height; (c) the ratio of  $d_b/D_t$  and (d) bubble rising velocities versus bubble aspect ratio for different Cases1-4 respectively, such data from Tomiyama et al. (2002) are included.

#### 4.4 Conclusion

Two dimensional (2D) CFD analysis were carried out using Level Set Volume of Fluid (CLSVOF) numerical method in the current study to investigate the effects of wall of trapezoidal columns to rising characteristics of a single bubble such as rise velocity, rising trajectory, bubble size and shape. The conclusions of the current study are

- The study shows that the bubble rising velocity reduced from 0.20 m/s to 0.06 m/s with the increase of trapezoidal inclination angles from  $0^\circ$  to  $9^\circ$  which measured from the vertical wall or the decrease of the top column width.
- The bubble rising vertical height at a given particular time of 0.16 s reduces with the increase of trapezoidal inclination angles.
- The trapezoidal column enhances the lateral spatial distribution of a bubble to left and right of the column and this may enhance mixing in the column.
- The trapezoidal column enhances the changes in bubble shape with the increase of the time or the vertical height representing a change in the bubble shape from elliptic to circle and vice versa.
- The use trapezoidal cavity give potential benefits of increase of residing time for bubble in a column which increase the gas hold up in column and enhancement the movement of bubble. Consequently, this may improve the heat and mass transfer in the column.

## CHAPTER 5

### STUDY OF BUBBLE COALESCENCE PROCESS USING CFD

This chapter describes the study of bubble coalescence processes in stagnant fluids. The work carried out in this chapter provides detailed information of co-axial and parallel bubble coalescence mechanism and rise characteristics under various operating conditions.

#### 5.1 Introduction

Gas–liquid bubble column reactors are commonly used in areas of engineering and technologies especially for chemical and petrochemical processes. The overall performance of a bubble column mainly depends on the bubble flow characteristics, bubbles coalescence and bubble break up phenomenon, which alter the bubble size distribution and enhance the gas–liquid contact area resulting a significant increase in heat and mass transfer as well as chemical reaction rate (Yang et al., 2011; Yang et al., 2007). Therefore, various studies have been carried out over a number of years to enhance the our understanding on bubble characteristics including the bubble rise in parallel arrangement in a quiescent liquid through experimental and numerical investigations e.g., the bubble rise velocities, the bubble shape variation and operating conditions etc., (Sanada et al., 2009; Fan et al., 2009; Legendre et al., 2003; Van Sint Annaland et al., 2006; Lui et al., 2013). For example, Legendre et al. (2003) investigated the rising behaviour of two parallel bubbles in a viscous fluid. They reported cohesive or repulsive hydrodynamic interactions between bubbles, which depends primarily on Reynolds number. Sanada et al. (2009) experimentally investigated the motion of a horizontally aligned pair of rising bubbles in silicone oil. They found that the bubble repulsion effect developed due to a large amount of fluid vortexes in the space between bubbles, which resulted in the bubbles movement in a

direction away from each other. Van Sint Annaland et al. (2006) simulated the coalescence dynamics of two bubbles in stagnant fluids in co-axial and oblique direction. The simulation results showed a reasonable agreement with that of experiment. Lin et al. (2013) also found that for two in-line bubbles, the acceleration of the trailing bubble to the leading bubble was caused by negative pressure; and the shear-thinning is caused by viscoelastic effect.

In summary, a detailed study of the coalescence process of co-axial bubble and parallel bubble in viscous liquid and how the shape of the bubbles evolves with time is not available. There are some works in which non-Newtonian are tested, which has a different physical property from the Newtonian fluid, e.g., see Refs (Legendre et al. 2003; Lin et al. 2013). The present study provides much detailed information on the co-axial and three parallel bubbles coalescence mechanism as well as rise trajectory under different operating conditions. The effect of the non dimensional liquid viscosity ( $1 < \mu^* < 0.1$ ) and the effect of non dimensional surface tension coefficient ( $1 < \sigma^* < 0.1$ ) on the co-axial and three parallel bubbles coalescence will be investigated using the VOF model.

## **5.2 Methods**

### **5.2.1 Governing equations**

In this chapter, the volume of fluid (VOF) method with continuum surface force (CSF) model was used to investigate the coalescence and the rise trajectory of a co-axial and three parallel bubble arrangements in 2D column. The governing equations for the present work are similar as that described in section 3.2.1 (Chapter 3).

### **5.2.2 Boundary conditions**

A two dimensional (2D) domain is used to represent the bubble rise dynamics in a quiescent liquid. A full 2D domain is used to investigate asymmetry in bubble shape

and rise characteristics from bottom to the top of the domain. The boundary condition and the numerical methods are similar as discussed in earlier in section 4.2.2 (Chapter 4) and in section 3.2.3 (Chapter 3), respectively.

### **5.2.3 Simulation cases**

A total of 83 simulation cases were carried out for the purpose of bubble coalescence process. A summary of all the simulation cases is given in Table 5.1.

#### (i) (Cases 1-12)

First twelve cases (Cases 1-12) were used for validation in which 4 to 10 mm sizes of bubble were set in different viscous fluids to rise from a rest condition and from an initial position of 12 mm vertical height of the domain. A rectangular domain with a height of  $H = 100$  mm and a width of  $D = 100$  mm have been used.

#### (ii) (Cases 13-46)

Eighteen cases (Cases 13-31) were used to investigate the effect of non dimensional liquid viscosity from  $1 < \mu^* < 0.1$ ; and another fifteen cases (Cases 32-46) were for investigations of the effect of non dimensional surface tension coefficient ( $1 < \sigma^* < 0.1$ ) on co-axial bubble coalescence. For these investigations, the same domain with dimension was used as mentioned in Case 1-12.

#### (iii) (Cases 47-49)

Three cases (Cases 47-49) were used to investigate the effect of non-dimensional horizontal intervals (i.e.,  $S = 1.5, 2.0$  and  $4.0$ ) between a pair of bubbles (parallel direction) with  $d_b = 6$  mm. The non-dimensional horizontal interval is defined as  $S = X_i/d_b$ , where  $X_i$  is the initial distance between the centres of bubbles pair and  $d_b$  is the initial bubble diameter.

#### (iv) (Cases 50-83)

Cases 50-68 were used to find a critical flat gap between three parallel bubbles at reduced surface tension and liquid viscosity. Finally the last fifteen cases (Cases 69-83)

have been used to investigate the repulsion behavior of the bubble after exit the critical flat gap between the bubbles. Figure 5.1 shows the computational domain of three parallel bubbles arrangement.

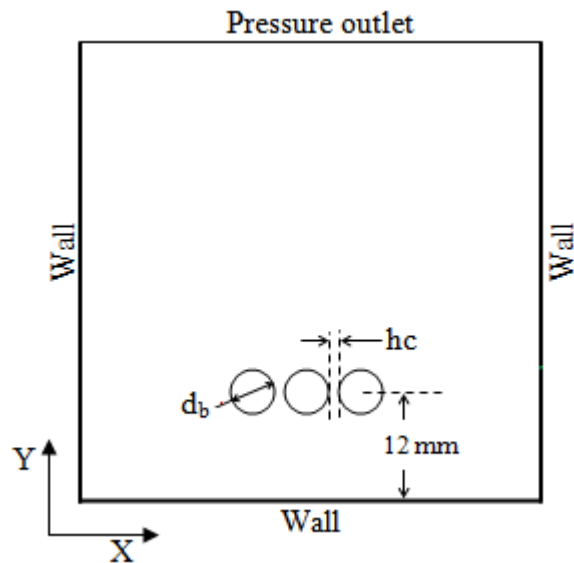


**Figure 5.1:** Parallel bubble arrangement in computational domain. Noted:  $hc$  represents critical flat gap between the bubbles.

For these investigation, the three parallel bubbles with different initial diameter were placed in S3 fluid. 12 mm height between the bottom wall and bubble centre was maintained for every Cases and different  $hc$  condition under different operating condition have been investigated.

**Table 5.1** Simulation cases.

Case	$\rho_l$ (kg/m <sup>3</sup> )	$\sigma$ (N/m)	$\mu_l$ (Pa.s)	$d_b$ (mm)	$\sigma^* = \sigma_l/\sigma$	$\mu^* = \mu_l/\mu_l$	Purpose
1-12	S1=1230 S2=1220 S3=1205	0.064;	0.24; 0.16; 0.076	4, 6, 8,10	3-20	4 -50	For validation of the present work.
13-31	1205	0.064	0.076 0.038 0.019 0.0123 0.0098 0.0076	4,6,8	1	1; 0.5; 0.25; 0.17; 0.13; 0.1	To investigate the effect of reduced liquid viscosity on two co-axial bubble coalescence.

Table 5.1 Continue

32-46	1205	0.064 0.0192 0.0134 0.0096 0.0077 0.0064	0.076	4,6,8	1; 0.3; 0.21; 0.15; 0.12; 0.1	1	To investigate the effect of reduced surface tension coefficient on two co-axial bubble coalescence.
47-49	1205	0.064	0.0098	6	1	0.13	To investigate the effect of horizontal interval between two parallel bubbles.
50-68	1205	0.064	0.076	3, 4,5 5,6,7, 8	1; 0.1	1; 0.1	To find the critical flat gap for three parallel bubble coalescence.
69-83	1205	0.064	0.076	4, 6,8	1; 0.1	1; 0.1	To investigate the bubble repulsion after exit the critical flat gap for three parallel bubble.

**Noted:**  $\mu_r$  and  $\sigma_r$  represents the reduced liquid viscosity and surface tension coefficient respectively

#### 5.2.4 Limitations

The limitations of the present work are similar as that described in section 3.2.5 (Chapter 3).

#### 5.2.5 Mesh dependency study

A uniform structured mesh was used everywhere in the domain. The effect of mesh sizes on results was investigated using four types of meshes i.e., 0.18 mm, 0.22 mm, 0.25 mm and 0.30 mm, resulting in a total number of elements of 308641, 206611, 160000 and 111111, respectively. An 8 mm size of bubble was patched in S3 fluid, at the centre and a 12 mm height from the bottom of the domain. The purpose of this test is to compare the bubble rise velocity of the four different meshes with the increase in simulation time, which is shown in Figure 5.2. The velocities of the meshes are almost overlapping with each other for the mesh size of 0.18 mm and 0.22 mm. However, a negligible deviation can be observed for the 0.25 mm and for the 0.3 mm mesh. Therefore, the mesh of 0.22 mm is selected for the current work to encompass accuracy and the computation cost.

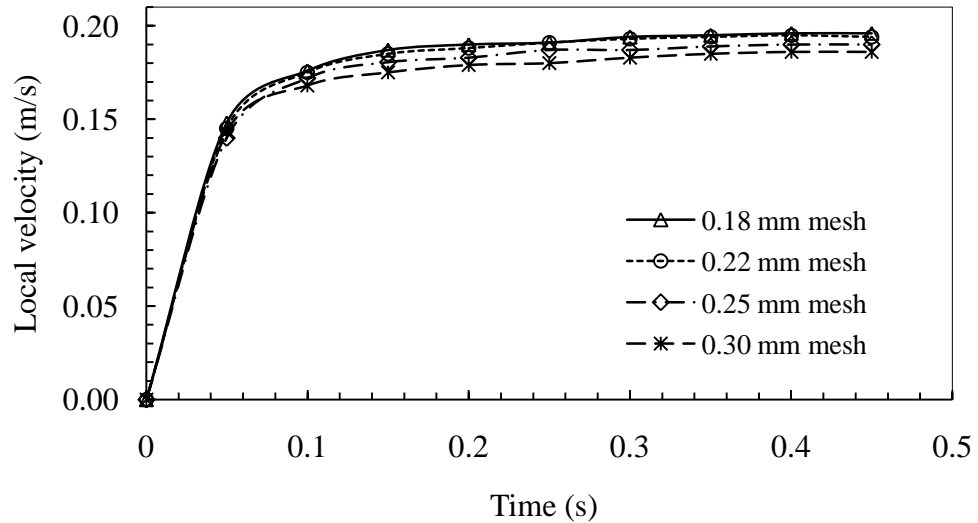


**Figure 5.2:** Grid dependency study using different size of meshes.

### 5.3 Results and Discussion

#### 5.3.1 Validation of CFD for bubble coalescence

For simulation Cases 1-12, a single air bubble of four different initial diameters (e.g., 4, 6, 8 and 10 mm) was imposed in three different viscous fluids (e.g., S1, S2 and S3). The results were compared with the available experimental data from literature, i.e., Raymond & Rosant (2000). Figure 5.3 shows the quantitative comparison between the results found from the simulations Cases of 1-12 and the experimental data from Raymond & Rosant, (2000) and those calculated using Jamialahmadi, Branch, & Müller-Steinhagen (1994) correlation (solid line). Authors developed the correlation between the bubble equivalent diameter and rising velocity of the bubble in water, as follows:  $V_T = V_b V_t^w / [(V_b)^2 + (V_t^w)^2]^{0.5}$ ; Where,  $V_b = [gd_e^2(\rho_l - \rho_g)] / 18\mu_l$  and  $V_t^w = [2\sigma/d_e(\rho_l - \rho_g) + gd_e^2/2]^{0.5}$  is the bubble rising velocity of a spherical bubble and the travelling wave velocity in front of bubble, respectively. It is observed from the figure 5.3, the bubble terminal velocity progressively increased with the increase of bubble diameter in three different viscous fluids (i.e., S1, S2, and S3). Comparing between Raymond & Rosant (2000) data from experiment and the present simulation, on average, the results are quite close to one another; some differences (i.e., less 20%

relative error) are observed for both experiment (Raymond & Rosant, 2000) and simulation with Jamialahmadi et al. (1994) correlation results and this may have resulted due to the different fluid properties, whereby the present study is based on air-glycerine solution and Jamialahmadi et al. (1994) correlation is based on air-water system.

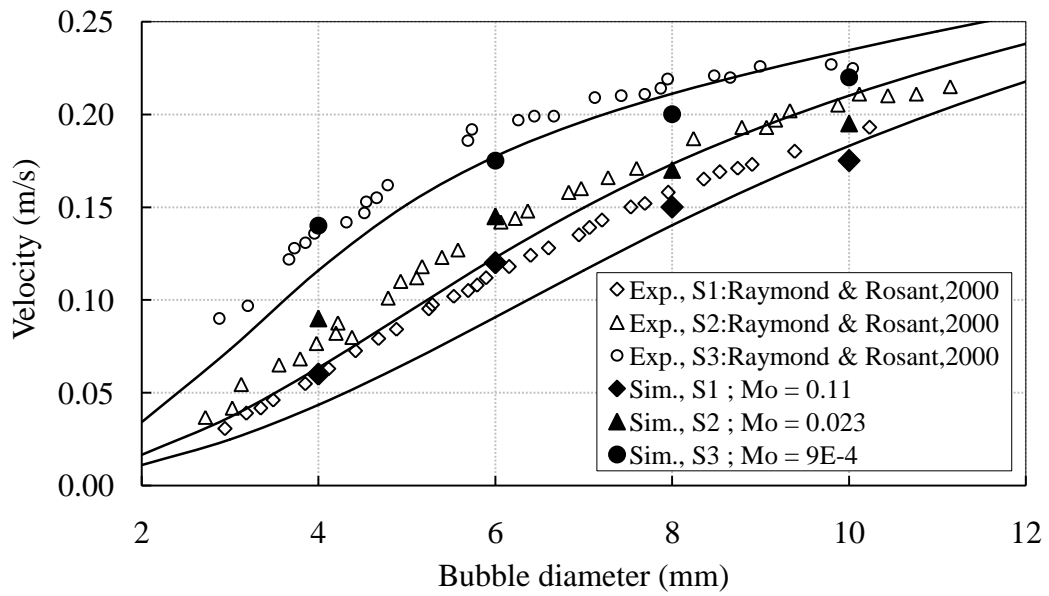


**Figure 5.3:** Bubble terminal velocity versus bubble diameter. The solid lines correspond to the correlation results of Jamialahmadi et al. (1994).

Figure 5.4 illustrates the bubble aspect ratio as a function of bubble diameter. The bubble aspect ratio is calculated as the ratio of the bubble height ( $h$ ) to width ( $w$ ) after the bubble reach a steady conditions (i.e., no more changes in the bubble shape). The solid lines correspond to fitted curves of the experimental data of Raymond & Rosant (2000). It is observed that the bubble aspect ratio decreases or more deforms (which indicates the change of bubble from a spherical shape to an ellipsoidal shape) with the increasing bubble diameter. In addition, the rise of a bubble in low Morton number ( $Mo$ ) fluid (S3) deforms more than the high  $Mo$  number fluid (S1 and S2). However, comparing between Raymond & Rosant, (2000) and the present simulation, on average, the results are quite close to one another and maximum less than 6% relative error is found.

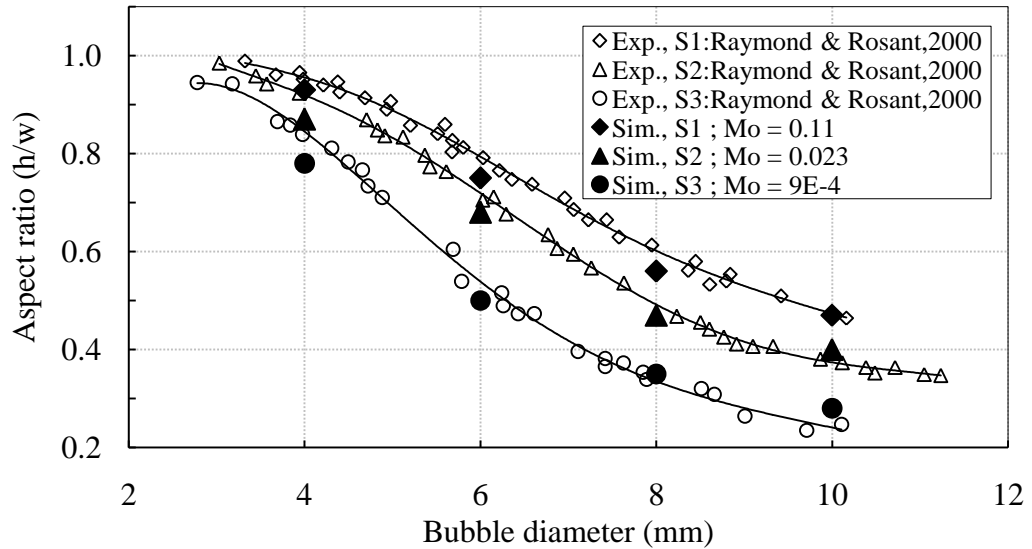


**Figure 5.4:** Bubble aspect ratio as function of bubble diameter.

In summary, the above comparison between experimental data, correlation results and the simulation results indicate, the present CFD method is capable to predict an accurate result. This method was then applied to study the effect of liquid viscosity, the surface tension coefficient on co-axial and parallel bubble coalescence process. The CFD method and the same domain has also been used to investigate the different initial horizontal interval of bubble for parallel bubble coalescence mechanism as well as rising of parallel bubbles into the changes of fluid properties.

### 5.3.2 Co-axial bubble coalescence

#### 5.3.2.1 Effect of liquid viscosity (Cases 13-31)

The effect of non-dimensional liquid viscosity ( $\mu^* = \mu_r/\mu_l$ ) on two co-axial bubble coalescence and how the shape of the bubbles changes during coalescence process are discussed, when the other parameter kept fixed. At initial condition at  $t = 0s$ , the spherical bubbles were set in a static position with an equal distance ( $\Delta Y$ ) of 8 mm. When the simulation started, the bubbles moved to rise due to the buoyancy and altered an ellipsoid shape because of the differential pressure between the top surface and the bottom surface of the bubbles with increasing time. The pressure differences depend on

the pushing action by the formation of liquid jets behind the bubbles. As the time progresses, the following bubble was moving toward the leading bubbles. It touched to each other within a short time due to the wake effect behind the leading bubble. Figure 5.5 illustrates the bubble coalescence time as a function of non-dimensional liquid viscosity. In general, it can be seen that the bubble coalescences time decreases gradually with reducing non-dimensional liquid viscosity of  $\mu^* > 0.25$ . After that the coalescence time of the bubbles decreases steeply from  $0.1 < \mu^* < 0.25$ . The shape of bubble has experienced a significant affect by the reduced  $\mu^*$ .

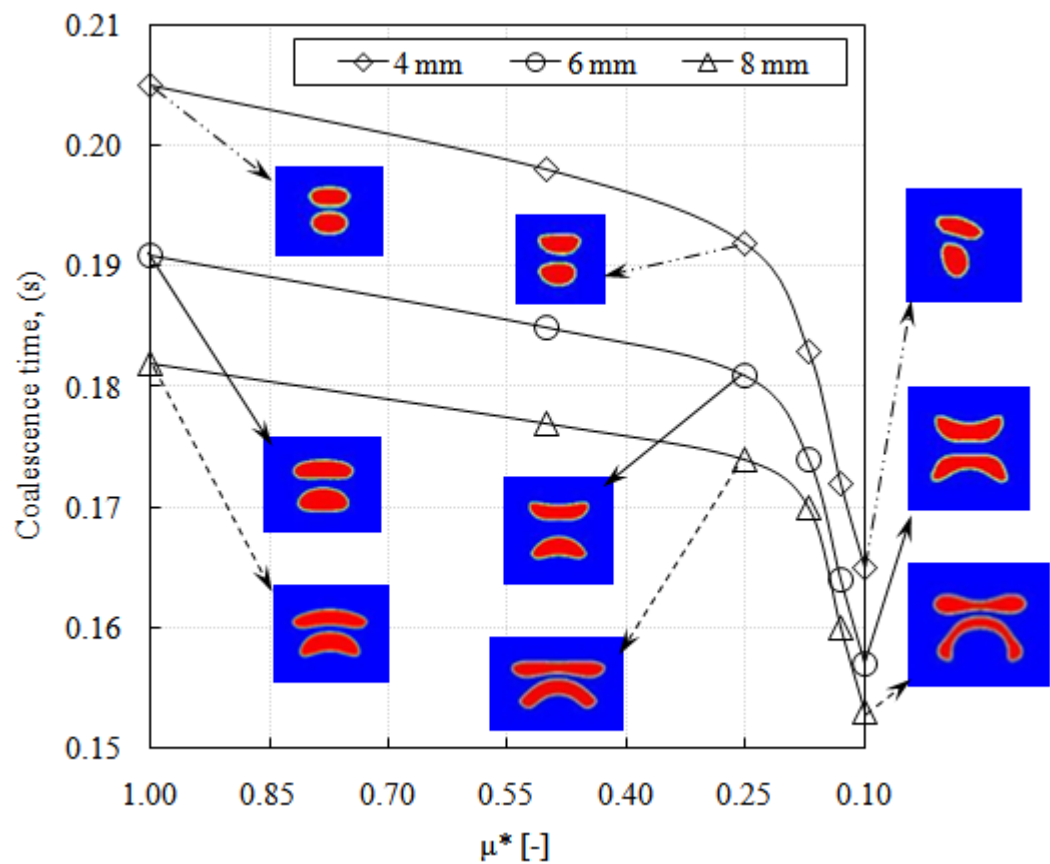


**Figure 5.5:** Bubble coalescence time as a function of non-dimensional liquid viscosity when  $\sigma^* = 1$ .

For example of  $\mu^* = 0.1$ , the following bubble with 4 mm alters an ellipsoidal shape and finally it has altered to oblate ellipsoidal cap shape and skirted shape for the increased size of 6 mm and 8 mm bubble, respectively. The change of shape deformations of the bubbles occurred due to the push of liquid jet with longer period behind the upper

bubble lower surface. Consequently, a stronger negative pressure region had developed between the bubble interactions regions. The wake (or negative pressure) region accelerates the quick rising of following bubbles in a short time. On the other side, the viscous force was continuously trying to maintain the liquid flow with a minimum stress. Thus, a harder stretch developed over the top surface of the following bubble in low of  $\mu^*$  and in results of an earlier coalescence of bubbles. Therefore, the bubbles of a high  $\mu^*$  of liquid collide lately than the bubbles of a low  $\mu^*$  of liquid, when the other properties remain the same. In Figure 5.6, the effect of non-dimensional liquid viscosity on three different initial sizes of bubble rise distance ( $\Delta Y$ ) in time is shown.

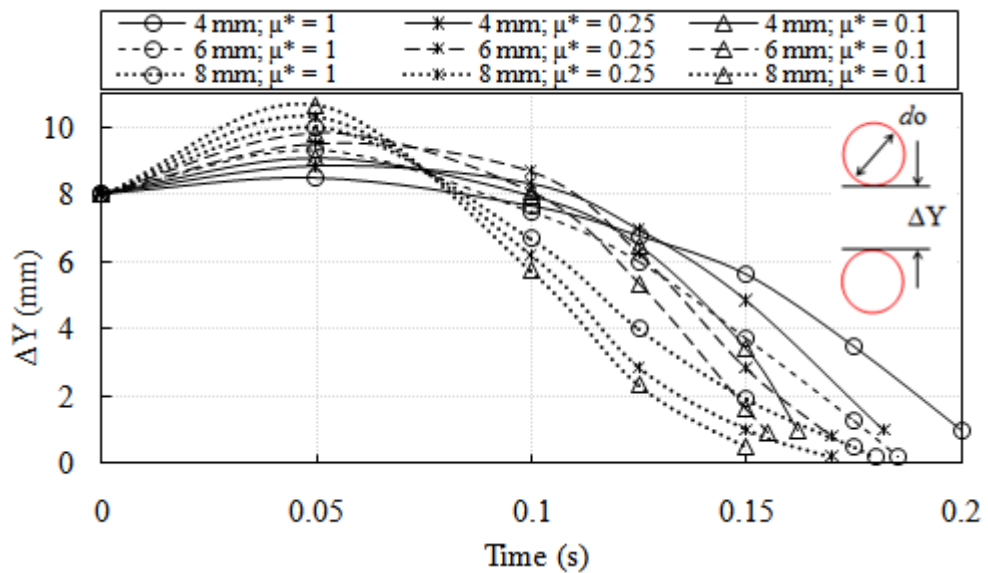


**Figure 5.6:** Co-axial bubble rising distance as a function of time when  $\sigma^* = 1$ .

It was found that the bubbles into a high viscosity of liquid,  $\mu^* = 1$  came to each other slowly than the decreasing of  $\mu^*$  and size of bubble. The slowest rising of the bubbles with higher of  $\mu^*$  occurred due to development of weaker vortex of liquid jet that unable to push strongly behind the bubbles. In addition, it can be seen that at  $t = 0.05s$ , the pick value of all bubbles indicated that the stronger weak region has developed behind the upper bubble in initial rising stages.

### 5.3.2.2 Effect of surface tension coefficient (Cases 32-46)

Figure 5.7 illustrates the bubble coalescence time as a function of non-dimensional surface tension coefficient ( $\sigma^*$ ). It can be seen that the bubbles coalescence time gradually decreases with reducing of  $\sigma^*$  for the initial size of 6 mm and 8 mm bubbles. But, the coalescence time of the 4 mm bubbles decreases steeply from  $\sigma^* = 0.25$  to 0.1. The shape of bubble has also experienced a significant affect by the reduction of  $\sigma^*$ .

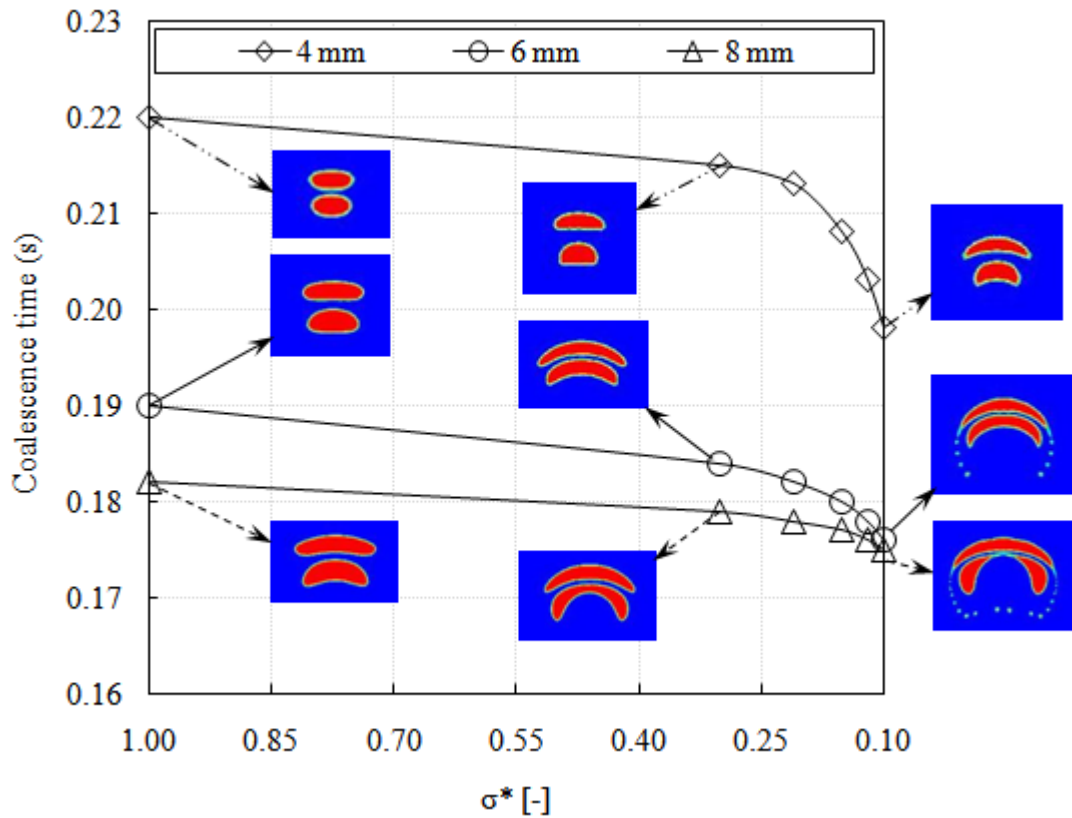


**Figure 5.7:** Bubble coalescence time as a function of non-dimensional surface tension coefficient when  $\mu^* = 1$ .

For example of  $\sigma^* = 0.1$ , the bubble with 4 mm and 6 mm alters an ellipsoidal cap shape. But the following bubble with 8 mm braked up before coalescence due to low obstruction to resist the change in shape of the bubble. It is observed that for the high value of  $\sigma^* = 1$ , the bubble altered an ellipsoidal shape for 4 mm and 6 mm bubble. But for the reducing of  $\sigma^*$  from 0.85 to 0.1, the bubbles is changing its shape from an ellipsoidal to ellipsoidal cap shape. The ellipsoidal cap shape formed due to strong push of the liquid jet behind the bubble that promotes stiff deformation of the bubbles. On the

other hand, the upper bubble forms a more ellipsoidal cap shape rather than the following bubble for  $\sigma^* = 0.1$ . It develops due to the increment of liquid drag over the upper bubble with a short time. However, a more deformation of the bubbles have seen for the low surface tension coefficient, because of low obstruction to resist the change in shape of the bubbles. Consequently, the effect of non-dimensional surface tension coefficient on three different initial sizes of bubble rise distance ( $\Delta Y$ ) in time is shown in Figure 5.8. It is found that the bubbles into a high  $\sigma^*$  of 1 rise slowly than the decreasing of  $\sigma^*$  and size of bubble. Additionally, the reason of the maximum pick value of all cases of bubble is found at  $t = 0.05$  s, as discuss in earlier.

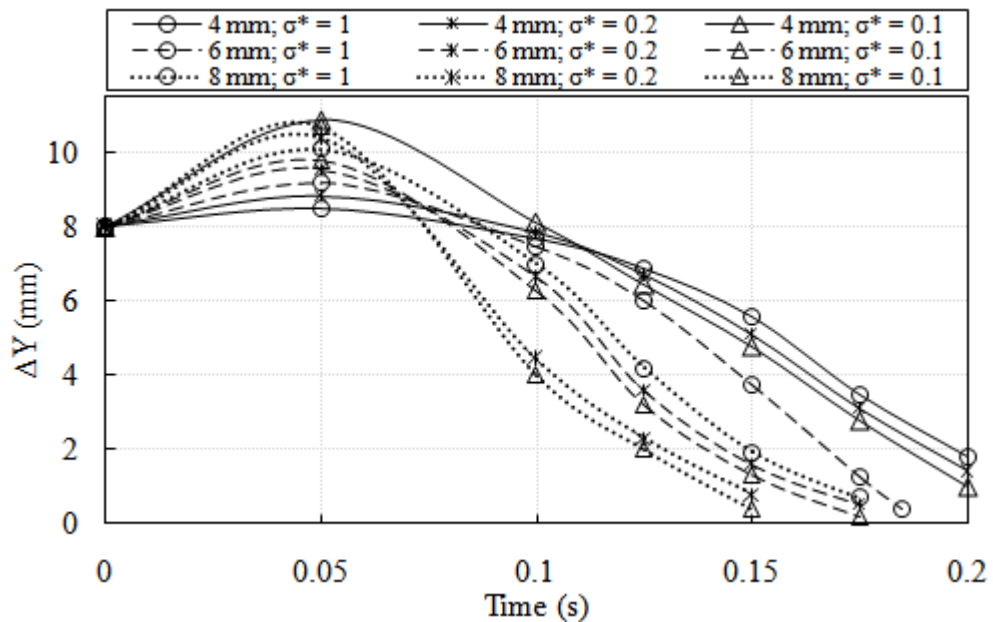


**Figure 5.8:** Co-axial bubble rising distance as a function of time when  $\mu^* = 1$ .

### 5.3.3 Tow parallel bubble rise dynamics (Cases 47-49)

Two parallel bubbles rising dynamics in horizontal direction are closely related to the initial horizontal bubble interval and the physical properties of fluids. The interaction of two parallel bubbles are investigated with three different non-dimensional initial horizontal intervals  $S = 1.5, 2.0$  and  $4.0$ . Figure 5.9 shows the 6 mm parallel bubble rising trajectories with three different initial bubble intervals. The results reveal that the

path, shape as well as velocity experience a significant variation with increasing the distance between the centres of the two bubbles. The bubble shape changes from spherical to wobbling shape (or irregular shape) for the three different initial bubble intervals. The two parallel bubbles rising trajectory are asymmetric along the perpendicular line in the middle of the vertical column, as can be seen from Figure 5.9. For  $S = 1.5$  (see Figure 5.9a) and  $S = 2.0$  (see Figure 5.9b), a stronger repulsive interaction between two parallel bubbles are observed rather than the interval of  $S = 4.0$  (see Figure 5.9c).

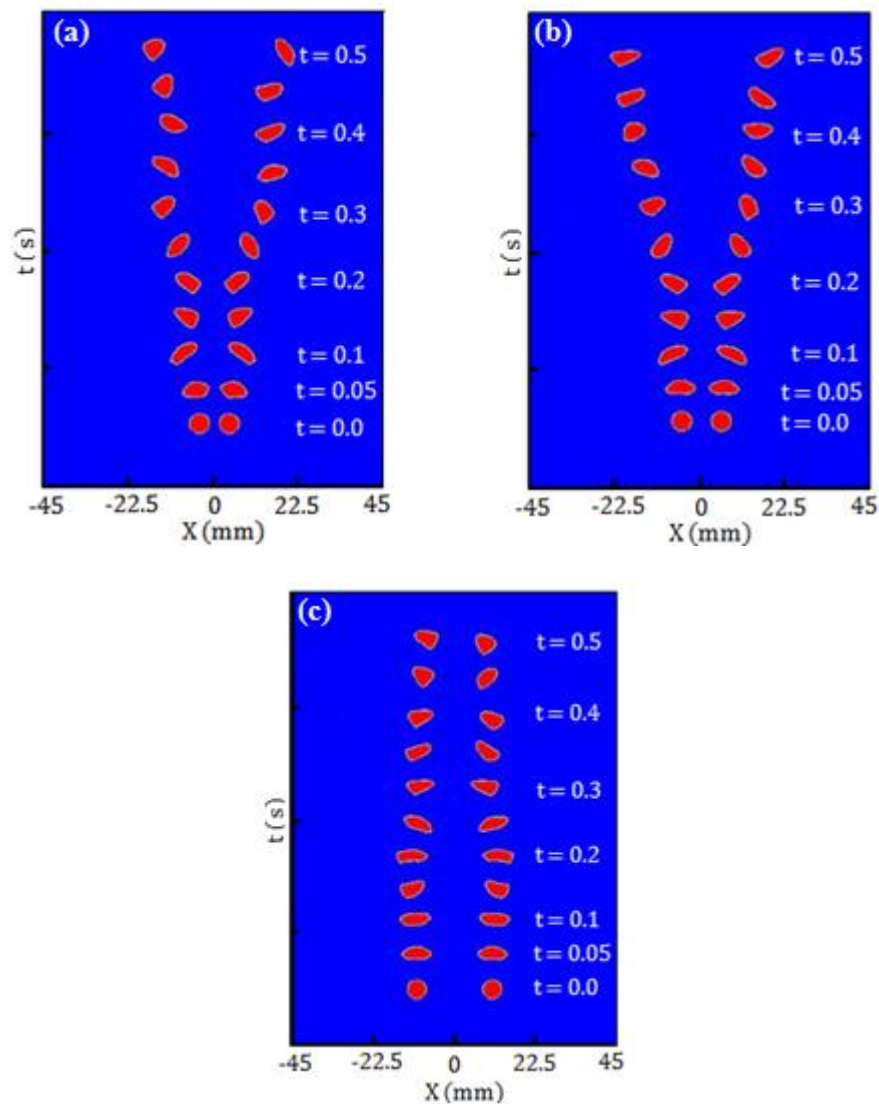


**Figure 5.9:** Two parallel bubble rising trajectory at different initial interval when (a)  $S = 1.5$ ; (b)  $S = 2.0$ ; (c)  $S = 4.0$ .

The results for bubble horizontal interval ratio, bubble aspect ratio (or the ratio of minimum to maximum deformation of bubble), bubble rising velocity and static pressure on bubble as a function of time at three different initial bubble intervals are shown in Figure 5.10a, 5.10b and 5.10c, respectively.

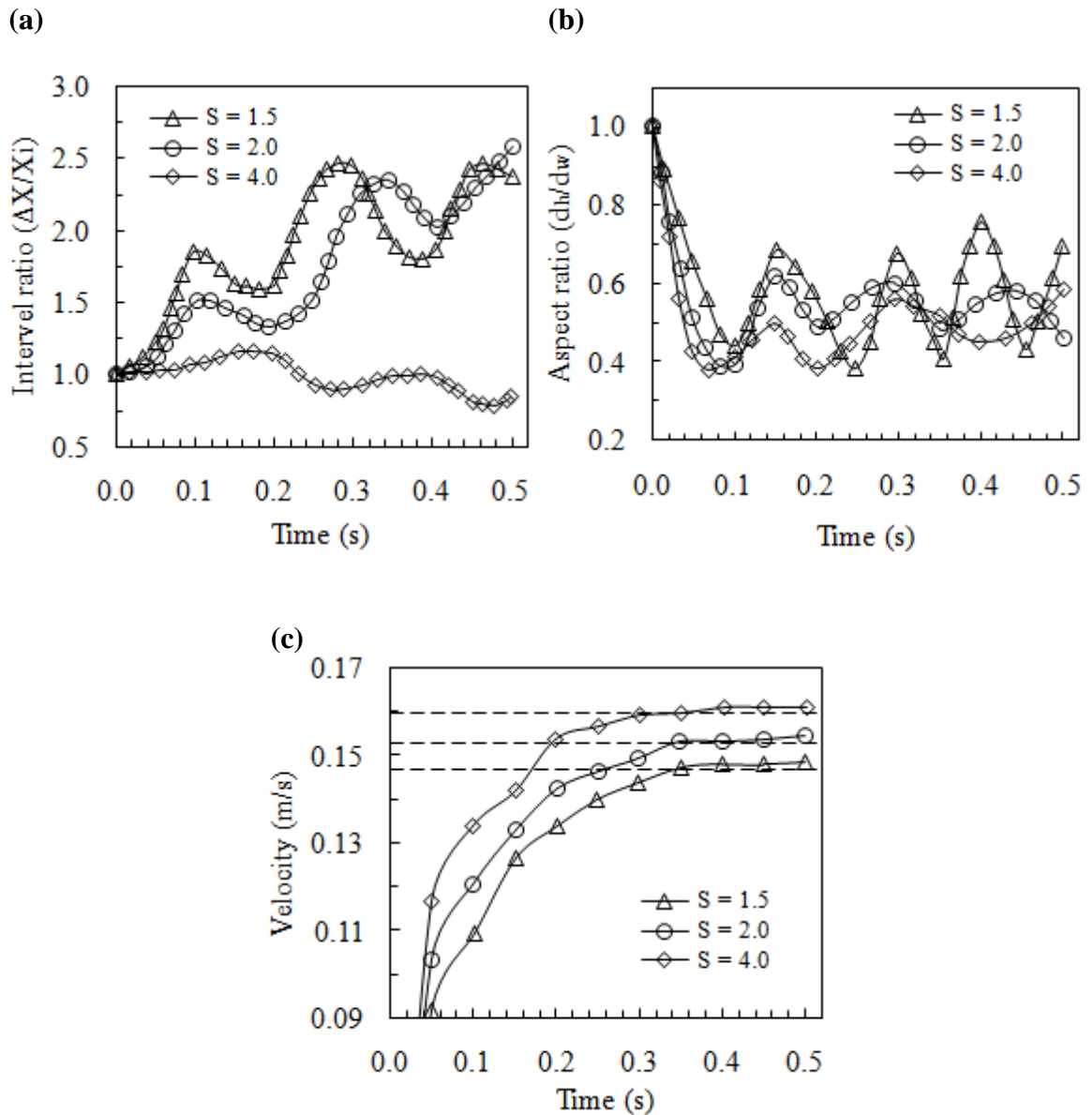


**Figure 5.10:** (a) Bubble interval ratio; (b) bubble aspect ratio; (c) and bubble rising velocity as a function of time at different initial bubble interval.

According to Figure 5.10a, the highest variation of bubbles rising trajectory, in horizontal direction, occurs for the low initial bubble intervals of  $S = 1.5$  and  $2.0$ . This is due to the stronger effect of repulsion as a result of large amount of vortices generated between the bubbles interval. While in the case of  $S = 4.0$ , the bubble rising trajectory in

horizontal direction remains less fluctuated, indicating the weak repulsion effect. Consequently from Figure 5.10b, for  $S = 1.5$ , the curve of bubble aspect ratio was fluctuated intensely, but less fluctuation was observed in  $S = 2.0$  curve. When the initial interval increased to  $S = 4.0$ , the variation of bubble shape was not varied so significantly compared to the other non-dimensional intervals. The change of bubble aspect ratio occurs due to the stronger vortexes field lying in the gap between bubbles pair that keep interacting with each other and also the interacting force in the horizontal direction which varies with time, as can be observed in Figure 5.11a and 5.11b.

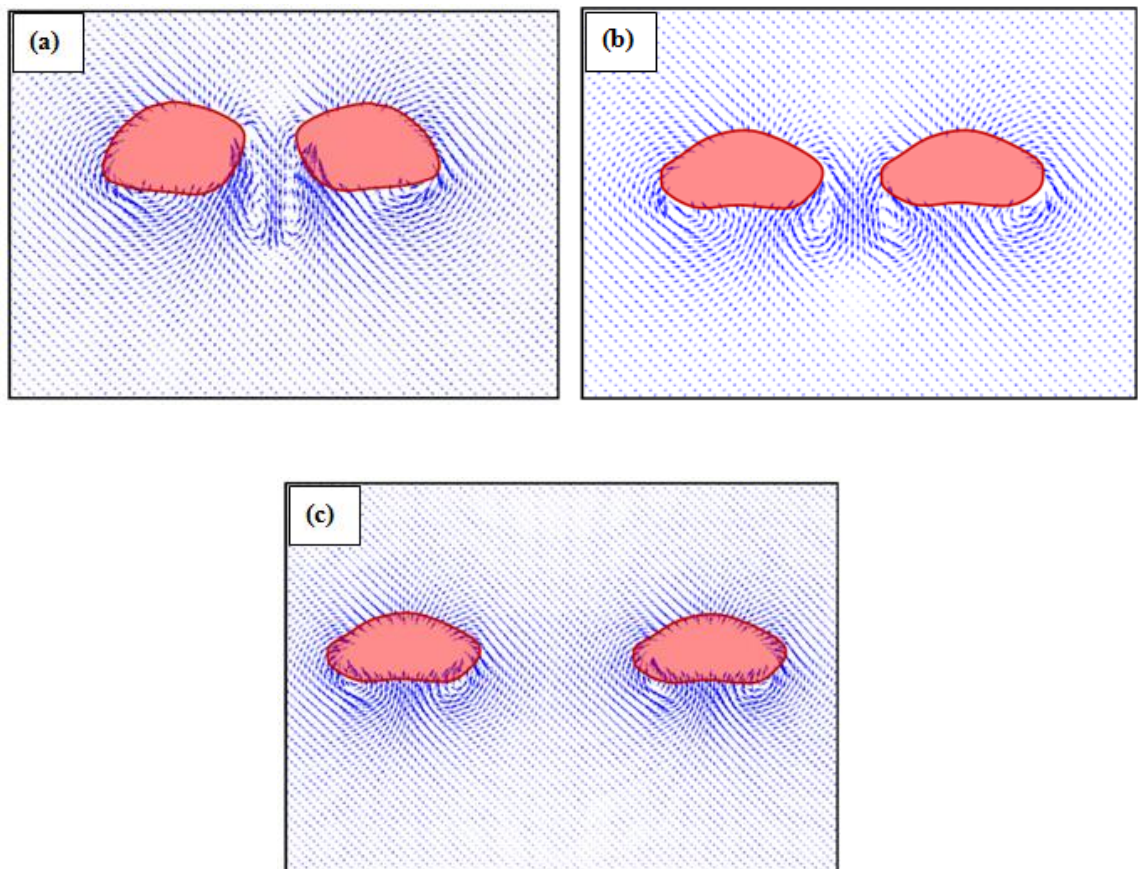


**Figure 5.11:** Velocity flow field around rising bubble pairs at  $t = 0.05s$ ; when (a)  $S = 1.5$ ; (b)  $S = 2.0$ ; (c)  $S = 4.0$ .

It is also worth noting that the bubbles rising velocity depends on the distance between bubbles. As can be seen in Figure 5.10c, the bubbles pair with initial interval  $S = 4.0$  was observed to reach the terminal velocity  $0.16 \text{ m/s}$ , which is higher than those with  $S$

= 2.0 and 1.5. It means that the vertical motion of bubbles with small distance is weakened by their repulsive effect in horizontal direction, and the terminal velocity of bubbles pair would increase with the increase of initial bubble interval due to weaker vortex field between the bubbles gap, as can be observed in Figure 5.11c. So it is reasonable to conclude that bubble-bubble interaction exhibits a repulsive effect, which decreases with the increase of distance between bubbles and the repulsive effect can be considered negligible at  $S \geq 4$ .

### 5.3.4 Three parallel bubble rise dynamics

#### 5.3.4.1 Lateral coalescence and breakup mechanism (Cases 50-68)

A coalescence mechanism of three parallel bubbles in horizontal direction is strongly linked to the initial flat gap between the bubbles and the properties of liquid. To find the critical flat gap, a trial and error method was considered. Figure 5.12 shows the non-dimensional critical flat gap ( $Sc$ ) of the bubble coalescence at different initial bubble sizes, non-dimensional liquid viscosities ( $\mu^*$ ) and surface tension coefficient ( $\sigma^*$ ). Considering as ‘ $Sc$ ’ is the non-dimensional critical flat gap of the bubble coalescence and defined as:  $Sc = hc/d_b$ . Where  $hc$  is the critical initial flat gap of the bubble for coalescence;  $d_b$  is the initial diameter of the bubble.

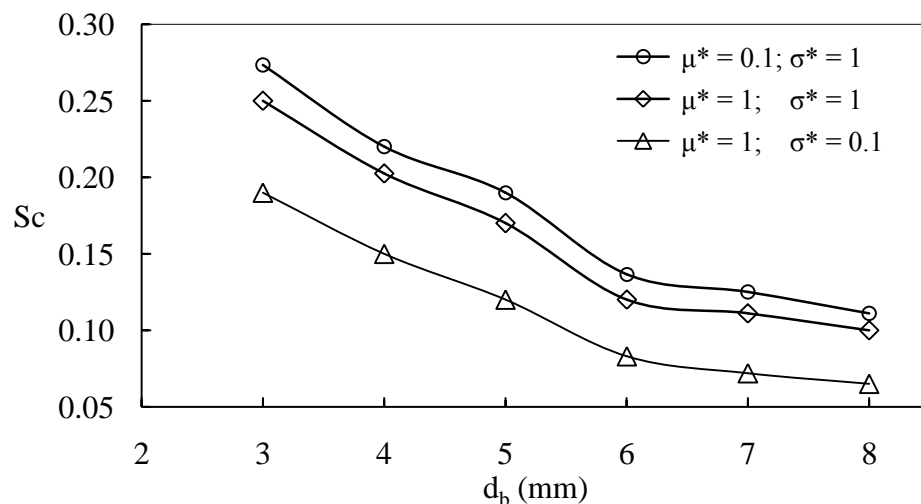


**Figure 5.12:** Non-dimensional critical flat gap of bubble coalescence with initial bubble diameter.

According to Figure 5.12, the non-dimensional critical flat gap ( $Sc$ ) of the bubble coalescence reduces with the increase of bubbles size. It has been found that, for reducing non-dimensional liquid viscosity,  $\mu^*$  from 1 to 0.1 at a fixed  $\sigma^* = 1$ , the critical flat gap of the bubble coalescence increases with the increase of bubble diameter. But the 'Sc' reduces with the reducing surface tension coefficient, at a constant  $\mu^* = 1$ ,  $\sigma^*$  is from 1 to 0.1.

Several lateral coalescence characteristic and breakup mechanism of the three parallel bubbles and shape of the bubble were displayed in Figure 5.13 at 'Sc' condition for the three different diameters of bubble, non-dimensional liquid viscosity ( $\mu^*$ ) and non-dimensional surface tension coefficient ( $\sigma^*$ ) of the fluid. As displayed in Figure 5.13a and 5.13b, the effect of initial bubble sizes of 4 mm and 6 mm diameter at a fixed liquid viscosity and surface tension coefficient ( $\mu^* = \sigma^* = 1$ ) are simulated. In this study, the lateral coalescence process of 4 mm size of three parallel bubbles (see in Figure 5.13a) is a similar approach through experiment and simulation observation by Sanada, Sato, Shirota, & Watanabe (2009) and RH Chen et al. (2011), respectively. The rising of three coalescing bubbles is deforming more in flat direction (typically at  $t = 0.020s$  to  $0.029s$ ) and finally adapted into ellipsoidal shape at  $0.13s$  as observed in Figure 5.13a. For initial size of 6 mm bubble (see in Figure 5.13b), a V-shaped bubble has developed first at  $t = 0.042s$ . The V-shaped bubble became dumbbell like shape at  $t = 0.081s$  and finally breakup into two daughter bubble at  $t = 0.091s$  as seen in Figure 5.13b. The velocity field surrounding the combined bubble before bubble breakup is shown in Figure 5.14a. It is observed that the fluid on the upper surface of the merge bubble is approximately stationary. It appeared that the right and left side portions of the merge bubble go up more rapidly than the intermediate portion. The intermediate portion of the combined bubble grew up as slender and ultimately it ruptured.

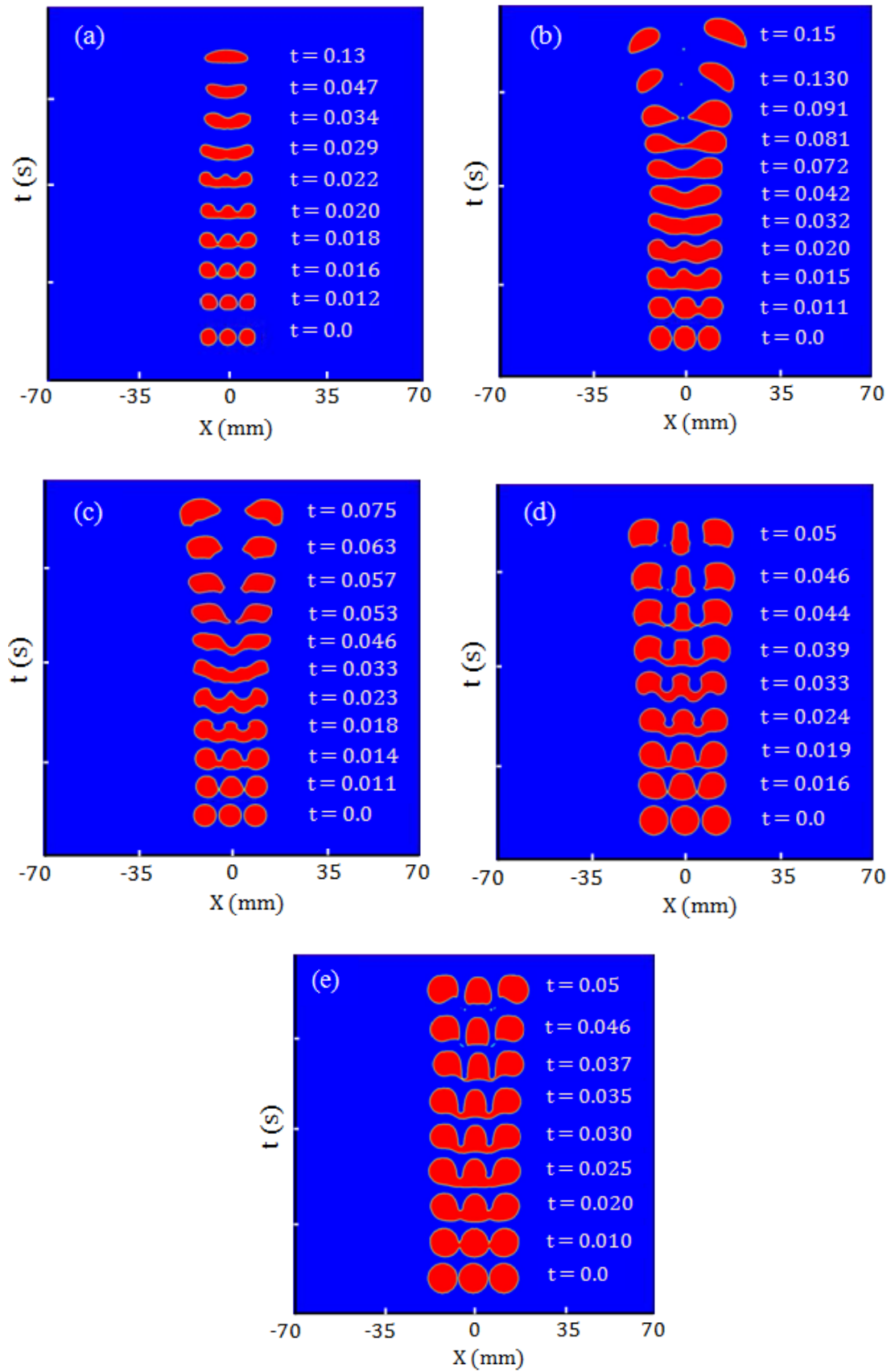


**Figure 5.13:** Three parallel bubble coalescence process; (a)  $d_b = 4$  mm,  $\mu^* = \sigma^* = 1$ ,  $Sc = 0.2025$ ; (b)  $d_b = 6$  mm,  $\mu^* = \sigma^* = 1$ ,  $Sc = 0.12$ ; (c)  $d_b = 6$  mm,  $\mu^* = 0.1$ ,  $\sigma^* = 1$ ,  $Sc = 0.136$ ; (d)  $d_b = 8$  mm,  $\mu^* = 0.1$ ,  $\sigma^* = 1$ ,  $Sc = 0.11$ ; (e)  $d_b = 8$  mm,  $\mu^* = 1$ ,  $\sigma^* = 0.1$ ,  $Sc = 0.05$ .

Figure 5.13c and 5.13d represent the effect of initial bubble diameter of 6 mm and 8 mm at a fixed surface tension ( $\sigma^* = 1$ ) and reduced liquid viscosity,  $\mu^*$  from 1 to 0.1. The bubble with initial size of 6 mm (see in Figure 5.13c), a W-shaped bubble develops earlier at  $t = 0.023$ s and finally breaks up into two daughter bubbles at  $t = 0.053$ s as shown in Figure 5.13c. The bubble with initial diameter of 8 mm as shown in Figure 5.13d, a W-shaped bubble has developed lately at  $t = 0.033$ s and quick breakup into three daughter bubble at  $t = 0.044$ s. Whereas the middle daughter bubble appears like a Taylor bubble which is also appears for the reducing  $\sigma^*$  of 0.1, as can be seen in Figure 5.13e. Figure 5.14b and 5.14c shows, the velocity fields of the coalescence bubble before breakup for  $d_b = 6$  mm,  $t = 0.046$ s and  $d_b = 8$  mm,  $t = 0.039$ s, respectively. The coalescence bubble of 6 mm and 8 mm deforms easily because of the action of liquid jet in the downward direction into the vapour bridge and speeds up the breakup of the coalescence bubble.

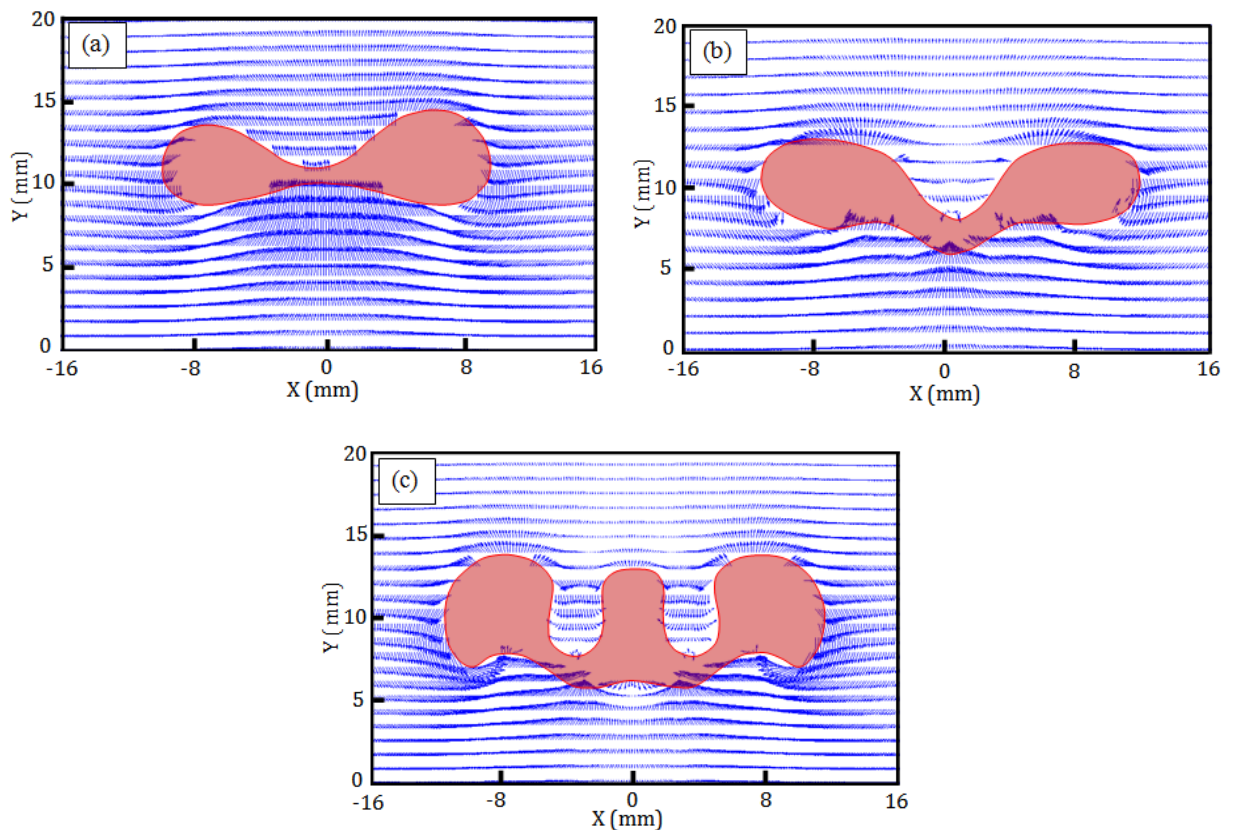
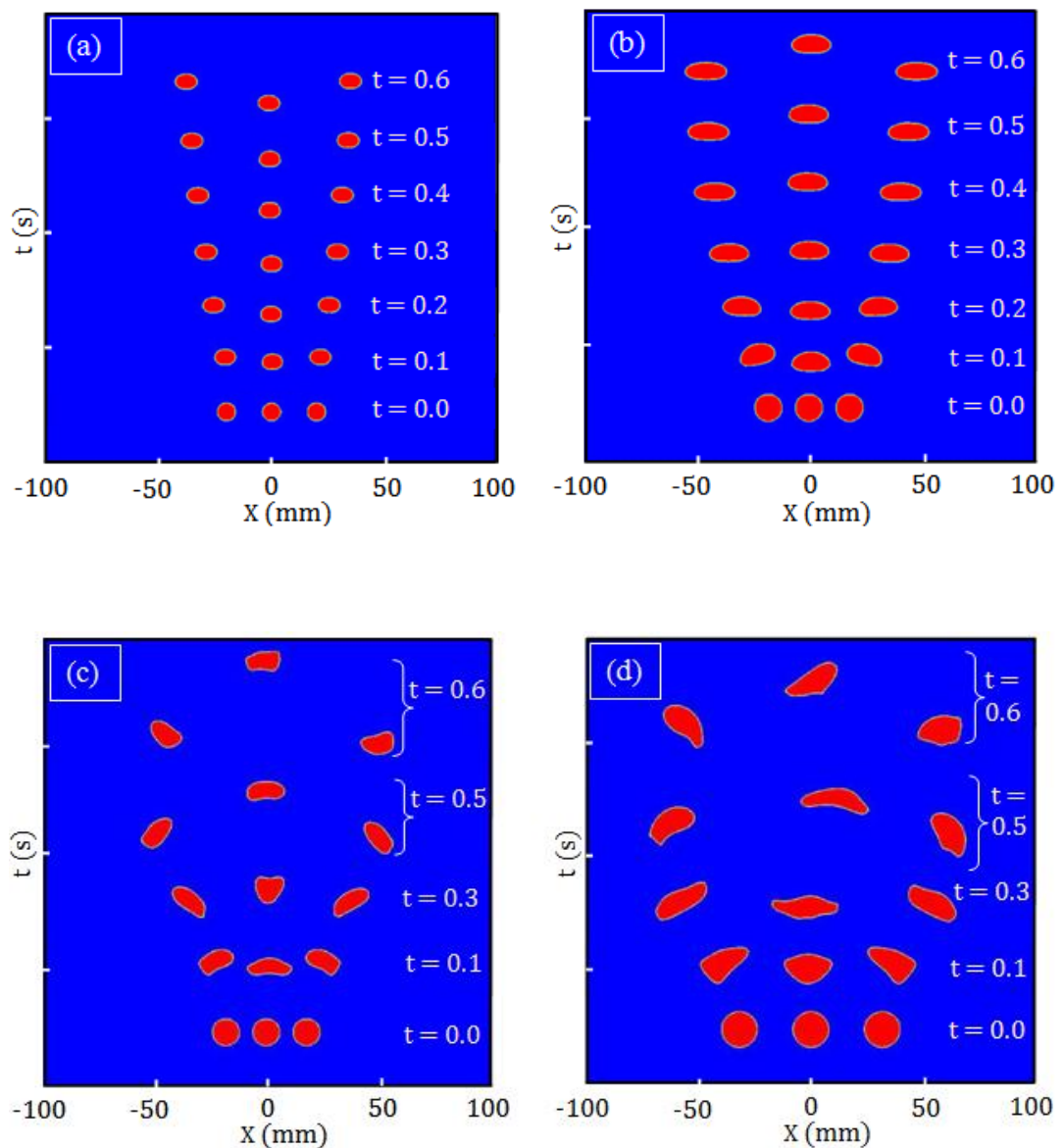


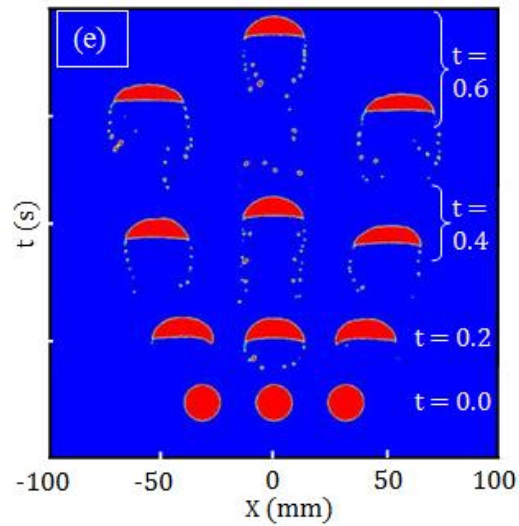
**Figure 5.14:** Velocity field around the coalescing bubble; (a)  $d_b = 6$  mm,  $\mu^* = \sigma^* = 1$ ,  $Sc = 0.12$ ,  $t = 0.081$ s; (b)  $d_b = 6$  mm,  $\mu^* = 0.1$ ,  $\sigma^* = 1$ ,  $Sc = 0.136$ ,  $t = 0.046$ s; (c)  $d_b = 8$  mm,  $\mu^* = 0.1$ ,  $\sigma^* = 1$ ,  $Sc = 0.11$ ,  $t = 0.039$ s.

### 5.3.4.2 Repulsive behaviour (Cases 69-83)

Figure 5.15 displays the rising trajectories of the three parallel bubbles with three different sizes in different non-dimensional fluid properties at different  $S$  conditions (after exit the  $Sc$  condition). As shown in Figure 5.15a, the initial size of bubbles is 4 mm,  $S = 1.5$  and as shown in Figure 5.15b, the initial size of bubbles is 6 mm,  $S = 0.5$  at a fixed  $\mu^* = \sigma^* = 1$ . It is observed that the bubble shape changes from very less ellipsoidal to more ellipsoidal shape (see in Figure 5.15a and 5.15b) and the rising path of the two side bubble was like as symmetric in these two cases.



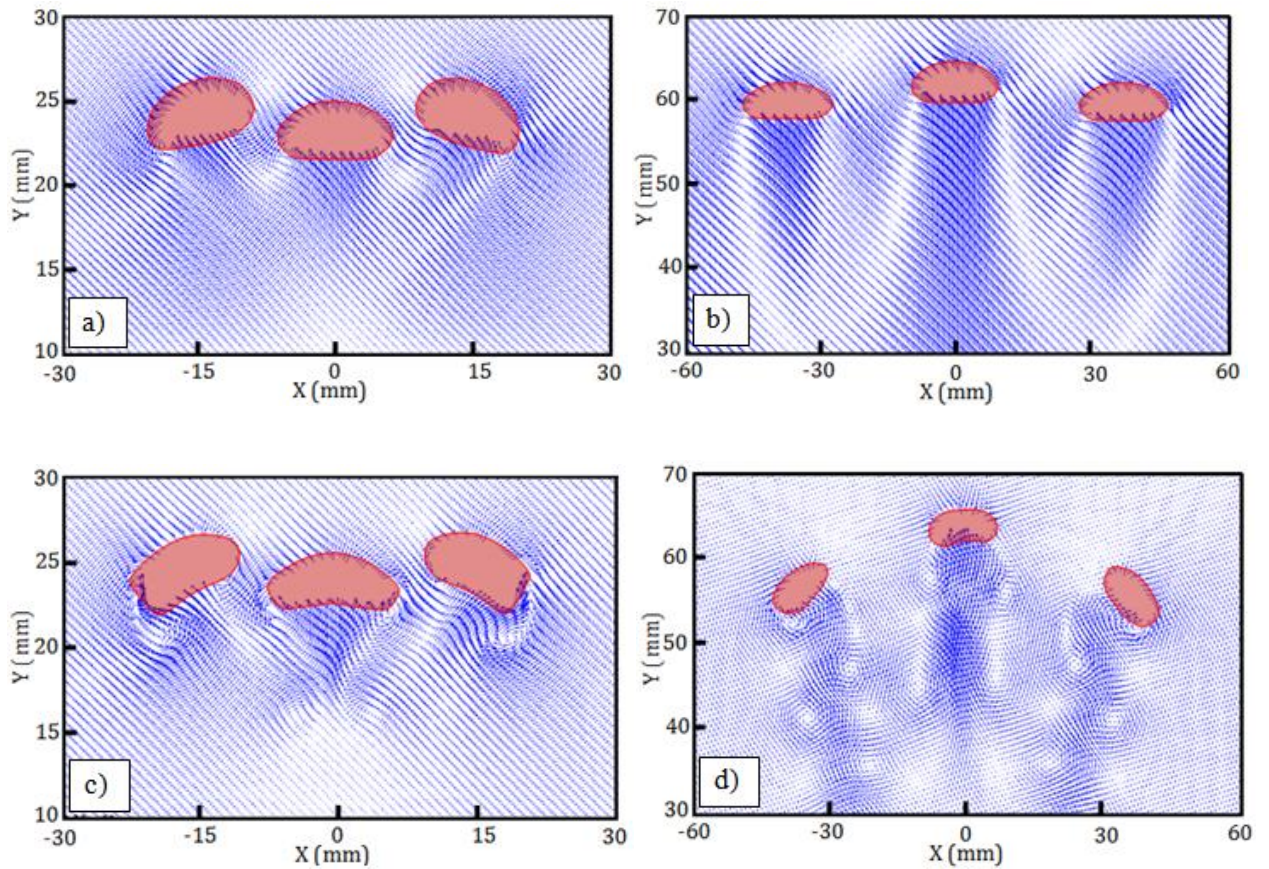
Continue Fig. 5.15



**Figure 5.15:** Three parallel bubble rising dynamics; (a)  $d_b = 4$  mm,  $\mu^* = \sigma^* = 1$ ,  $S = 1.5$  (b)  $d_b = 6$  mm,  $\mu^* = \sigma^* = 1$ ,  $S = 0.5$ ; (c)  $d_b = 6$  mm,  $\mu^* = 0.1$ ,  $\sigma^* = 1$ ,  $S = 0.5$ ; (d)  $d_b = 8$  mm,  $\mu^* = 0.1$ ,  $\sigma^* = 1$ ,  $S = 1$ ; (e)  $d_b = 8$  mm,  $\mu^* = 1$ ,  $\sigma^* = 0.1$ ,  $S = 1$ .

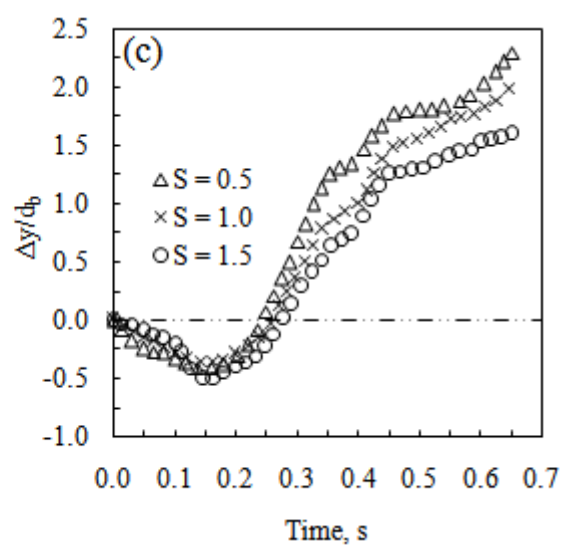
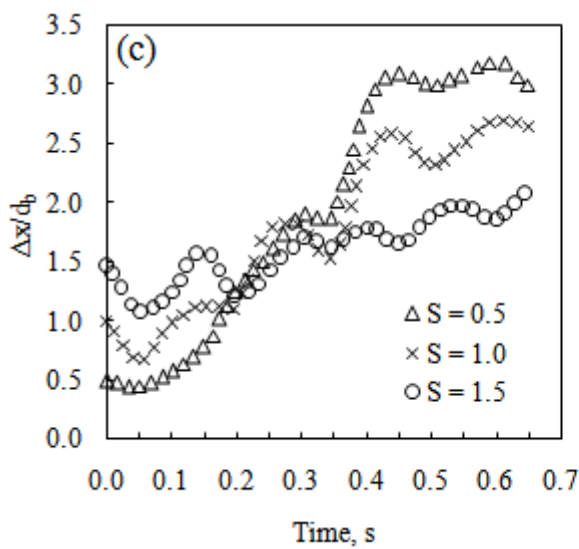
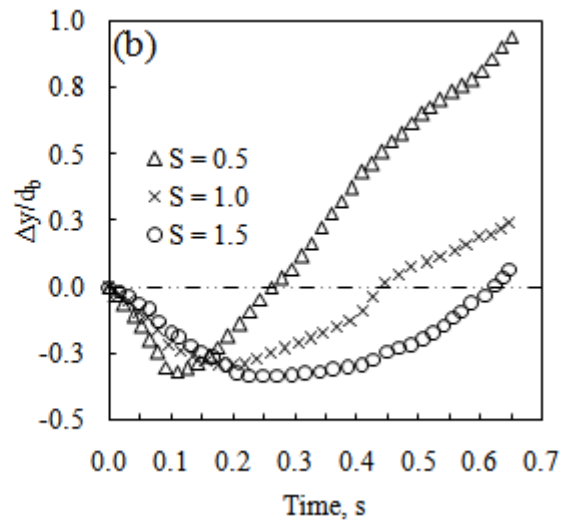
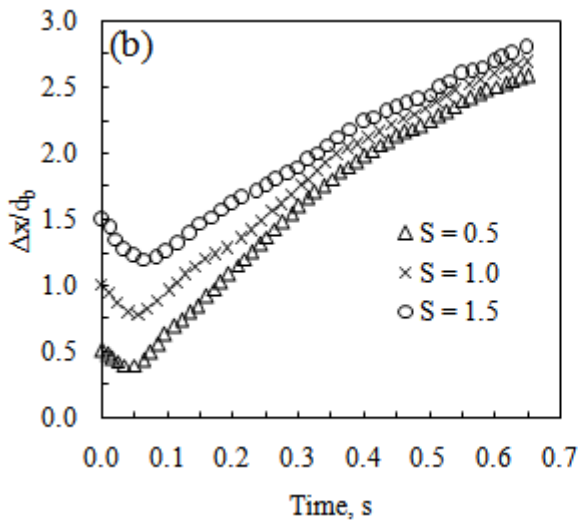
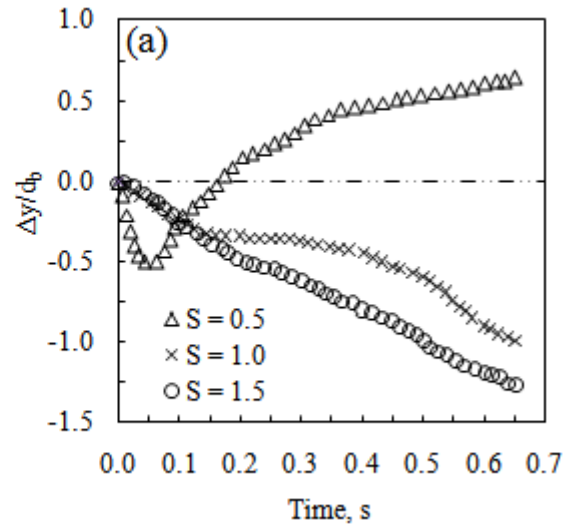
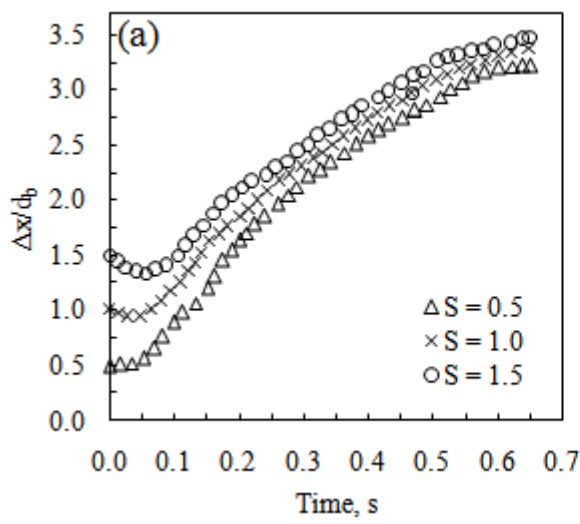
From the Figure 5.15b at  $S = 0.5$ , the middle bubble rise faster than the two side bubbles. These occurred due to over-lapped of liquid jet between the bubbles when  $S$  is relatively small, as shown in Figure 5.16a at  $t = 0.1$ s. Finally a stronger liquid jet pushed behind the middle bubble as can be seen in Figure 5.16b at  $t = 0.5$ s. Therefore, force of the buoyancy is stronger than the gravitation force on the middle bubble.

Figure 5.17 shows the non-dimensional horizontal distance ( $\Delta X/d_b$ ) and vertical distance between the middle and two side bubbles ( $\Delta Y$ ) that normalized by initial bubble size ( $d_b$ ). As illustrated in Figure 5.17a and 5.17b, with the increases of  $S$  (initial bubble gap), the vertical distance between the middle and two side bubbles ( $\Delta Y/d_b$ ) reduces negatively in value of 0.5 at  $S = 0.5$  (Figure 5.17a). Particularly at  $S = 1.5$ , representing that the interactions between the three bubbles have no significant result on vertical distance. Because of the increment of  $S$ , the strength of the interaction between the three bubbles was reduced by velocity flow field and the flat gap of the bubble moves to stable condition.



**Figure 5.16:** Velocity field around the middle bubble for (a)  $d_b = 6$  mm,  $\mu^* = \sigma^* = 1$ ,  $S = 0.5$ ,  $t = 0.1$ s; (b)  $d_b = 6$  mm,  $\mu^* = \sigma^* = 1$ ,  $S = 0.5$ ,  $t = 0.5$ s; (c)  $d_b = 6$  mm,  $\mu^* = 0.1$ ,  $\sigma^* = 1$ ,  $S = 0.5$ ,  $t = 0.1$ s; (d)  $d_b = 6$  mm,  $\mu^* = 0.1$ ,  $\sigma^* = 1$ ,  $S = 0.5$ ,  $t = 0.5$ s.

As shown in Figure 5.15c, when the bubbles with initial size  $d_b = 6$  mm rising in low viscosity of  $\mu^* = 0.1$ , the bubbles adopted typical irregular shape from ellipsoidal shape. The irregular shape of bubble developed due to development of an excess vortex of fluid as can be seen in Figure 5.16c at  $t = 0.1$ s. The excess vortex of fluid is continuing until the bubble reaches the top of the column as evidence in Figure 5.16d at  $t = 0.5$ s. It can be seen that from Figure 5.17c, the value of  $\Delta Y/d_b$  is also reducing when the increase of  $S$  from 0.5 to 1.5. But a variation has been observed in the non-dimensional horizontal distance value of  $\Delta X/d_b$ . Especially at  $S = 0.5$ , the bubble moves faster in horizontal direction. Thus the reduction of  $S$  in low viscosity of fluid, the oscillation of the bubbles in horizontal direction is significant than the vertical distance.



Continue Fig. 5.17

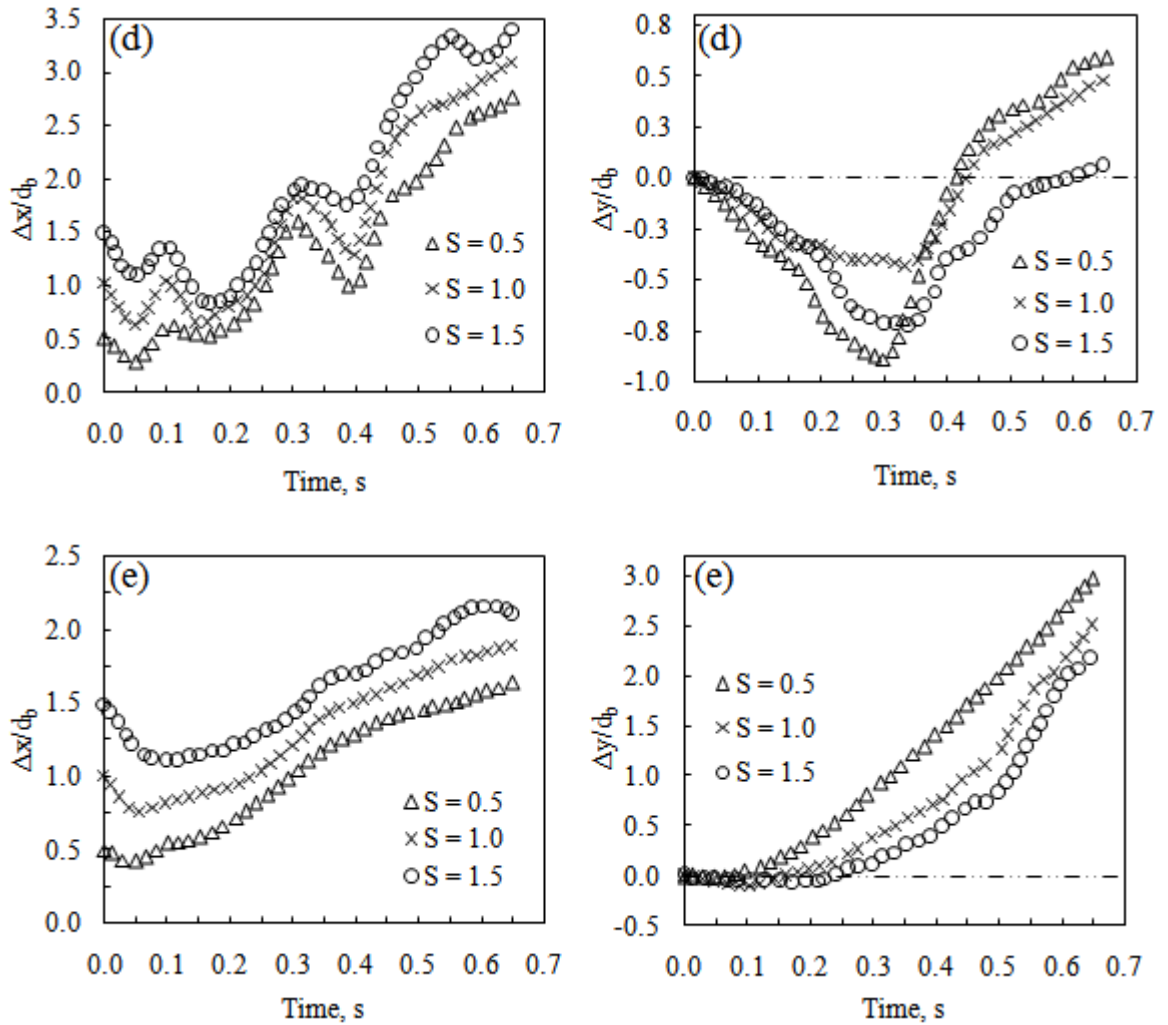


**Figure 5.17:** Effect of initial bubble gap for (a)  $d_b = 4$  mm,  $\mu^* = \sigma^* = 1$ ; (b)  $d_b = 6$  mm,  $\mu^* = \sigma^* = 1$ ; (c)  $d_b = 6$  mm,  $\mu^* = 0.1$ ,  $\sigma^* = 1$ ; (d)  $d_b = 8$  mm,  $\mu^* = 0.1$ ,  $\sigma^* = 1$ ; (e)  $d_b = 8$  mm,  $\mu^* = 1$ ,  $\sigma^* = 0.1$ .

As shown in Figure 5.15d, the shape of bubble has become more irregular and more oscillation of the bubbles, when the initial bubble size has increased to 8 mm. Figure 5.17d, e, the increment of  $\Delta Y/d_b$  was negative value in a certain period typically,  $t = 0.3$ s and again increased with positive value with the increasing of  $S$ . Furthermore, an oscillation of the bubble for the value of  $\Delta X/d_b$  which occurred due to strong resistance from fluid over increase size of bubble as well as the force of the liquid jet becomes weakened. Figure 5.15e represents the bubble with initial size of 8 mm, the rise and shape changed behaviour in low surface tension fluid,  $\sigma^* = 0.1$ . It has also been observed that the bubble changes the ellipsoidal cap shape and break up as a number of

small daughter bubbles. These types of bubble breakup may enhance the mixing as well as heat and mass transfer rate. As we can see from Figure 5.17e, the value of  $\Delta Y/d_b$  increases positively with decrease of  $S$ ; no oscillation of the bubble with the horizontal distance between the middle and two side bubbles ( $\Delta X/d_b$ ) with increasing time.

It can be seen from Figure 5.15, the rising behaviour of the three parallel bubbles in horizontal direction is similar as the rise behaviour of the two parallel bubbles in viscous fluid (Legendre et al., 2003; Yu et al., 2011). However, it is found that there are no attraction behaviour in flat direction to rise of the three parallel bubbles, when ' $S$ ' was increased from ' $S_c$ '. The initial bubble size and fluid properties have great impact on rise dynamics and shape of bubbles. Additionally, it is considered that there are two opposing mechanism that affect the rising velocities of multiple bubbles. The first one is the hydrodynamics interference between bubbles reduces the middle bubble rise velocity. The 2<sup>nd</sup> one is that the reduction of fluid viscosity and surface tension coefficient increase the rise velocity of the bubbles.

#### **5.4 Conclusion**

In this study, the VOF-CSF method have been used to investigate the effect of reduced viscosity and surface tension coefficient on co-axial and three parallel bubble coalescence process as well as rise characteristics. The conclusions of this study are-

- It is found that the coalescence time of two co-axial bubbles decreases with the reducing surface tension coefficient and reducing liquid viscosity.
- For the parallel bubbles coalescence, non-dimensional critical flat gap of bubble coalescence reduces with the increase of bubble diameter under reduction of surface tension coefficient. But it increases with reduction of liquid viscosity.
- When the initial flat gaps of bubble ( $S$ ) are larger from the critical flat gap ( $S_c$ ) of bubble coalescence, the parallel bubble enchanted itself by repulsive effect.

## CHAPTER 6

### CONCLUSION AND RECOMANDATIONS

#### 6.1 Contributions of this study

The main objectives of the present work was to obtain a detail information of a single bubble formation through an orifice and to rise characteristics of a free bubble in a bubble column using computational fluid dynamics (CFD). The results were carried out with different parametric condition. The work has demonstrated the capacity and accuracy of the CFD method to predict bubble formation, bubble shape, bubble departure diameter and bubble coalescence process etc., for all the cases simulated. The following part provides a summary of the main conclusions of this work.

#### *Effect of orifice diameter*

Computational methods of VOF-CSF have been used to study the effect of orifice diameter at constant inlet gas velocity, the effect of Bond number (which represent the variation of surface tension coefficient) and the effect of Reynolds number (which represent the variation of liquid viscosity) on bubble formation. The study shows that under the constant gas inlet velocity boundary condition, the use of a larger orifice diameter (1.5 mm) accelerates the decreasing of the bubble contact angle from an obtuse angle ( $100^\circ$  to  $42^\circ$ ) to an acute angle ( $45^\circ$  to  $130^\circ$ ). A larger orifice diameter (1.5 mm) forms a bigger bubble and the bubble requires a shorter time (0.11 s) to detach from the orifice. A leading bubble requires a longer time to detach from an orifice in comparison to the following the second bubble but interestingly the third bubble detaches much quicker than the second bubble. An increase of Bond from 0.047 to 0.16 speeds up the bubble pinch-off. However, a further increase in  $Bo_\sigma$  (e.g., 0.17~ 0.47) slows down the bubble pinch-off. An increase of Reynolds number from 1.58 to 120 speeds up the

bubble pinch-off and forms a smaller bubble neck height due to strong vortex ring near the bubble neck region.

### ***Effect of column angle to rise a single bubble***

Two dimensional (2D) CFD analysis were carried out using a couple level set volume of fluid (CLSVOF) numerical method in the current study to investigate the effects of wall of trapezoidal columns to rising characteristics of a single bubble such as rise velocity, rising trajectory, bubble size and shape. The study shows that the bubble rising velocity reduced from 0.20 m/s to 0.06 m/s with the increase of trapezoidal inclination angles from 0° to 9°. The bubble rising vertical height at a given particular time of 0.16s reduces with the increase of trapezoidal inclination angles. The trapezoidal column enhances the lateral spatial distribution of a bubble to left and right of the column and this may enhance mixing in the column. It also enhances the changes in bubble shape with the increase of the time or the vertical height representing a change in the bubble shape from elliptic to circle and vice versa. The use trapezoidal cavity give potential benefits of increase of residing time for bubble in a column which increase the gas hold up in column and enhancement the movement of bubble. Consequently, this may improve the heat and mass transfer in the column.

### ***Bubble coalescence process***

In this work, the VOF-CSF method was used to investigate the effect of reduced viscosity and the effect of surface tension coefficient on co-axial and three parallel bubble coalescence processes as well as rising characteristics. For co-axial bubble coalescence, the study shows that the bubble coalescence time decreases with reduced liquid viscosity and surface tension coefficient. Faster bubble coalescence has been obtained for the reduction of liquid viscosity of  $\mu^* < 0.25$ . The bubble shape shows a

noticeable alteration, when the bubble diameter has been increased in reduced liquid viscosity and surface tension coefficient. Consequently, an ellipsoidal, oblate ellipsoidal cap and skirted shape of following bubble were found.

For the three parallel bubbles coalescence, the non-dimensional critical flat gap of bubble coalescence decreased with the increase of bubble diameter under reduction of surface tension coefficient but increased with reduced liquid viscosity. After that, the coalescing of three parallel bubbles broke up into two daughter bubbles, while the initial bubble diameter was increased or the fluid viscosity was reduced. The three initial parallel bubbles diameter was further increased in reduced fluid viscosity or surface tension coefficient. As a consequence, three daughter bubbles formed. When the initial flat bubble gaps were larger than the critical flat gap of bubble coalescence, the parallel bubble enchanted itself by repulsive effect. The normalized vertical and horizontal distance between the bubbles varied dramatically for increased bubble size and reduced liquid viscosity due to the velocity field structure.

## **6.2 Suggestion for future study**

Main future extensions can include follows:

- The bubble formation in non-Newtonian fluids through the single or multiple orifices using varied inlet gas velocity condition may represent the better understanding. Because, non-Newtonian fluids mainly use in industrial purposes.
- The experimental study of changes of column angle should be carried out, which has the potential to provide the better mathematical development and to increase the confidence level of the numerical study.
- Multiple bubble coalescence in non-Newtonian fluid should be carried out, which provide a better physical understanding of complex bubble coalescence process.

## REFERENCES

- Ahmadzadeh, M, Saranjam, B, Hoseini Fard, A, & Binesh, AR. (2013). Numerical simulation of sphere water entry problem using Eulerian–Lagrangian method. *Applied Mathematical Modelling*.
- Akhtar, Abid, Pareek, Vishnu, & Tadé, Moses. (2007). CFD simulations for continuous flow of bubbles through gas-liquid columns: Application of VOF method. *Chemical Product and Process Modeling*, 2(1).
- Albadawi, A, Donoghue, DB, Robinson, AJ, Murray, DB, & Delauré, YMC. (2013). Influence of surface tension implementation in Volume of Fluid and coupled Volume of Fluid with Level Set methods for bubble growth and detachment. *International Journal of Multiphase Flow*, 53, 11-28.
- Badam, VK, Buwa, V, & Durst, F. (2007). Experimental investigations of regimes of bubble formation on submerged orifices under constant flow condition. *The Canadian Journal of Chemical Engineering*, 85(3), 257-267.
- Bari, Sergio Di, & Robinson, Anthony J. (2013). Experimental study of gas injected bubble growth from submerged orifices. *Experimental Thermal and Fluid Science*, 44, 124-137.
- Bhaga, D, & Weber, ME. (1980). In-line interaction of a pair of bubbles in a viscous liquid. *Chemical Engineering Science*, 35(12), 2467-2474.
- Bhaga, Dahya, & Weber, ME. (1981). Bubbles in viscous liquids: shapes, wakes and velocities. *Journal of Fluid Mechanics*, 105(1), 61-85.
- Bhavaraju, SM, Mashelkar, RA, & Blanch, HW. (1978). Bubble motion and mass transfer in non-Newtonian fluids: Part I. Single bubble in power law and Bingham fluids. *AIChE Journal*, 24(6), 1063-1070.
- Bolaños-Jiménez, R, Sevilla, A, Martínez-Bazán, C, & Gordillo, JM. (2008). Axisymmetric bubble collapse in a quiescent liquid pool. II. Experimental study. *Physics of Fluids*, 20(11), 112104-112104-112112.
- Bozzano, G, & Dente, M. (2001). Shape and terminal velocity of single bubble motion: a novel approach. *Computers & chemical engineering*, 25(4), 571-576.
- Brackbill, JU, Kothe, Douglas B, & Zemach, C1. (1992). A continuum method for modeling surface tension. *Journal of computational physics*, 100(2), 335-354.
- Buwa, Vivek V, & Ranade, Vivek V. (2002). Dynamics of gas–liquid flow in a rectangular bubble column: experiments and single/multi-group CFD simulations. *Chemical Engineering Science*, 57(22), 4715-4736.
- Cai, Ziqi, Bao, Yuyun, & Gao, Zhengming. (2010). Hydrodynamic behavior of a single bubble rising in viscous liquids. *Chinese Journal of Chemical Engineering*, 18(6), 923-930.

- Chakraborty, I, Biswas, G, & Ghoshdastidar, PS. (2011). Bubble generation in quiescent and co-flowing liquids. *International Journal of Heat and Mass Transfer*, 54(21), 4673-4688.
- Chakraborty, I, Ray, B, Biswas, G, Durst, F, Sharma, A, & Ghoshdastidar, PS. (2009a). Computational investigation on bubble detachment from submerged orifice in quiescent liquid under normal and reduced gravity. *Physics of Fluids (1994-present)*, 21(6), 062103.
- Chakraborty, I, Ray, B, Biswas, G, Durst, F, Sharma, A, & Ghoshdastidar, PS. (2009b). Computational investigation on bubble detachment from submerged orifice in quiescent liquid under normal and reduced gravity. *Physics of Fluids*, 21, 062103.
- Chen, Li, Li, Yuguo, & Manasseh, Richard. (1998). *The coalescence of bubbles-a numerical study*. Paper presented at the Third International Conference on Multiphase Flow, ICMF.
- Chen, RC, & Chou, IS. (1998). Wake structure of a single bubble rising in a two-dimensional column. *Experimental thermal and fluid science*, 17(3), 165-178.
- Chen, RH, Tian, WX, Su, GH, Qiu, SZ, Ishiwatari, Yuki, & Oka, Yoshiaki. (2011). Numerical investigation on coalescence of bubble pairs rising in a stagnant liquid. *Chemical Engineering Science*, 66(21), 5055-5063.
- Chesters, A. K. (1991). The modelling of coalescence processes in fluid-liquid dispersions: a review of current understanding. *Chemical engineering research & design*, 69(A4), 259-270.
- Chi, BK, & Leal, LG. (1989). A theoretical study of the motion of a viscous drop toward a fluid interface at low Reynolds number. *Journal of Fluid Mechanics*, 201, 123-146.
- Clift, Grace. (1978). Weber 1978 R. Clift, JR Grace, ME Weber, Bubbles, drops: and particles Academic Press, New York.
- Clift, Roland. (2005). *Bubbles, drops, and particles*: Dover Publications. com.
- Coutanceau, Madeleine, & Thizon, Patrick. (1981). Wall effect on the bubble behaviour in highly viscous liquids. *Journal of Fluid Mechanics*, 107, 339-373.
- Crabtree, JR, & Bridgwater, J. (1971). Bubble coalescence in viscous liquids. *Chemical Engineering Science*, 26(6), 839-851.
- Davidson, JF, & Schüler, BOG. (1997). Bubble formation at an orifice in a viscous liquid. *Chemical Engineering Research and Design*, 75, S105-S115.
- Davies, RM, & Taylor, Geoffrey. (1950). The mechanics of large bubbles rising through extended liquids and through liquids in tubes. *Proceedings of the Royal Society of London. Series A. Mathematical and Physical Sciences*, 200(1062), 375-390.

- Deckwer, W-D, & Schumpe, A. (1993). Improved tools for bubble column reactor design and scale-up. *Chemical Engineering Science*, 48(5), 889-911.
- Di Bari, S, Lakehal, D, & Robinson, AJ. (2013). A numerical study of quasi-static gas injected bubble growth: Some aspects of gravity. *International Journal of Heat and Mass Transfer*, 64, 468-482.
- Di Marco, P, Forgione, N, & Grassi, W. (2005). Quasi-static formation and detachment of gas bubbles at a submerged orifice: experiments, theoretical prediction and numerical calculations. *Paper presented at the XXII Congresso Nazionale UIT sulla Trasmissione del Calore, Parma, Guigno*.
- W. Fritz (1963). Grundlagen der Wärmeübertragung beim Verdampfen von Flüssigkeiten. *Chemie Ingenieur Technik*, 35(11), 753 - 764.
- Fan, Liang-Shih, & Tsuchiya, Katsumi. (1990). *Bubble wake dynamics in liquids and liquid-solid suspensions*: Butterworth-Heinemann Stoneham.
- Fluent, Fluent. (2006). 6.3 user's guide. *Fluent Inc*.
- Gaddis, ES, & Vogelpohl, A. (1986). Bubble formation in quiescent liquids under constant flow conditions. *Chemical Engineering Science*, 41(1), 97-105.
- Gerlach, D, Alleborn, N, Buwa, V, & Durst, F. (2007). Numerical simulation of periodic bubble formation at a submerged orifice with constant gas flow rate. *Chemical engineering science*, 62(7), 2109-2125.
- D. Gerlach, D, Biswas, G, Durst, F & Kolobaric, V. (2005). Quasi-static bubble formation on submerged orifices. *Int. J. Heat Mass Transf.*, 48 (2), 425-438.
- Grace, JR. (1973). Shapes and velocities of bubbles rising in infinite liquids. *Trans. Inst. Chem. Eng.*, 51(2), 116-120.
- Gupta, Ankur, & Roy, Shantanu. (2013). Euler–Euler simulation of bubbly flow in a rectangular bubble column: Experimental validation with Radioactive Particle Tracking. *Chemical Engineering Journal*, 225, 818-836.
- Higuera, FJ. (2005). Injection and coalescence of bubbles in a very viscous liquid. *Journal of Fluid Mechanics*, 530, 369-378.
- Hirt, Cyril W, & Nichols, Billy D. (1981). Volume of fluid (VOF) method for the dynamics of free boundaries. *Journal of computational physics*, 39(1), 201-225.
- Hua, Jinsong, & Lou, Jing. (2007). Numerical simulation of bubble rising in viscous liquid. *Journal of Computational Physics*, 222(2), 769-795.
- Jamialahmadi, M, Branch, C, & Müller-Steinhagen, H. (1994). Terminal bubble rise velocity in liquids. *Chemical engineering research & design*, 72(1), 119-122.
- Jamialahmadi, M, Zehtaban, MR, Müller-Steinhagen, H, Sarrafi, A, & Smith, JM. (2001). Study of bubble formation under constant flow conditions. *Chemical Engineering Research and Design*, 79(5), 523-532.

- Kim, Ieewan, Kamotani, Yasuhiro, & Ostrach, Simon. (1994). Modeling bubble and drop formation in flowing liquids in microgravity. *AIChE journal*, 40(1), 19-28.
- Krishna, R, & Sie, ST. (2000). Design and scale-up of the Fischer–Tropsch bubble column slurry reactor. *Fuel Processing Technology*, 64(1), 73-105.
- Krishna, R, Urseanu, MI, Van Baten, JM, & Ellenberger, J. (1999). Wall effects on the rise of single gas bubbles in liquids. *International communications in heat and mass transfer*, 26(6), 781-790.
- Krishna, R, & Van Baten, JM. (1999). Rise characteristics of gas bubbles in a 2D rectangular column: VOF simulations vs experiments. *International communications in heat and mass transfer*, 26(7), 965-974.
- Krishna, R, Wilkinson, PM, & Van Dierendonck, LL. (1991). A model for gas holdup in bubble columns incorporating the influence of gas density on flow regime transitions. *Chemical engineering science*, 46(10), 2491-2496.
- Krishna, Rajamani, De Swart, Jeroen WA, Hennephof, Danielle E, Ellenberger, Jürg, & Hoefsloot, Hubertus CJ. (1994). Influence of increased gas density on hydrodynamics of bubble-column reactors. *AIChE journal*, 40(1), 112-119.
- Kulkarni, AA, Ekambara, K, & Joshi, JB. (2007). On the development of flow pattern in a bubble column reactor: experiments and CFD. *Chemical Engineering Science*, 62(4), 1049-1072.
- Kulkarni, Amol A, & Joshi, Jyeshtharaj B. (2005). Bubble formation and bubble rise velocity in gas-liquid systems: A review. *Industrial & engineering chemistry research*, 44(16), 5873-5931.
- Legendre, Dominique, Magnaudet, Jacques, & Mougin, Guillaume. (2003). Hydrodynamic interactions between two spherical bubbles rising side by side in a viscous liquid. *Journal of Fluid Mechanics*, 497, 133-166.
- Li, H, & Prakash, A. (2000). Influence of slurry concentrations on bubble population and their rise velocities in a three-phase slurry bubble column. *Powder technology*, 113(1), 158-167.
- Li, Qiang, Ouyang, Jie, Yang, Binxin, & Li, Xuejuan. (2012). Numerical simulation of gas-assisted injection molding using CLSVOF method. *Applied Mathematical Modelling*, 36(5), 2262-2274.
- Li, Yong, Zhang, Jianping, & Fan, Liang-Shih. (2000). Discrete-phase simulation of single bubble rise behavior at elevated pressures in a bubble column. *Chemical engineering science*, 55(20), 4597-4609.
- Lin, T-J, Tsuchiya, K, & Fan, L-S. (1998). Bubble flow characteristics in bubble columns at elevated pressure and temperature. *AIChE journal*, 44(3), 545-560.
- Liu, Jingru Z, Chunying Fu, Taotao Ma, Youguang Li & Huaizhi. (2013). Numerical simulation of the interactions between three equal interval parallel bubbles rising in non Newtonian fluids. *Chemical Engineering Science*, 93 (3), 55-66.

- Ma, Dou, Liu, Mingyan, Zu, Yonggui, & Tang, Can. (2012). Two-dimensional volume of fluid simulation studies on single bubble formation and dynamics in bubble columns. *Chemical Engineering Science*, 72, 61-77.
- Manasseh, Richard, Yoshida, Shizuo, & Rudman, M. (1998). *Bubble formation processes and bubble acoustic signals*. Paper presented at the Third International Conference on Multiphase Flow, Lyon, France.
- Martinez, Jean-Michel, Chesneau, Xavier, & Zeghmati, Belkacem. (2005). Numerical and experimental studies of air bubbles coalescence in a quiescent water column. *International Journal of Chemical Reactor Engineering*, 3(1).
- Mendelson, Harvey D. (1967). The prediction of bubble terminal velocities from wave theory. *AIChE Journal*, 13(2), 250-253.
- Moo-Young, M, & Blanch, HW. (1981). *Design of biochemical reactors mass transfer criteria for simple and complex systems*: Springer.
- Ohta, Mitsuhiro, Kikuchi, Daisuke, Yoshida, Yutaka, & Sussman, Mark. (2007). Direct numerical simulation of the slow formation process of single bubbles in a viscous liquid. *Journal of chemical engineering of Japan*, 40(11), 939-943.
- Ohta, Mitsuhiro, Kikuchi, Daisuke, Yoshida, Yutaka, & Sussman, Mark. (2011). Robust numerical analysis of the dynamic bubble formation process in a viscous liquid. *International Journal of Multiphase Flow*, 37(9), 1059-1071.
- Okawa, Tomio, Tanaka, Tomoe, Kataoka, Isao, & Mori, Michitsugu. (2003). Temperature effect on single bubble rise characteristics in stagnant distilled water. *International journal of heat and mass transfer*, 46(5), 903-913.
- Oolman, Timothy O, & Blanch, Harvey W. (1986). Bubble coalescence in stagnant liquids. *Chemical Engineering Communications*, 43(4-6), 237-261.
- Osher, Stanley, & Fedkiw, Ronald P. (2001). Level set methods: an overview and some recent results. *Journal of Computational physics*, 169(2), 463-502.
- Otake, T, Tone, S, Nakao, K, & Mitsuhashi, Y. (1977). Coalescence and breakup of bubbles in liquids. *Chemical Engineering Science*, 32(4), 377-383.
- Pinto, AMFR, Pinheiro, Coelho, & Campos, Jblm. (1998). Coalescence of two gas slugs rising in a co-current flowing liquid in vertical tubes. *Chemical engineering science*, 53(16), 2973-2983.
- Rabha, Swapna S, & Buwa, Vivek V. (2010). Volume-of-fluid (VOF) simulations of rise of single/multiple bubbles in sheared liquids. *Chemical Engineering Science*, 65(1), 527-537.
- Raymond, F, & Rosant, J-M. (2000). A numerical and experimental study of the terminal velocity and shape of bubbles in viscous liquids. *Chemical Engineering Science*, 55(5), 943-955.

- Ribeiro Jr, Cláudio P, & Mewes, Dieter. (2006). On the effect of liquid temperature upon bubble coalescence. *Chemical engineering science*, 61(17), 5704-5716.
- Rider, W. J., & Kothe D.B. (1998). Reconstructing volume tracking. *Journal of Computational Physics*, 141 (2), 112-152.
- Salomons, Erik M, Blumrich, Reinhard, & Heimann, Dietrich. (2002). Eulerian time-domain model for sound propagation over a finite-impedance ground surface. Comparison with frequency-domain models. *Acta Acustica united with Acustica*, 88(4), 483-492.
- Sanada, Toshiyuki, Sato, Ayaka, Shirota, Minori, & Watanabe, Masao. (2009). Motion and coalescence of a pair of bubbles rising side by side. *Chemical Engineering Science*, 64(11), 2659-2671.
- Schäfer, R, Merten, C, & Eigenberger, G. (2002). Bubble size distributions in a bubble column reactor under industrial conditions. *Experimental Thermal and Fluid Science*, 26(6), 595-604.
- Stover, Richard L, Tobias, Charles W, & Denn, Morton M. (1997). Bubble coalescence dynamics. *AIChE journal*, 43(10), 2385-2392.
- Takada, Naoki, Misawa, Masaki, Tomiyama, Akio, & Hosokawa, Shigeo. (2001). Simulation of bubble motion under gravity by lattice Boltzmann method. *Journal of nuclear science and technology*, 38(5), 330-341.
- Tomiyama, A, Celata, GP, Hosokawa, S, & Yoshida, S. (2002). Terminal velocity of single bubbles in surface tension force dominant regime. *International Journal of Multiphase Flow*, 28(9), 1497-1519.
- Tryggvason, Grétar, Bunner, Bernard, Esmaeeli, Asghar, Juric, Damir, Al-Rawahi, N, Tauber, W, Jan, Y-J. (2001). A front-tracking method for the computations of multiphase flow. *Journal of Computational Physics*, 169(2), 708-759.
- Tse, Kathryn, Martin, Thomas, Mcfarlane, Caroline M, & Nienow, Alvin W. (1998). Visualisation of bubble coalescence in a coalescence cell, a stirred tank and a bubble column. *Chemical engineering science*, 53(23), 4031-4036.
- Tsuchiya, Katsumi, & Fan, Liang-Shih. (1988). Near-wake structure of a single gas bubble in a two-dimensional liquid-solid fluidized bed: vortex shedding and wake size variation. *Chemical engineering science*, 43(5), 1167-1181.
- Tsuge, Hideki, Hamamoto, Shin-ichi, & Hibino, Shin-ichi. (1984). Wall effect on the behaviour of single bubbles rising in highly viscous liquids. *Journal of chemical engineering of Japan*, 17(6), 619-623.
- Uno, Seiji, & Kintner, RC. (1956). Effect of wall proximity on the rate of rise of single air bubbles in a quiescent liquid. *AIChE Journal*, 2(3), 420-425.
- Valencia, A, Cordova, M, & Ortega, J. (2002). Numerical simulation of gas bubbles formation at a submerged orifice in a liquid. *International communications in heat and mass transfer*, 29(6), 821-830.

- Van sint Annaland, M, Dijkhuizen, W, Deen, NG & Kuipers, J. (2003). Numerical simulation of behaviour of gas bubbles using a 3D front tracking method. *AIChE Journal*, 52 (1), 99-110.
- Wellek, RM, Agrawal, AK, & Skelland, AHP. (1966). Shape of liquid drops moving in liquid media. *AIChE Journal*, 12(5), 854-862.
- Yang, GQ, Du, Bing, & Fan, LS. (2007). Bubble formation and dynamics in gas-liquid-solid fluidization—A review. *Chemical Engineering Science*, 62(1), 2-27.
- Yang, GQ, Luo, X, Lau, R, & Fan, LS. (2000). Bubble formation in high-pressure liquid-solid suspensions with plenum pressure fluctuation. *AIChE journal*, 46(11), 2162-2174.
- Yang, Ning, Wu, Zongying, Chen, Jianhua, Wang, Yuhua, & Li, Jinghai. (2011). Multi-scale analysis of gas-liquid interaction and CFD simulation of gas-liquid flow in bubble columns. *Chemical Engineering Science*, 66(14), 3212-3222.
- Youngs, DL. (1982). Time-dependent multi-material flow with large fluid distortion. *Numerical methods for fluid dynamics*, 24, 273-285.
- Yu, Zhao, Yang, Hui, & Fan, Liang-Shih. (2011). Numerical simulation of bubble interactions using an adaptive lattice Boltzmann method. *Chemical Engineering Science*, 66(14), 3441-3451.
- Zhang, Lei, & Shoji, Masahiro. (2001). Aperiodic bubble formation from a submerged orifice. *Chemical Engineering Science*, 56(18), 5371-5381.
- Zhang, Yali, Xiao, Zongyuan, & Tan, Reginald BH. (2005). Interfacial element modeling of bubble formation with liquid viscosity. *Journal of chemical engineering of Japan*, 38(7), 478-485.
- Zudin, Yu B. (1995). Calculation of the rise velocity of large gas bubbles. *Journal of engineering physics and thermophysics*, 68(1), 10-15.

## APPENDIX A

### Publications

Peer-reviewed international journal (ISI-index)

**Md. Tariqul Islam**, P. Ganesan, Ji Chang, “A pair of bubbles rising dynamics in xanthan gum solution: A CFD study” *Royal Society of Chemistry Advances*, Vol. (5), 2015, 7819 -7831.

**Md. Tariqul Islam**, P. Ganesan, J. N. Sahu, S. C. Sandaran, “Effect of orifice size and Bond number on bubble formation characteristics: A CFD study” *Canadian Journal of Chemical Engineering* (Accepted for publication).

P. Ganesan, **Md. Tariqul Islam**, J. N. Sahu, S. C. Sandaran, “Effect of column angles to rise velocity of a single bubble: A CFD study” *Progress in Computational Fluid Dynamic: An International Journal* (Accepted for publication).

### Conference

**Md. Tariqul Islam**, P. Ganesan, J. N. Sahu “Single bubble rise dynamic in glycerine solution: A CFD study” *IMiEJS2014*, Malaysia, 25th – 26th June 2014.

